Geomorphology of the deglaciated Eglinton Valley, Fiordland: new insights into the origin of hummocky terrain

A thesis presented in partial fulfillment
of the requirements for the degree of

Master of Science
in Geography

at Massey University, Manawatu, New Zealand.

Goldie Sky Walker

November 28, 2016

Abstract

The distribution and types of landforms within deglaciated valleys provide information on past processes and indicate the potential for future changes and associated hazards. This study is the first to characterise the landform assemblages within Eglinton Valley, Fiordland, New Zealand, and develop a model for the post-glacial evolution of the valley. In particular, it assesses the origins of hummocky topography on the valley floor which, like in many other parts of the world, have previously been interpreted to be glacial in origin.

Geomorphic field mapping, GPR, sedimentology (clast and agglomerate identification), and a novel terrestrial cosmogenic nuclide dating (TCND) method of extracting meteoric ^{10}Be from pyroxene minerals were utilised to reconstruct the geomorphology of the valley during the Holocene.

Glacial deposits were confirmed at Knobs Flat and Eglinton Flat while RA deposits were conclusively found at Knobs Flat, Deer Flat, and adjacent to Lake Malvora. Eglinton Valley has been completely blocked on (a minimum of) three separate occasions, forming a large lake each time, with only Lake Gunn and a few minor swamps and lakes (e.g. Lake Malvora) remaining today. Relative age dating evidence suggests the first lake was formed by the large Deer Flat RA, the next formed due to the extensive Wesney Creek alluvial fan, and the youngest, Lake Gunn, as a result of the Lake Gunn Landslide ~7.6 kyrs BP. TCND was uncompleted due to lab contamination at the final step, however, the methods attempted here appeared to yield promising results.

The Eglinton Valley has been sculpted by glacial, mass movement, and fluvial processes. This work advances the knowledge of the processes responsible for the hummocky terrain found throughout Eglinton Valley, and adds to the currently limited pool of research into the reinterpretation of hummocky deposits within deglaciated valleys in a global and New Zealand context.

Acknowledgments

First and foremost I must acknowledge the immense support given to me by my family during this research. Mum, without your epic food boxes (and financial support), I would be very hungry and unhealthy. Papa, Chris, and Helen, without your financial support, I would have struggled to put the amount of time into my work as I have been able to, had I needed a part-time job. And a special thank you to my little sister, Gemma, for hosting me, without question, for seven weeks while I undertook lab work at Victoria University of Wellington (VUW).

The research carried out for this thesis would not have been possible without permission to access the DOC land, and financial support from the British Society of Geomorphology Postgraduate Research Grant, Graduate Women Manawatu Postgraduate Scholarship, Massey Foundation new New Zealand Grant, and Massey's Geography Student Research Fund.

I would like to offer my sincerest gratitude to my supervisor, Dr. Sam McColl, who has supported me throughout my thesis with his patience, knowledge, and essential editing, whilst also leaving me to my own devices. I must also acknowledge Dr. Kevin Norton of VUW, whom I essentially 'hijacked' as a second supervisor. I immensely appreciate the large amount of time, effort, and energy you expended (all while you had a completely full calendar of your own students and projects) in order to help me learn the aspects of preparing difficult samples for TCND. On this note, I must say a huge thank you to all the staff I encountered while I was working at VUW. In particular, Jane Chewings and Sabrina Lange, as they, for some reason, accepted me as one of their own students and allowed me to work in their specialist labs. A special thank you to Professor Diane Seward for your genuine chats, moral support, and expertise in mineral identification.

I express my gratitude towards my field assistant and LaTeXtutor, Dr. Alastair Clement, who had to deal with snow in the middle of summer and angle-grinding rocks in the rain. Your support, endurance, and rock-carrying skills were immensely helpful! I can not forget the staff at Massey University who challenged my thoughts and ideas throughout this process and gave their time to meet my deadlines. Associate Professor Bob Stewart - thank you for your XRD skills; Niki Murray - cheers for your enthusiasm and humour when analysing my SEM stubs; Dr. Clel Wallace

- thank you for your input on weird and random metamorphic minerals in my thin sections; Anja Moebis - thanks for allowing me to take over the corner of the lab and trusting me with random machinery; and Szabolcs Kosik - thank you for showing me that the rock saw will not cut my fingers off.

Finally, I can not forget my friends. While working on this project I have pretty much removed myself from the world of the living. I really, really appreciate you all still being there for me, especially as I have been prioritising this work over you. You guys are the best.

"Let us try to recognise the precious nature of each day." Dalai Lama XIV.

Contents

List of Figures

List of Tables

Chapter 1

Introduction

1.1 The nature of the problem

There is still debate over the processes responsible for many landforms, particularly in deglaciated landscapes, where the concept of equifinality *(when multiple differing processes can result in visually similar deposits)* commonly applies. Where equifinality occurs, for example, hummocky ground as a product of glacial or rock avalanche (RA) processes, there is a tendency to favour explanations that are more familiar, potentially leading to false interpretations. This misinterpretation has occurred in glacial landscapes in New Zealand (Hancox and Perrin, 1994; McColl and Davies, 2011; Reznichenko et al., 2012a; Barth, 2014) and globally (Hewitt, 1999; Ballantyne and Stone, 2004; Davies et al., 2013; Reznichenko et al., 2013; Robinson et al., 2014), where hummocky ground is assumed to be a result of glacial processes yet has later been found to be the product of rock slope failures (Hewitt, 1999; Weidinger et al., 2014).

The misinterpretation of landslide deposits for glacial ones can have two crucial implications:

1. It miscounts the hazards and geomorphic significance of rock slope failures (Ballantyne and Stone, 2004; McColl and Davies, 2011).

2. It provides an inaccurate representation of regional paleo-climate reconstructions (Larsen et al., 2005; Reznichenko et al., 2012a),

This thesis investigates the Late Quaternary geomorphology of the deglaciated Eglinton Valley, Fiordland, New Zealand. The valley is abundant with alluvial fans, relict landslide deposits, hummocky topography, a wide floodplain, and a wandering river with many tributaries cascading from the valley walls. A number of the hummocks of varying sizes are currently protected as glacial kames in the New Zealand Geopreservation Inventory. However, hummocky topography can be produced by different processes including RA's, glacial deposits, and debris flows. This thesis uses quantitative methods to examine the morphology, sedimentology, and geomorphic significance of the varying features found throughout the Eglinton Valley.

1.2 Aims

The primary aim of this research is to develop a geomorphological model for the major landforms on the Eglinton Valley floor. The scope of this research aims to better describe and understand the morphology and internal sedimentology of hummocks and other features in the deglaciated Eglinton Valley. Previous observations of deposit morphology indicate RA processes may have occurred within the valley in the past (S. McColl, personal communication, December, 2014) yet this is currently unattested. The information gathered during this research should provide a better understanding and acknowledgment of the processes responsible for the hummocks on the valley floor.

A subsidery aim of this research explores a novel method of TCND which will assist in building up a global database for using ^{10}Be in pyroxene minerals.

1.3 Objectives

In order to fulfill the aims of this research, the primary objectives are:

- To produce a morphological map of the valley using aerial imagery and 12 days of field mapping. This will help assess landform distribution throughout the valley,
- To characterise clast shape and lithology from valley floor landforms (floodplain, alluvial fans, hummocky topography) to assess modes of sediment transport and sediment provenance,
- To characterise the micro-textures of fine-grained deposits within hummocky topography, to help distinguish between deposits of glacial or RA origin,
- To utilise a novel TCND technique measuring in situ cosmogenic Beryllium-10 (^{10}Be) in pyroxene minerals to determine exposure ages of boulders on top a number of hummocks. ^{10}Be is commonly extracted out of the mineral quartz, however, many landscapes, including Eglinton Valley, lack quartz-rich rocks.

Chapter 2

Literature Review

2.1 Introduction

This background chapter is intended to outline how glacial and RA processes can dramatically alter alpine landscapes, both globally and in New Zealand, and identifies the importance of careful assessment of geomorphic deposits in such regions. Hummocky topography on valley floors can be indicative of glacial (Hoppe, 1952), RA (McColl and Davies, 2011), and volcanic or fluvial debris-flow (Siebert, 1984) processes, therefore, careful examination of the internal structures and sedimentology of such deposits is crucial as these attributes can differ between processes. In this research, volcanic and debris flow processes are are not discussed as the study region is not considered to have been affected by such processes to a large extent.

Glacial landforms are widely used to infer regional climatic patterns which are then correlated globally, however, this is reliant on correct identification of the landforms (Chinn, 1979). RA's are common in glaciated landscapes, particularly in tectonically active regions, and such deposits have been misidentified, based on visual observation, globally and in New Zealand (Hewitt et al., 2008; McColl and Davies, 2011). Therefore, the current understanding of glacial and RA deposit morphology and internal sedimentology is explained, highlighting the importance of using multiple techniques to determine geomorphic deposit origins.

Slope stability factors and hazards associated with RA's will be discussed, using well-documented rock slope failures as examples, and the glacial history of New Zealand is outlined, with a focus on sediment transport and deposition dynamics of valley glaciers, focusing particularly on kame deposits.

2.2 Landslide geomorphology, processes, and hazards

2.2.1 Slope stability in alpine environments

Mass movements are a significant process influencing slope evolution in mountainous regions (McColl, 2012). The influence of steepened slopes, harsh environments, and sources of strong seismisity renders deglaciated environments prone to instability (Korup et al., 2007; McColl, 2012; McColl and Draebing, in press.). Glacier retreat, providing an 'unloading' effect on the previously stabilised valley walls, and a warming climate have been identified as catalysts for mass movements to occur in these environments (McColl, 2012; Deline et al., 2015).

2.2.1.1 States of stability

Where inherent slope stresses exceed the shear strength of the slope (i.e. the opposing stresses that resist movement) a slope failure can occur. This can be viewed on a 'margin of stability' spectrum (Figure 2.1). Slopes with a 'stable' state include slopes with a high enough margin of stability to withstand destabilising forces such as earthquakes and rainfall. The 'marginally stable' state involves slopes that are susceptible to failure should external forces exceed a strength certain threshold within the slope. Finally, the 'actively unstable' state represents slopes that are undergoing continuous or intermittent movement (Glade and Crozier, 2005b). These three states are affected by preconditioning, preparatory, and triggering factors. Understanding how these factors interact in any given region is important for geomorphic reconstructions, hazard estimation, and potential forecasting of future RA events.

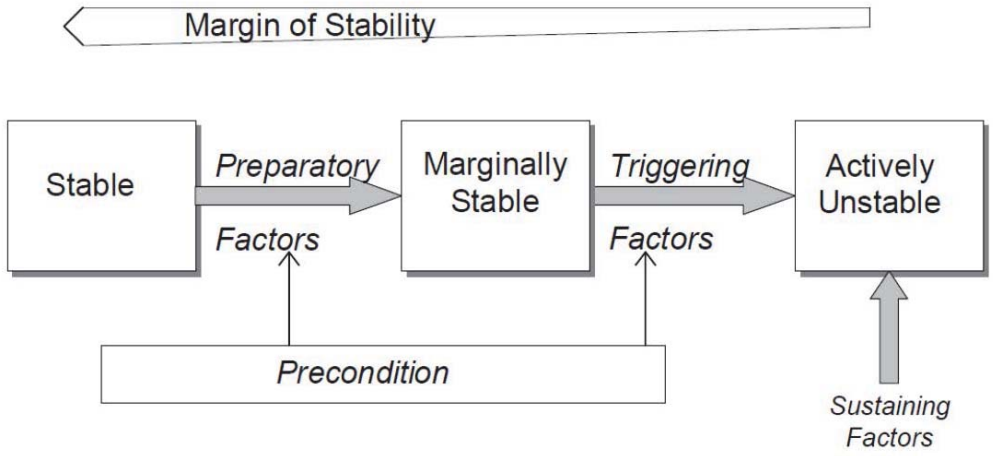

Figure 2.1: Slope stability states and destabilizing factors (Glade and Crozier, 2005b).

2.2.1.2 Preconditioning, preparatory, and triggering factors

The factors involved with the change in state of mountainous slopes are grouped into three types: preconditioning, preparatory, and triggering factors.

1. *Preconditioning factors*
   These are static factors that are inherent to the slope. They influence the overall margin of stability and allow destabilizing factors to operate more effectively (Glade and Crozier, 2005b). They include lithology, geological bedding structure, joint characteristics, and overall rock strength (McColl, 2012).

2. *Preparatory factors*
   Preparatoy factors can reduce the stability of a slope over time without initiating movement. These include strength reduction by weathering or glacial retreat (McColl and Davies, 2013), climate change, tectonic uplift, erosion causing slope oversteepening, or disturbance to the slope by human activity (Glade and Crozier, 2005b; Crozier, 2010).

3. *Triggering factors*
   These factors initiate movement; taking a slope from marginally to actively unstable. The most common triggering factors are external influences (e.g. intense rainfall or seismic shaking) however, where no apparent trigger is identified, it can be assumed that in internal threshold within the slope has been surpassed by a progressive failure mechanism (Schumm, 1979).

Mass movements in New Zealand are commonly triggered by rainfall (Crozier, 2005) and earthquakes, however, no large RA's are thought to have been triggered directly by rain. Large RA's are commonly triggered by earthquakes $>M_w$ 6.5 (Hancox et al., 1997; Keefer, 1999; Hancox et al., 2013), however, a number of New Zealand's largest RA's have occurred without a discernible trigger (e.g. Mt Cook, 1991).

2.2.2 Mass movement classification

Mass movement is a geological phenomenon that includes a wide range of ground movement and differing materials such as rock falls, debris flows, and mudslides which can occur when a triggering stress exceeds the strength of the slope (Glade and Crozier, 2005b). The most commonly used classifications are based on material type, mechanisms of movement, and degree of disruption of the displaced mass (Table 2.1; Glade and Crozier, 2005b). This chapter will focus on complex (where the material can change behaviour downslope) RA processes as this has commonly been found to produce hummocky topography in alpine terrain (e.g. McColl, 2012).

Table 2.1: Mass movement classification based on Dikau et al., (1996).

Process	Material		
	Rock	Debris	Earth
Fall	Rockfall	Debris fall	Earthfall
Topple	Rock topple	Debris topple	Earth topple
Rotational slide	Single (slump)	Single	Single
	Multiple	Multiple	Multiple
	Successive	Successive	Successive
Translational slide	Block slide	Block slide	Slab slide
Planar	Rockslide	Debris slide	Mudslide
Lateral spreading	Rock spreading	Debris spread	Earth spreading
Flow	Rockflow (Sackung)	Debris flow	Earthflow
Complex	e.g. Rock avalanche	e.g. Flow slide	e.g. Slump - earthflow

Note: A *complex* mass movement is where one form of failure develops into a second form of movement, i.e. the same material changes behaviour downslope.

2.2.3 Rock avalanches

The definition of a RA, also termed *sturzstrom* (lit. 'fall stream'; Heim, 1932) or *bergsturz* (lit. 'mountain torrent'; Glade and Crozier, 2005a), varies from paper to paper. A generally accepted definition is that a RA is an extremely rapid flow movement of fragmenting rock particles originating from the failure of all or part of a mountainside, under the influence of gravity, that can instantaneously modify the landscape (Whitehouse, 1983; Deline, 2009; Hewitt, 2009). For example the 1991 Mount Cook RA lowered the mountain by 10 m when the debris fell 2,720 m in two minutes (McSaveney, 2002).

The term 'rock avalanche' is also loosely applied in literature, with some referring to the phenomenon as rock-fall avalanche, rock-slide avalanche, debris avalanche, and rock slides, all of which imply a specific mechanism of motion (Dunning, 2004). The term RA will be applied in this study, not as a definite description of the movement, but as a term for the characteristic mass movement resulting in a particular type of deposit (outlined in Subsubsection 2.2.3.2). The kinematics of a RA are ultimately what determines the overall deposit morphology (Dufresne et al., 2016).

2.2.3.1 Rock avalanche kinematics

RA's are rarely viewed in real-time. However, they have been reported to seemingly 'flow' over and around obstacles and can even travel upslope due to their high speeds (commonly in excess of tens of metres per second; Heim, 1932; Hewitt, 1999; Davies and McSaveney, 2002; McSaveney and Davies, 2007). The motion of RA's is controlled by the phenomenon of grain flow and the frictional resistance of the constituent rock grains (McSaveney and Davies, 2007). RA's are generally dry (Glade and Crozier, 2005b), therefore, the flow-like mechanism and extensive run-out lengths (where topography allows) is thought to occur due to the reduction in inter-granular friction as a product of intensive fragmentation as opposed to the influence of water (Davies et al., 1999; Smith et al., 2006; Imre et al., 2010).

The minimum volume of rock required to initiate the flow-like behaviour of a RA is on the order of 0.5 million cubic metres though this can vary with triggering factor, geological setting, and parameters of runout path (Hewitt, 2002; Reznichenko, 2012). A large RA is considered to have a depositional volume of $>$1 million cubic metres (10^6 m^3; Davies, 1982; Angeli et al., 1996).

2.2.3.2 Rock avalanche deposit morphology

The geomorphic characteristics of RA's can be used to distinguish their deposits from other types of deposits found within deglaciated valleys. These are shown in Figure 2.2. The morphology can be described as follows:

1. Long runout deposits following topography (Heim, 1882; Heim, 1932),

2. Lateral and terminal margins are clearly defined (Shreve, 1968),

3. Ridges and troughs, parallel to flow direction, are found on the surface (Hewitt, 2002; Dufresne and Davies, 2009),

4. Run-up of deposits (also known as *brandung*) on opposite valley walls or outside bends (Heim, 1932; Crosta et al., 2007),

5. Source scar (Whitehouse and Griffiths, 1983),

6. Deposit radiates from source area where topography allows (Dufresne and Davies, 2009; McColl and Davies, 2011).

While some RA deposits might show several or all of these characteristics, not every RA deposit will exhibit all of the mentioned morphologies as they are a product of the internal characteristics of the rock and slope mechanisms involved (Nicoletti and Sorriso-Valvo, 1991; Davies et al., 1999; Strom and Korup, 2006). Therefore, the geomorphology alone can not be used to determine the depositional process, therefore, the internal sedimentology must also be considered.

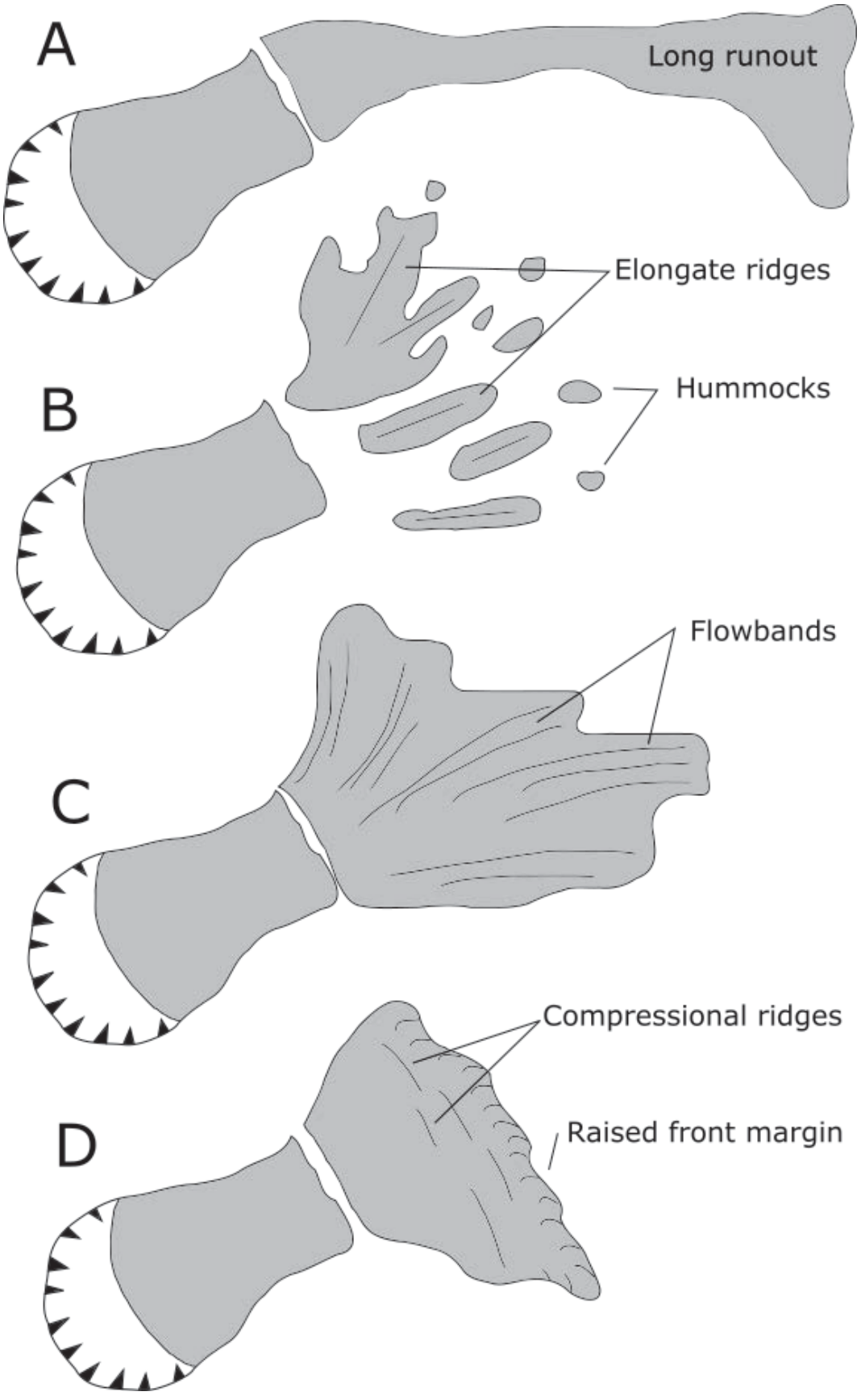

Figure 2.2: Diagram of the typical morphological features that a RA can form. A) Where topography allows, a long runout can occur. B) Radiating deposits forming natural ridges and hummocky topography. C) Flowbands e.g. less-pronounced ridges forming in the flow direction. D) Compressional ridges forming perpendicular to the flow direction, usually due to a topographical constraint or abrupt slowing down of movement.

2.2.3.3 Rock avalanche deposit sedimentology

The internal sedimentology of RA deposits is a major component of this research as recent work has shown the sediment can be a crucial diagnostic tool for identifying RA deposits where morphological characteristics alone are not sufficient for unequivocal identification, either because of equifinality or post-depositional modification (Davies et al., 1999; Dunning, 2006; McSaveney and Davies, 2006; Crosta et al., 2007; Reznichenko et al., 2012a; Weidinger et al., 2014). The commonly held distinguishing criteria of RA deposits are outlined in Figure 2.3 and include:

1. *Fragmented yet relatively undisaggregated clasts.*
   Also termed 3-D jigsaw puzzle texture, crackle breccia, jigsaw clasts, or mosaic texture (Davies et al., 1999; Hewitt, 1999; Dunning, 2004; Dufresne et al., 2016), fragmented yet relatively undisaggregated clasts are highly diagnostic of RA deposits and reflect the role of fragmentation processes (Davies and McSaveney, 2002; Dunning, 2006; Crosta et al., 2007). They are reported by almost all studies where the deposit interior can be viewed (Davies et al., 1999; Hewitt, 1999; Dunning, 2004; Wassmer et al., 2004; Dunning et al., 2005; Smith et al., 2006; McColl and Davies, 2011; Barth, 2014; Weidinger et al., 2014), however, their degree of development is strongly influenced by lithology and travel distance (Dufresne et al., 2016).

2. *Preservation of source-rock structures.*
   The presence of source stratigraphy within a deposit is a key diagnostic feature for RA deposits (Whitehouse, 1983; Dunning, 2004; Abdrakhmatok and Strom, 2006; Strom and Korup, 2006). It is supported by many case studies including the Frank Slide (Cruden and Hungr, 1986), the Falling Mountain RA deposit (McSaveney, 2002), and the Cascade RA (Barth, 2014). It is dependent on the presence of source rock stratigraphy which allows recognition in the deposit.

3. *Monolithic.*
   In many RA deposits the composition is monolithic, from boulders to dust, representing the local bedrock (Hewitt, 1999). However, the lithological composition can also include multiple lithologies if they are present in the source areas or have been entrained during transport.

4. *Angular to very angular clasts.*
   The shape of clasts is inherited from transportation mechanisms and weathering. The Power's Scale of Roundness (Powers, 1953) is a visual comparison chart widely used to clarify roundness of clasts within a RA deposit. A RA exhibits angular to very angular clasts as they are sourced directly from bedrock and a result of intense comminution and fragmentation during runout (McSaveney and Davies, 2007; Shulmeister et al., 2009). Softer lithologies (or weathered deposits) may present slightly *snubbed* corners, however, faceting

and striations (typical glacial features) are absent for RA sediment (Hewitt, 1999).

5. *Agglomerates.*
   Agglomerates form when fragments, resulting from rapid, high-stress comminution in strongly confined conditions, can not disperse when they are formed. They also form in fault shear zones but has not been found to occur during glacial transport of sediments. Where agglomerates are found in glacial deposits it can be inferred that a RA probably fell onto the glacier and was entrained (Reznichenko et al., 2012a; Deline et al., 2015).

6. *Coarse carapace topping matrix-supported clasts.*
   The internal and basal debris of a RA deposit are generally topped with the coarsest unit; a carapace of less-fragmented rocks (McSaveney and Davies, 2006; Dunning and Armitage, 2011; McColl and Davies, 2011; Weidinger et al., 2014; Dufresne et al., 2016). The carapace is clast supported and can retain source stratigraphy (Strom, 2006; Dunning and Armitage, 2011).

7. *Source scar.*
   The presence of a source scar above the deposit is a tell-tale feature, however, it may not always be visible due to vegetation, further erosion, or the RA may have been large enough to remove the entire ridge or face. There is also the implication that the source scar may be confused for a glacial cirque basin (Turnbull and Davies, 2006).

In addition to these features, a number of studies argue for inverse grading and poor sorting as distinguishing features (e.g. Cruden and Hungr, 1986; Blair, 1999; Hewitt, 1999). However, a common observation that RA deposits exhibit crude inverse grading has been shown to be a misconception (Dunning, 2006; Dunning and Armitage, 2011). The phenomenon of boulders becoming more prevalent from the base to the surface is not found in all deposits, e.g. Flims RA in Switzerland (Wassmer et al., 2004) and Falling Mountain in New Zealand (McSaveney, 2002), and can be confused with the coarse carapace of deposits if the entire section is not visible. Poor sorting, also termed 'immature' (Hewitt, 1999), within a RA deposit reflects rapid transport and emplacement that can be observed and measured directly. However, the sorting of a RA deposit cannot be used as a diagnostic tool as other forms of mass movement (e.g. debris flows) and glacial deposits (e.g. moraines) can also be poorly sorted (Dunning, 2004).

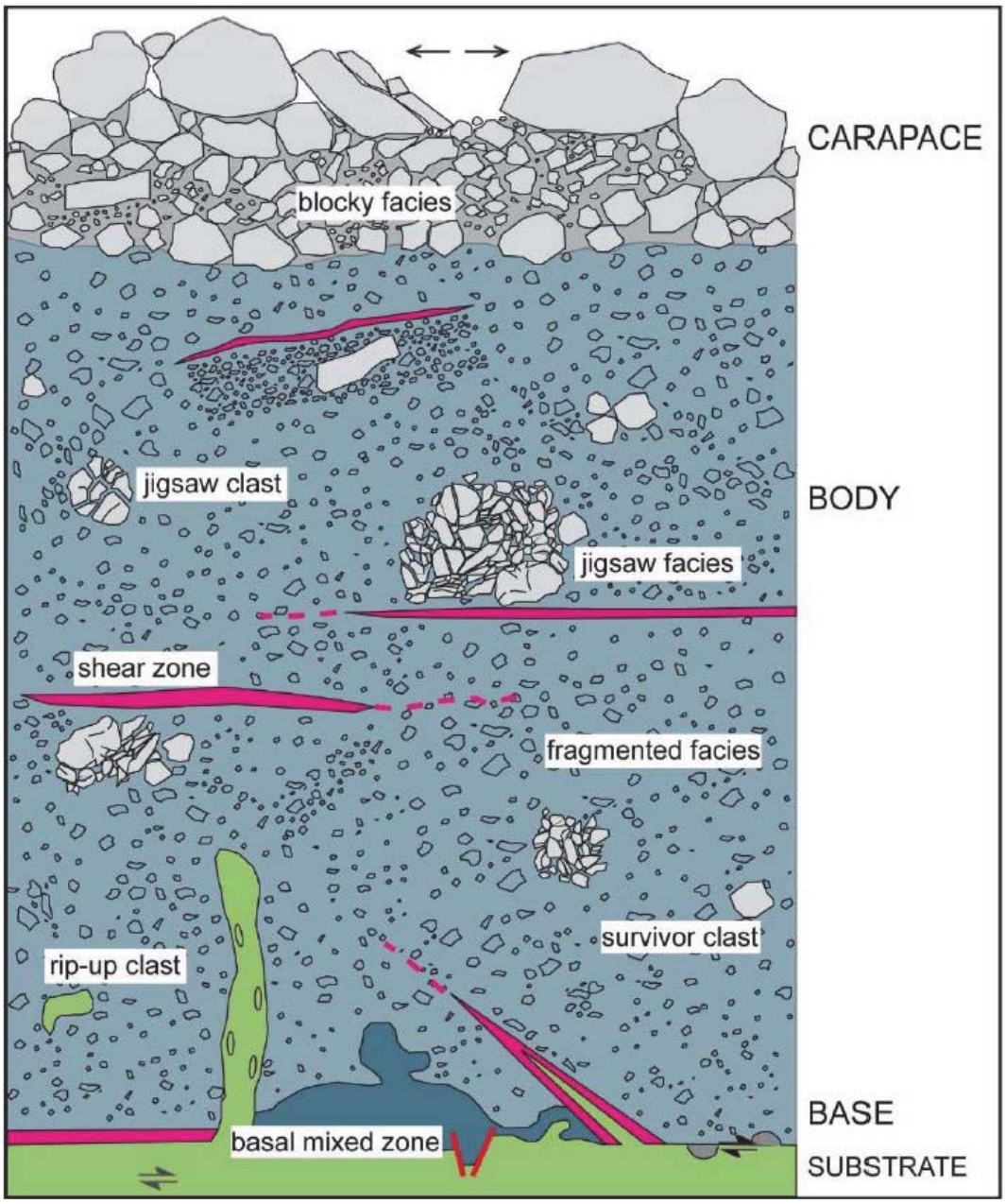

Figure 2.3: Diagram of common features found within RA deposits. From Dufresne et al., (2016).

2.2.3.4 Rock avalanche distribution in alpine regions

RA slope failures are infrequent but not an uncommon occurrence in most mountainous regions of the world e.g. Scotland (Ballantyne and Stone, 2004); the Italian Alps (Crosta et al., 2007); the Himalayas (Hewitt, 1999; Weidinger and Korup, 2009); the Southern Alps of New Zealand (Whitehouse and Griffiths, 1983); and the Rocky Mountains (Jackson, 2002). The most recent (yet still incomplete) inventory of landslides in the southwest New Zealand region shows 778 mass movements (Figure 2.4) as compiled by Korup (2005), however, this does not readily identify RA-type mass movements and only accounts for events which were identifiable in DEM's and aerial photographs. The methods used in Korup's study disregard some much older (Holocene) events where their geomorphic evidence and debris may have been eradicated by erosional processes (Hancox, 1999) thus providing only a minimum number of events with the opportunity for more to be identified and mapped, particularly by field investigation.

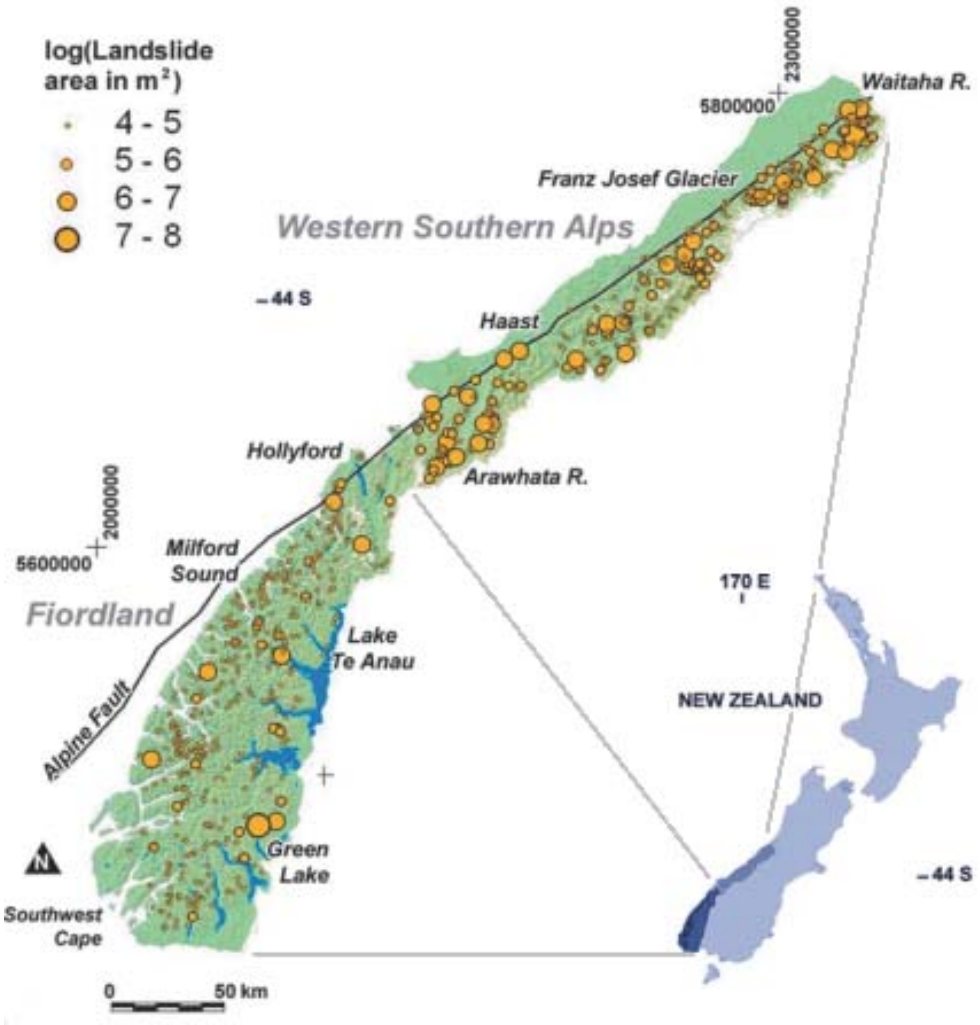

Figure 2.4: Distribution of 778 mapped mass movements within the western Southern Alps and Fiordland regions. Note that RA events are not identified separately. Adapted from Korup (2005).

2.2.4 Hazards associated with rock avalanches

RA's are a considerable threat to communities living in the vicinity of mountainous topography. They can destroy entire villages, kill thousands of people, and cause significant short- and long-term health problems (Heim, 1932; Cruden and Krahn, 1978; Whitehouse and Griffiths, 1983; Hewitt, 1999; Hewitt et al., 2008; Petley, 2012; Kennedy et al., 2015). The direct hazard from a RA to life, infrastructure, communication networks, and property increases as population grows and land-use expands into upland areas (Whitehouse and Griffiths, 1983; Dunning, 2006).

RA's act as fundamental agents of erosion (McSaveney, 2002), sediment production, and sediment impedance (Korup et al., 2004; McColl and Draebing, in press.) in alpine regions thus understanding the local effect in these areas is of significant importance.

2.2.4.1 Landslide dams

In a valley-confined setting, RA's are among the most common processes to form natural dams in fluvial systems (Costa and Schuster, 1988; Korup, 2002; Dunning, 2006). The impact of a RA in a fluvial system can result in complete channel blockage, constriction, diversion, avulsion, or can act as a buffer for further sediment input from upstream (Korup, 2002). Channel blockages by RA's generally have a short longevity e.g. Costa and Schuster (1988) studied 73 landslide-dam failures and found 27% failed in less than 1 day while ~50% failed within 10 days. Catastrophic outburst floods from naturally dammed rivers can cause loss of life, housing, and infrastructure (Costa and Schuster, 1988; Korup, 2002). Not all dams burst catastrophically; some may be emplaced for many years, allowing fine-grained lacustrine sediments to accumulate (Reading, 2009).

2.2.4.2 Global impacts of rock avalanches

RA's are a global phenomenon, altering mountainous landscapes dramatically and potentially affecting thousands of people. The legacies of such events are unmissable e.g. the Hattian Bala RA (Kashmir) that destroyed a village, killed ~1000 people, and formed the 130 m deep ZalZal and Bani Hafiz lakes that still threaten to flood the settlements down-valley (Table 2.2).

Table 2.2: Large global rock avalanches and their geomorphic impact.

Location	Date	Mass failure volume (10^6 m^3)	Geomorphic impact
Hattian Bala, Kashmir	2005	68	Debris formed two lakes (ZalZal Lake and Bani Hafiz Lake, still in place) and destroyed 5 villages[1]
Yigong, Tibet	2000	0.3 x 10^9	1,500 m vertical rockfall before entraining older deposits and flowing ~10 km where it dammed the Yigong river for 62 days[2]
Mount Adams, New Zealand	1999	10-15	120 m high rock-debris dam impounded a lake with a volume of 5-7 million m^3 before overtopping 1 day later and breaching a further 5 days later. Since, the Poerua river has aggraded and avulsed[3]
Mount Cook, New Zealand	1991	11.8 ± 2.4	10 m of former summit lost initially. This has dropped to 30 m total due to ongoing erosion[4] and reduced ablation of the Tasman Glacier due to the excess addition of supraglacial sediment[5]
Grisons, Switzerland (Flims RA)	1939	120	400 m high dam, 40 km-long lake formed, possibly two overtopping events[6]
Falling Mountain, New Zealand	1929	55	Removed the western face and former summit of Falling Mountain. Incision into the deposit by way of a gorge[7]
Turtle Mountain, Canada (Frank Slide)	1903	30	Infilled 120 m of the valley[8]

[1] Dunning et al., (2007); [2] Xu et al., (2012); [3] Hancox et al., (2005);
[4] McSaveney (2002); [5] Reznichenko et al., (2012b); [6] Wassmer et al., (2004);
[7] McSaveney et al., (2000); [8] Cruden and Krahn (1978).

2.3 Glaciers

Glacial processes are a major factor in influencing sediment dynamics and depositional landform development within alpine valleys. Glaciers provide different transport pathways for sediment transport and deposition throughout the travel path.

2.3.1 Sediment transport in a glacial system

Two forms of valley glaciers have been recognised: low-relief glaciers that form in old 1-2 km high mountain belts such as in Norway, and high-relief glaciers that form in young, seismically active, mountains with several km high peaks e.g. the Southern Alps of New Zealand (Benn and Evans, 2010). High-relief glaciers transport a demonstrably larger amount of supraglacial (on the ice surface of the glacier) debris as a result of rapid sub-aerial denudation of the steepened slopes by rock slope failure (Boulton and Deynoux, 1981; Korup and Clague, 2009). High-relief glaciers produce copious amounts of deposits with sediment of a range of sizes from house-size boulders to fine silts (Hallet et al., 1996). However, before sediment can be deposited it must be incorporated within the glacial system. The two primary sources of sediment incorporation are:

1. Erosion of basal material by subglacial (the zone of contact with the substrate) abrasion and plucking processes,
2. Mass movements (including RA's) onto the top of the glacier which generally get transported supra- and en-glacially (Figure 2.5).

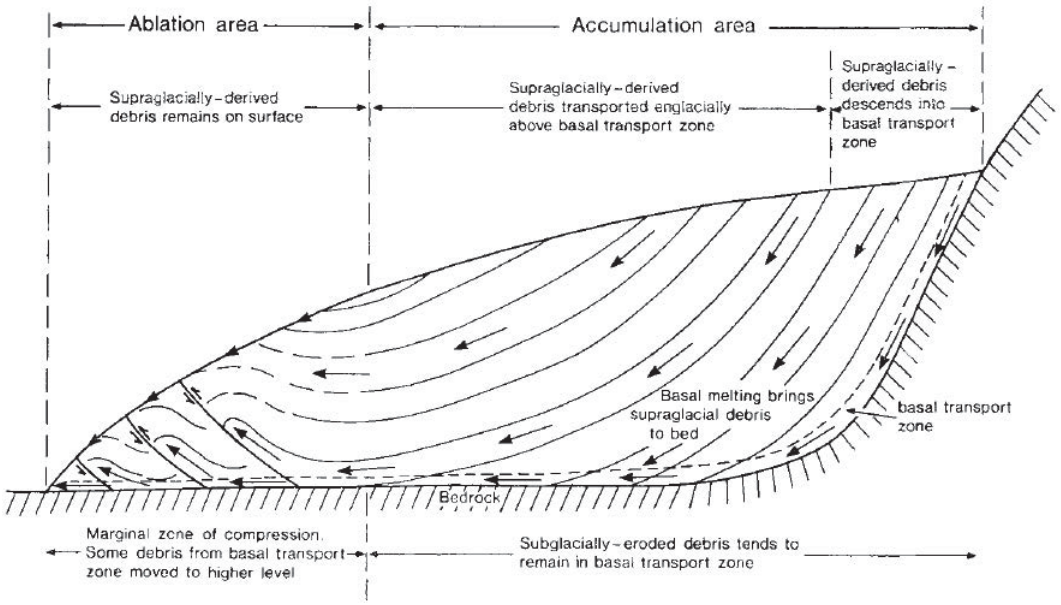

Figure 2.5: Transport paths of debris in a temperate valley glacier (Boulton, 1978).

The transport pathway of sediment in and on a glacier plays a significant role on the overall clast morphology (form) that is found in glacial deposits. The form of

clasts reflects the physical properties of the bedrock source material and subsequent modification by erosion, transport, and weathering (e.g. frost shattering; Boulton, 1978; Benn and Ballantyne, 1994) allowing interpretations of transport pathways and potentially source locations based on lithology and angularity.

1. *Supraglacial transport*
   Debris that falls onto the glacier surface in the ablation zone is carried passively on top of the ice, unless sufficient snowfall buries it in the upper accumulation area allowing the debris to reach near the glacier bed (Figure 2.5; Alley et al., 1997). Debris produced by fracturing rock above the glacier (e.g. rock fall/avalanche) is dominantly coarse and angular (Boulton, 1978) and commonly stays this way due to the lack of abrasion, though this can be partially dependent on rock type (Benn and Ballantyne, 1994). Deposits exhibiting angular material can therefore be representative of supraglacially transported debris, however, rock slope failures that fell directly onto a non-glacierized valley floor also include angular debris. Therefore, angularity alone cannot sufficiently be used to infer depositional processes.

2. *Englacial transport*
   Sediment transport within the glacial ice is relatively passive; with little to no break down or comminution of the clasts (Boulton, 1978). This form of transport can result in relatively angular clasts within the final deposits so lithologies and other depositional mechanisms (e.g. rock slope failures) must be carefully considered.

3. *Subglacial transport*
   Many factors influence the active subglacial entrainment properties of any particular glacier and these are covered in Alley et al., (1997) and beyond the scope of this thesis. The key factor of subglacial transport is the ability of the glaciers movement to break down and cause significant modification (e.g. striations and sharp-edge fracture planes on relatively smooth boulders; Boulton, 1978) and rounding of the clasts either on the bed or along the base of the glacier (Hewitt, 1999; Reznichenko, 2012).

2.3.2 Glacial history of New Zealand

New Zealand has a sufficient morphological record (based on interpretations of glaciogenic landforms) of Quaternary glaciations with fragmented records dating back to the Late Pliocene (*c.* 2.6 Mya; Suggate, 1990). The most recent synthesis of current knowledge of Quaternary glaciers in New Zealand is outlined in extensive detail in Barrell (2011) so only key points are mentioned here. In New Zealand the glaciers were at their largest extent during the Late Otira, otherwise known as the Last Glacial Maximum (LGM) *c.* 20-30 ka.

During the LGM, glaciers were prevalent throughout the South Island and small valley glaciers occurred in the central North Island and highest parts of the Tararua Ranges. In the South Island, glacial moraines have been found extending into the lowlands on the eastern side of the Main Divide and glaciers potentially reached to the sea on the western side (Figure 2.6; Almond et al., 2001; Barrell, 2011). As such, accurate interpretations of landforms as glacial or non-glacial are crucial in past climate reconstructions and in the formation of maps such as Figure 2.6.

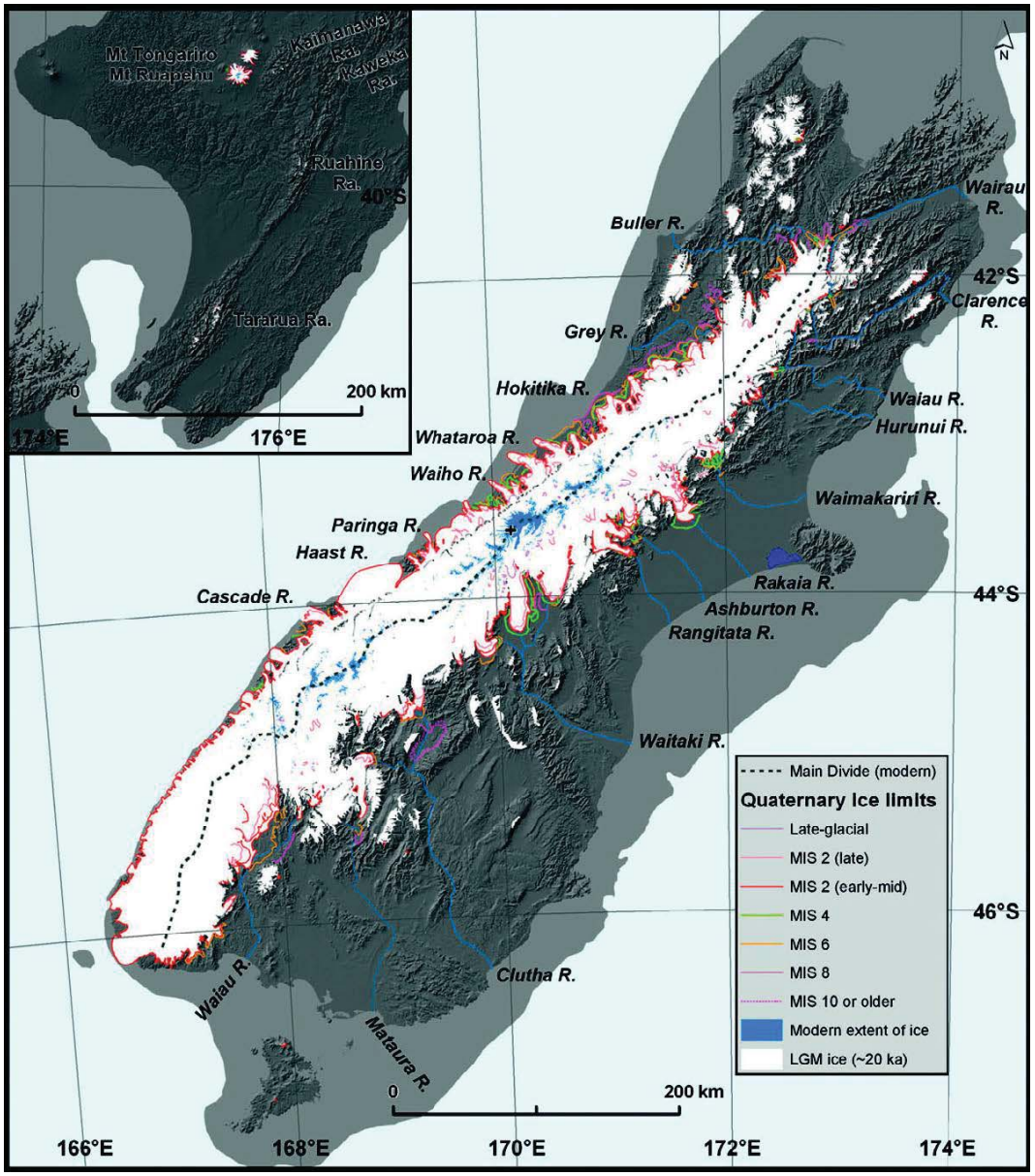

Figure 2.6: Interpretation of Middle to Late Pleistocene ice extents in New Zealand. Light grey indicates approximate land extent with sea-level ~125 m lower. Black dotted line indicates the Main Divide (Barrell, 2011).

2.3.3 Glacial deposits

A note on terminology:
The term *till* has, in the past, been used casually to describe generic glacial deposits, various subtypes of till, and till-like sediments (Brevik and Konen, 2003). In this research, the term *till* will follow the definition proposed following a 14-year discussion by the International Union for Quaternary Research (INQUA) as it clearly details the process involved:

"Till is a sediment that has been transported and deposited by or from glacier ice, with little or no sorting by water" (Brevik and Konen, 2003, p. 65).

All available debris is reworked by the glacier and eventually deposited as till in the valley as the glacier retreats. The deposits include medial, lateral, and terminal moraines, eskers, drumlins, and kames (Figure 2.7).

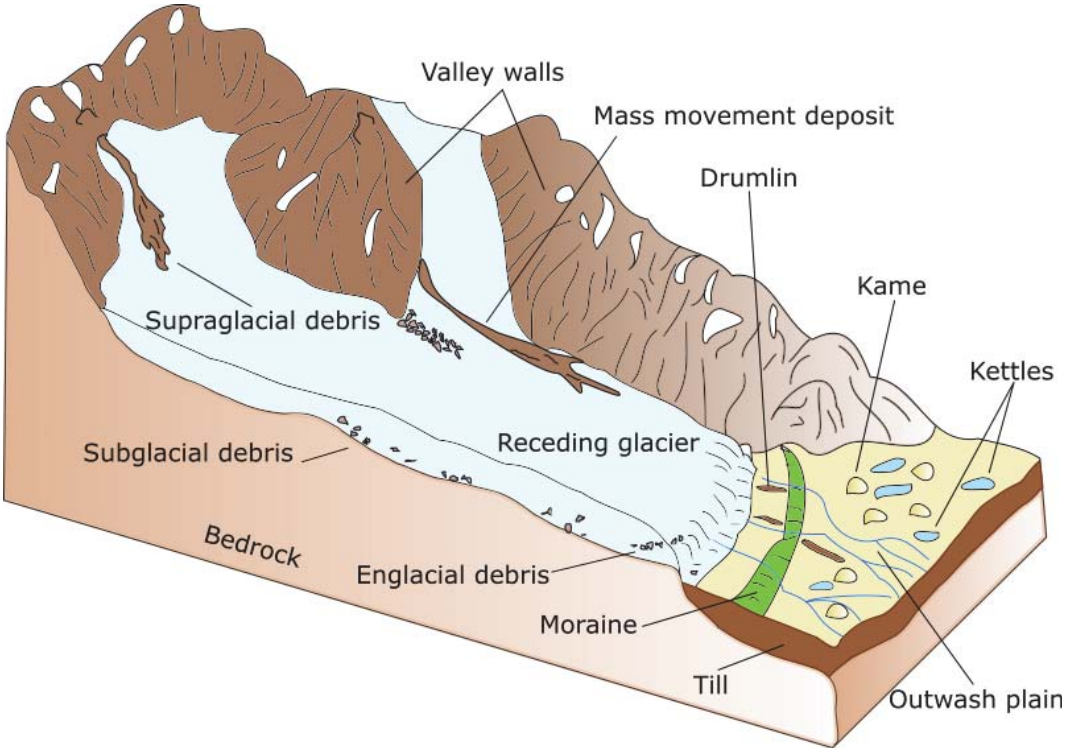

Figure 2.7: Schematic of typical valley glacier deposits.

The size of the deposit reflects the amount of sediment transported by the glacier. Low relief glaciers with little to no supraglacial sediment can only produce small (<10 m) eskers or moraines (e.g. Brigsdalsbreen Glacier moraines, Norway; Winkler and Nesje, 1999). In contrast, high relief glaciers with large amounts of available sediment can produce large (>100 m high) moraines and, where climatic conditions allow, fluvial processes can rework some of the sediment, altering the deposit morphology and that of the deglaciated valley (Swift et al., 2002; Reznichenko, 2012).

2.3.4 Primary and secondary deposition

When considering the depositional processes of a particular landform, the overall morphology cannot always be used as an indicator. Two depositional process groups have been recognised: primary and secondary. Primary processes release and deposit till directly from the glacier ice. Secondary processes involve further mobilisation and reworking of the deposit by external factors such as fluvial action (Lawson, 1981; Sharp, 1983),faulting, and folding, which can all have a demonstrable effect on the overall deposit morphology.

2.3.5 Glacial deposit sedimentology

Processes of deformation, flow, sliding, lodgement, and ploughing all coexist at the basal zone of temperate glaciers therefore sediment can be mobilised, transported, and deposited in a wide range of features. Valley glaciers deposit till under relatively low-stress conditions (in comparison with the high stresses of RA deposition), thus the sedimentology of glacial deposits directly reflects these low stress conditions. The internal sedimentology of such features can vary from folded and faulted stratified material to texturally homogeneous diamicton (unconsolidated till). Further information about the formation of glacial deposits is provided in a review paper by Evans et al., (2006) so is not covered in detail here.

2.3.6 Complex kame morphology

This research has a particular focus on glacial kames as their appearance can be strikingly similar to that of RA deposits. This similarity has led to misinterpretations in the past. For example, The Hillocks 'moraine', identified in the Dart Valley, NZ, has recently been reinterpreted as a RA deposit (Figure 2.8 McColl and Davies, 2011). This recognition has altered the preconception of past climate within the valley while recognising the geomorphic importance and potential hazard for future RA's within the region. This type of reinterpretation has also occurred in a small number of glaciated regions around the world (e.g. Hewitt et al., 2008).

Glacial kames can take on a range of forms such as terraces (e.g. Iceland; Evans and Twigg, 2002) and ridges (e.g. where a kame is produced within an ice crevasse; Niewiarowski, 1965), though they are generally found as conical hillocks/hummocks (Holmes, 1947; Benn and Evans, 2010; Livingstone et al., 2010; McColl, 2012). This diversity makes them one of the most complex and diverse depositional features within a deglaciated valley (Livingstone et al., 2010).

The term 'kame' has generally been used to describe the form of the deposit only, without regard to internal characteristics (Holmes, 1947) and is often used in conjunction with kettle topography (e.g. *"kame and kettle topography";* Niewiarowski, 1965; Price, 1969).

Figure 2.8: Annotated image showing some of The Hillocks RA deposits that were previously interpreted as glacial deposits, Dart Valley, NZ. Photo by S. McColl.

2.3.7 Kame sedimentology

The internal sedimentology of glacial kames can be used to help distinguish them from deposits formed by other processes. The kame formation process is commonly referred to as *melt-out till*; dead ice covered in debris melts out as the glacier retreats, leaving primary till behind (Figure 2.9; Boulton and Deynoux, 1981; Paul and Eyles, 1990; Livingstone et al., 2010; Larson et al., 2015). The primary till is further reworked by secondary processes (e.g. fluvial processes) as the glacier continues to retreat, leaving the classic hummocky topography behind.

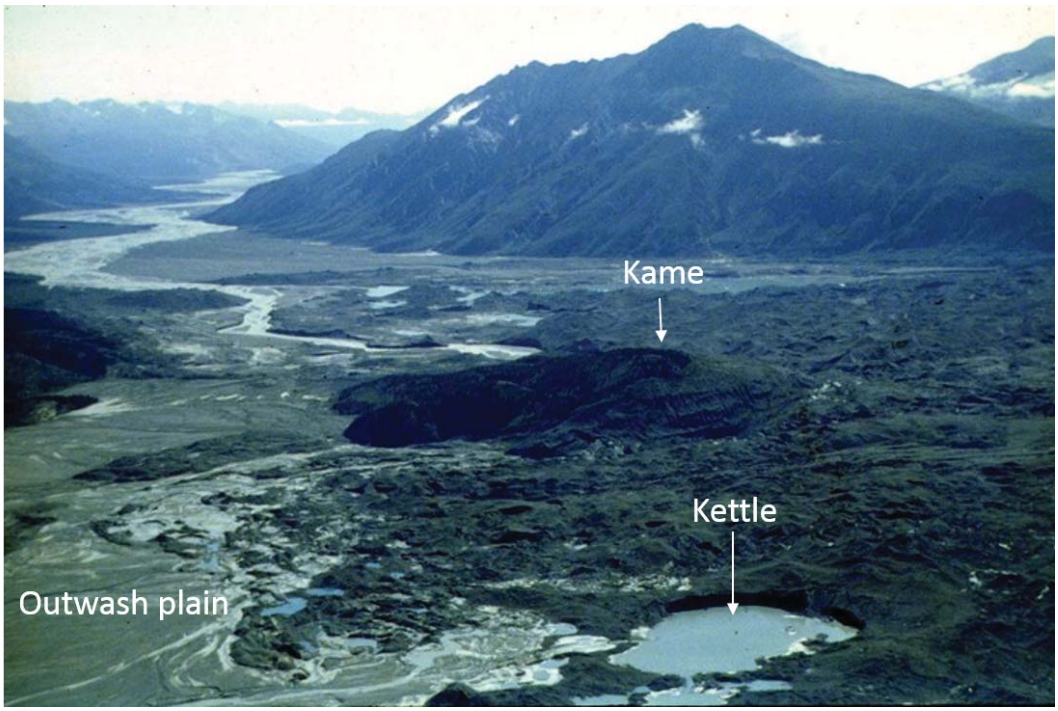

Figure 2.9: Typical kame and kettle topography (Shepherd, 2015).

The following conditions outline the most common sedimentological characteristics for glacial kame deposits:

1. *Matrix-supported.*
   The till produced by a glacier ranges in size from <63 µm to house-sized boulders. Beneath temperate glaciers, fluvial processes act to disperse the fine sediment throughout empty spaces, as a deposit is forming, before dewatering occurs as a result of increasing deposit depth. This process may then result in the base of a deposit being more matrix-supported than the top of the deposit (Evans et al., 2006).

2. *Varying clast roundness.*
   The active transport processes throughout the glacier can result in a range of sub-angular to rounded clasts in the final deposit depending on the travel distance (of the clasts) and the hardness of the lithologies (Benn and Ballantyne, 1993).

3. *Varying lithologies.*
   As a glacier travels down a valley it incorporates sediment and bedrock from throughout its travel path. In most valleys the lithologies vary, therefore, it is logical that the deposits would include a range of lithologies (Hambrey, 1994).

4. *Clast wear patterns.*
   Grain crushing and abrasion is common near the basal zone of temperate glaciers. Typical features of worn clasts include striations on individual clasts and/or flat and polished faces. The subglacial strain and drainage conditions will determine the spatial and temporal presence of such wear patterns and they may not be found on every clast (Benn and Evans, 1996).

5. *Widespread occurrence.*
   As discussed by McColl (2012), the presence of kame deposits would be expected to occur throughout the valley, though probably localised to patches of dead ice. This differs for RA deposits which are generally restricted to a runout path. However, due to the complexity and variety of run-out styles, it may be difficult to distinguish a ~km-long partly-buried RA deposit.

2.4 Differentiating rock avalanche deposits from glacial deposits

On the surface, a hummocky glacial deposit can look like a debris flow deposit (e.g. The Murimotu debris flow, Mt Ruapehu) or a RA deposit. Where the difference lies is within the internal sedimentology, though they can also be distinguished based on morphology and overall landform distribution within the depositional area (e.g. McColl and Davies, 2011).

As both processes (RA and glacial) can produce fine material by abrasion and crushing of rocks, specific differences in the physical process itself can be discovered by assessing the sedimentology at a microscopic level. The discovery that agglomerates can form during RA events allowed a distinction between glacially derived deposits and RA deposits (Reznichenko, 2012). However, agglomerates are not only related to RA's. They are also found in fault, crush zones and meteorite impact craters (Weidinger et al., 2014).

While the presence of agglomerates within a deposit may indicate a RA origin of the sediments, the final deposition process may in fact be glacial. This can occur where a RA falls onto a glacier, the sediment is carried actively or passively, and is then deposited as glacial moraine (e.g. Waiho Loop moraine, NZ; Tovar et al., 2008; Shulmeister et al., 2009).

2.5 Rock avalanche effect on glacier behaviour

A RA deposited onto glacial ice can dramatically alter the behaviour of a glacier (Shulmeister et al., 2009). The ice is protected from ablation which can prompt a glacial advance (e.g. Purdie and Fitzharris, 1999) and sediment delivery is increased (Deline, 2005; Hewitt, 2009; Shulmeister et al., 2009; Shugar et al., 2012; Deline et al., 2015). Glacial deposits, particularly terminal moraines, are widely regarded as proxy's for climate changes (e.g. Tschudi et al., 2000; Anderson and Mackintosh, 2006; Ivy-Ochs et al., 2006), however, a number of moraines found globally can not be correlated with cooling events. The Waiho Loop Moraine, in Westland, South Island, NZ, is one such deposit that has recently been identified as forming due to a landslide-initiated glacial advance that is not recognised in deposits elsewhere in the region. This re-interpretation was first discovered when the sedimentology was found to be prominently angular and monolithic (Shulmeister et al., 2009). This was later confirmed when agglomerates were found within the microsediments (Reznichenko et al., 2012a; Alexander et al., 2014; Reznichenko et al., 2015). Thus the influence of debris cover must be accounted for when interpreting climatic changes (Deline, 2005).

Chapter 3

Regional setting

3.1 Introduction

This regional setting chapter describes the geological setting and the geomorphic processes (including mass movement and glacial processes) and hazards of the Fiordland region of New Zealand. The overall geomorphology of the Entire Eglinton Valley is presented and a site description is provided. An outline of previous work on interpreting landforms within Eglinton Valley is also explained.

3.2 Geological setting - regional overview

Fiordland region is situated in the far southwest of New Zealand and is renowned for its harsh, mountainous terrain carved with bountiful fjords, parabolic valleys, and glacial-trough lakes such as Te Anau, Manapouri, and Monowai (Figure 3.1) which attract hundreds of thousands of tourists every year. Most of the region is covered by the Fiordland National Park, and at 12, 120 km^2, is New Zealand's largest national park.

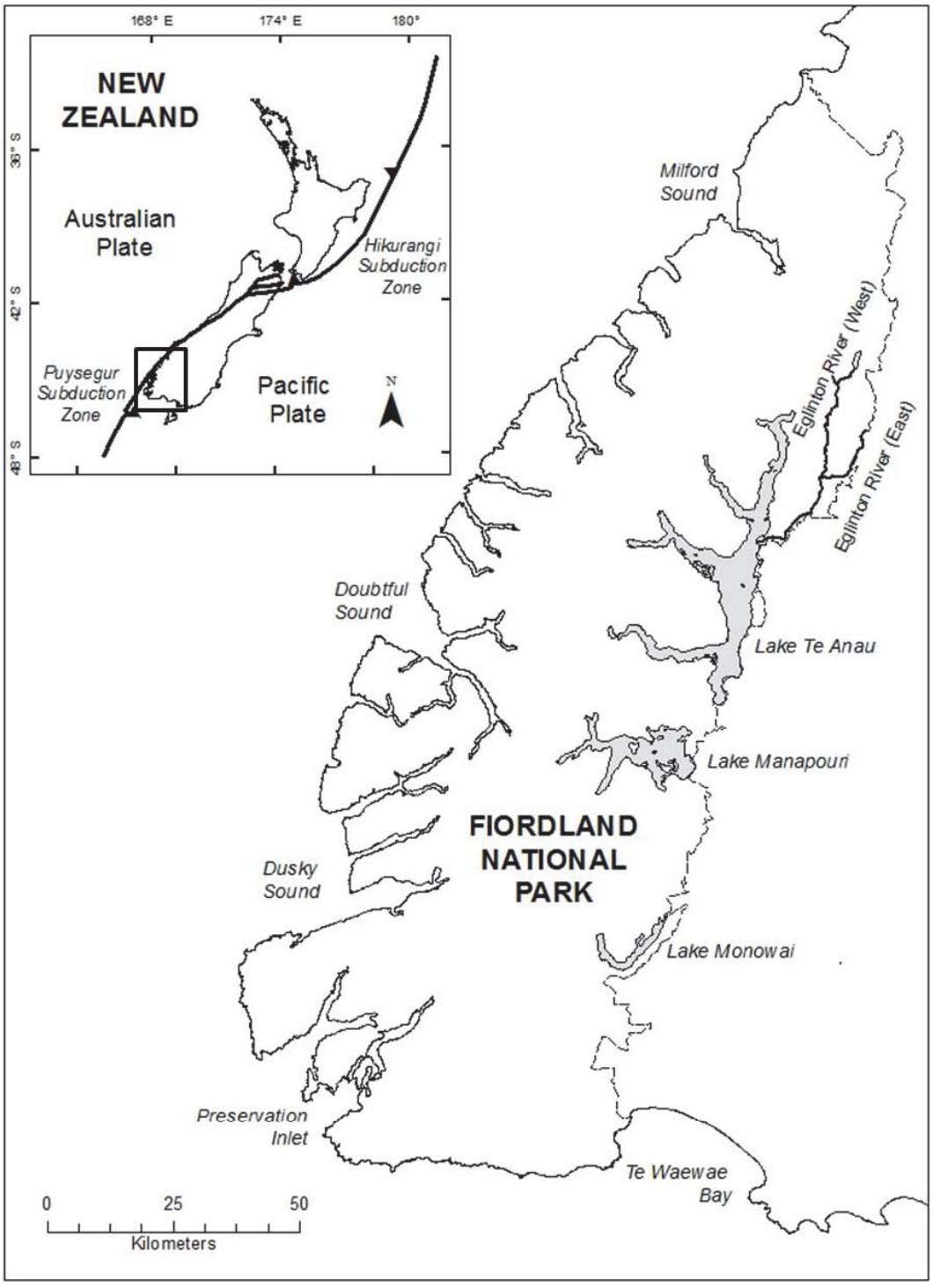

Figure 3.1: Location map of Fiordland National Park (outlined by the dashed line), major lakes, and the Eglinton Rivers (East branch and West branch). Inset shows the boundary of the Australian and Pacific plates (black line) and relative movement direction indicated by arrows.

Fiordland's mountains are formed of massive, well-indurated, low-grade metamorphic, un-weathered rocks, including Paleozoic to Mesozoic diorites, andesites, gabbros, amphibolites and granites (Korup, 2005; Hancox and Perrin, 2009) providing a strong and stable basement. The major active tectonic features in the Fiordland

region include the Alpine Fault, which comes on-shore north of Milford Sound, and the Puysegur Subduction Zone (PSZ) which dips to the east and underlies the Fiordland region (Figure 3.2). The smaller tectonic features within Eglinton Valley are further discussed in Subsection 3.2.2.

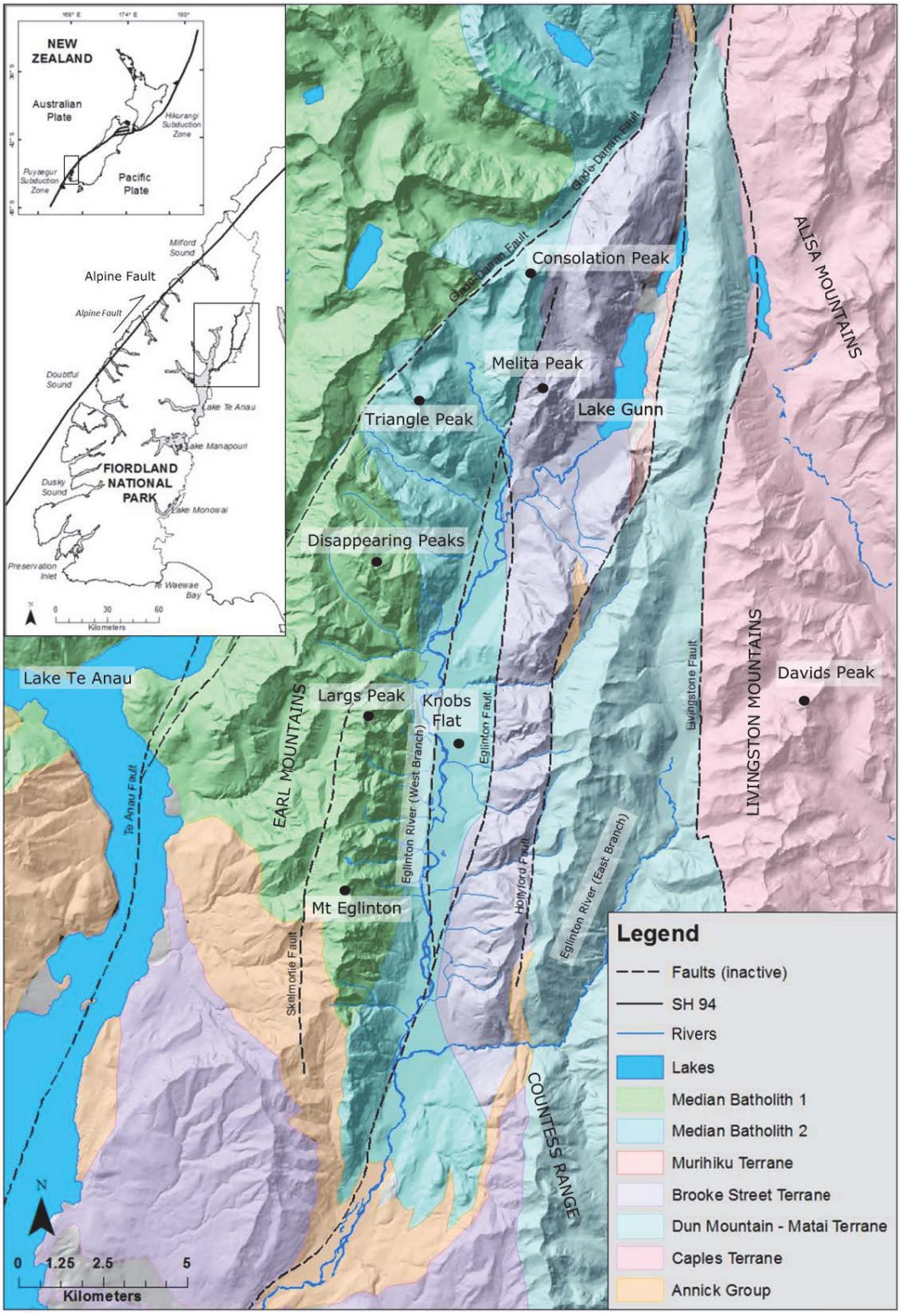

Figure 3.2: Basement geology of the Fiordland/Eglinton Valley region, subdivided into terranes, batholiths, and groups. Major faults are shown and the main mountains are labeled for reference. Knobs Flat is in the centre of Eglinton Valley. Inset shows location within New Zealand. Geological basemap adapted from (Turnbull, 2000).

3.2.1 Eglinton Valley geology

The bedrock geology was primarily mapped by Grindley (1958) and Williams (1975) and has since been compiled by Turnbull (2000). Eglinton Valley is 'sandwiched' between the North-South trending belts of the Cretaceous Median Batholith to the far west, a sliver of Late Triassic Median Batholith running down the western side of the valley floor, and the Permian Brook Street Terrane lining the east side of Eglinton Valley. This is then bounded farther east by the Early Permain-Triassic Dun Mountain-Matai Terrane and the Permian Caples Terrane (Figure 3.2; Turnbull, 2000).

3.2.1.1 Median Batholith

The Cretaceous and Late Triassic Median Batholith forms the Earl Mountains in the far north-western end of the catchment (including Disappearing Peaks, Consolation Peak, and Triangle Peak). It is comprised primarily of igneous granites and diorites, while farther south, Largs Peak and Mt Eglinton are formed of volcanic andesites, tuffs, and breccias (Turnbull, 2000).

3.2.1.2 Brook Street Terrane

The Permian Brook Street Terrane is generally faulted against the Median Batholith (Mortimer et al., 1999). This Terrane is primarily volcaniclastic and includes andesites. Metamorphism has altered much of it to prehnite-pumpellyite. Melita Peak, at the head of the valley on the south-western shore of Lake Gunn, and the eastern peaks of Eglinton Valley are formed of serpentinised gabbro, bedded sandstone and siltstone, volcanic breccia, and minor diorite (Williams, 1975; Turnbull, 2000).

3.2.1.3 Dun Mountain-Matai Terrane

The Dun Mountain-Matai Terrane is comprised of the Dun Mountain Ophiolite sequence (Landis, 1980), and weakly metamorphosed sedimentary rocks including hematitic siltstone. It occurs in a sliver running north-south and makes up the majority of the Eglinton River (East Branch) catchment. The peaks of the eastern mountains are formed of slightly older ultramafics (e.g. serpentinised gabbro and pyroxenite).

3.2.1.4 Caples Terrane

The Alisa and Livingston Mountain Ranges on the far west of the catchment are primarily composed of the sedimentary Early Jurassic to Cretaceous sandstone with minor mudstone and conglomerates (Graham and Mortimer, 1992; Turnbull, 2000).

3.2.2 Plate boundary tectonics

The Alpine Fault currently represents the primary structure of the Australian/Pacific Plate boundary in the South Island (Dykstra, 2012; Norris and Toy, 2014). The Fiordland region has a relatively low contemporary uplift rate (~0.5-1 mm a^{-1}; Kim and Sutherland, 2004) which is thought to be due to the predominantly strike-slip motion of the Alpine Fault in this area (Dykstra, 2012). The Alpine Fault is capable of significantly hazardous large (M_w >7.0) to great (M_w >8.0) earthquakes (Howarth et al., 2015). It has a mean recurrence time of ~330 years with the last great earthquake occurring in 1717 AD (Yetton, 2000; Rhoades and Van Dissen, 2003; Hancox and Perrin, 2009; Berryman et al., 2012; Robinson and Davies, 2013; Howarth et al., 2015).

Fiordland has experienced three earthquakes greater than M_w 7 and seven greater than M_w 6 over the last 150 years (Hancox et al., 2002) that have been correlated with large landslides and RA's. The probability of a large Alpine Fault earthquake in the next 50 years is considered to be as high as 45%, with potentially disastrous ground and slope damage (Hancox and Perrin, 2009) including the potential for major RA's and landsliding throughout the Fiordland region.

A number of (the now inactive) major faults running throughout the Eglinton Valley have previously played a significant role in the regions' geomorphology that can be seen in the rugged landscape today (Figure 3.2; Howarth et al., 2015). The faults include: the Eglinton Fault, which is predominantly buried under the modern floodplain of the Eglinton River West Branch and separates the Median Batholith from the Brooke Street Terrane (Williams, 1975; Turnbull, 2000), the Skelmorlie Fault (Grindley, 1958), and the Hollyford and Livingston Fault systems which once partition slipped away from the Alpine Fault (Campbell, 2005). The Hollyford Fault defines the eastern margin of the Brooke Street Terrane while the Livingston Fault marks the boundary between the Dun Mountain-Matai Terrane and the Caples Terrane (Williams, 1975).

3.3 Geomorphic processes and hazards - regional overview

The Southern Alps represent a particularly dynamic geomorphological setting with the central ranges experiencing uplift of ~5 mm a^{-1} (Kim and Sutherland, 2004; Korup, 2005; Beavan et al., 2010), and exceptionally high annual precipitation of up to 14 m a^{-1} (Henderson and Thompson, 1999). These components combine to stimulate a range of geomorphological processes including mass movement, glaciation, and fluvial erosion and deposition. As a consequence, the processes represent a significant challenge to geohazard management within this region. Seismic, mass

movement, and flood hazards pose risks to regional infrastructure, tourists, and the local population.

3.3.1 Mass movement history

The steep (35-65°) valley walls in Fiordland are vegetated with primarily silver and red beech (*Nothofagus menziessi* and *N. fusca* respectively; O'Donnell et al., 1999) up to 1,000 m.a.s.l., but are broken with many scars caused by shallow, small to large (10^2-10^5 m^3) mass movements of all types that, historically, have been triggered by intense rain events and moderate to large (M_W 6 to 7) earthquakes (Hancox et al., 2004; Hancox and Perrin, 2009; Hancox et al., 2013). Over 50 very large (10^6 - 10^7 m^3) to giant (>100 Mm^3) landslides have been identified in Fiordland, including the 300 Mm^3 Lake Gunn Landslide near the head of Eglinton Valley (Figure 3.3; Hancox et al., 2013).

Earthquakes over at least M_w 6 (and more commonly around M_w 9) are generally considered to be the primary trigger of such large mass movements in New Zealand (Hancox et al., 2002; Hancox et al., 2013). Lake Gunn Landslide has been dated with a minimum age of 7,630 years BP (Hancox et al., 2013) corresponding with a large Alpine Fault earthquake (Berryman et al., 2012). While the landslide would have undoubtedly blocked the Eglinton River (West Branch) for a period of time (Hancox et al., 2013), fluvial processes and retreat of the glaciers due to a warming climate (outlined in Section 3.3.2) have allowed the Eglinton River to erode a narrow gorge that carves its way through the hummocks and mounds of the post-glacial landslide debris, reaching it's current position in the valley.

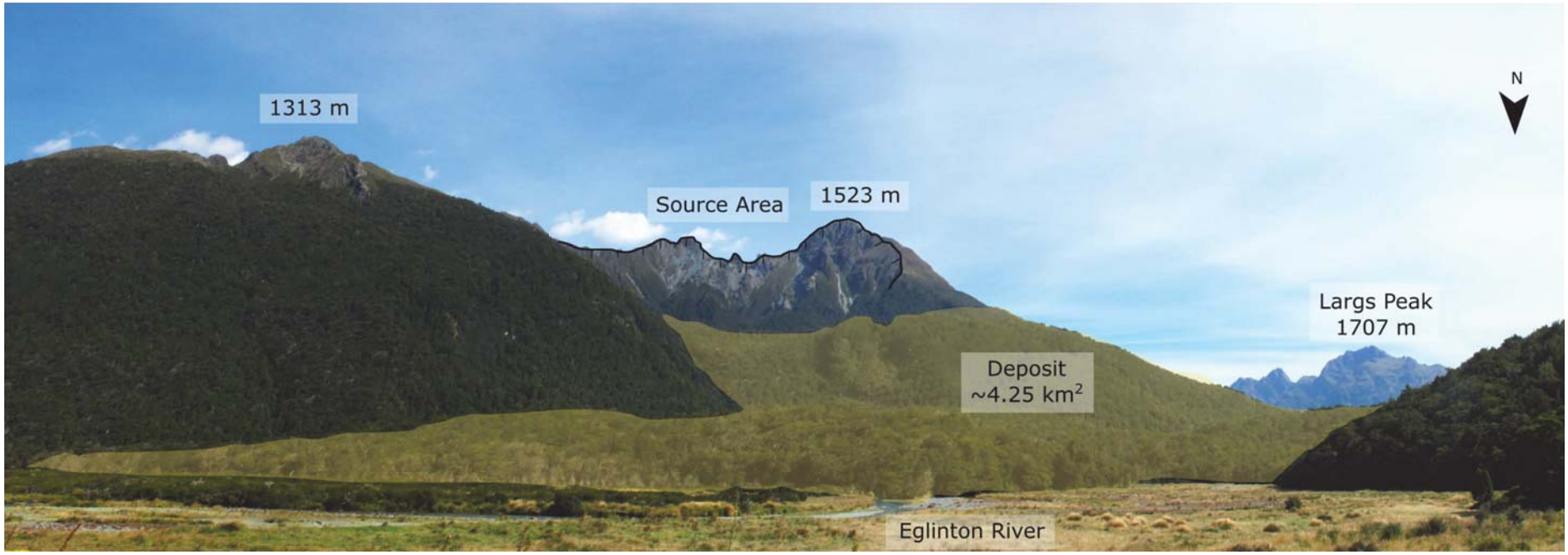

Figure 3.3: Annotated image looking SW towards the Lake Gunn Landslide depositional area with Eglinton Valley extending further southwards. The Eglinton River has since cut a winding channel through the debris.

3.3.2 Late-glacial history

As with many of the major valleys in Fiordland and the Southern Alps, Eglinton Valley has experienced extensive glacial modification during the LGM. The exact timing and extent of the glacial fluctuations within the valley is currently poorly known, though it can be inferred from glacial patterns in other parts of the region. The major valleys and lakes in the region were shaped by glacial erosion during previous ice ages, with the most recent glaciation ceasing between *c.* 11,500 and *c.* 14,000 years ago (Hancox and Perrin, 2009; Barrell, 2011).

3.3.2.1 The Last Glacial Maximum

In the northern hemisphere (NH), where glacial chronologies are well supported, the LGM is considered to have begun 32-28 ka (Rother et al., 2015). Most NH ice sheets are thought to have reached their LGM extent around 25-24 ka with subsequent warming and retreat occurring from about 20 ka (Vandergoes et al., 2005; Clark et al., 2009; Dykstra, 2012). The southern hemisphere (SH) is considered to have reached its LGM extent up to 6-8 kyrs earlier (Almond et al., 2001; Suggate and Almond, 2005; Vandergoes et al., 2005; Sutherland et al., 2007; Rother et al., 2015). At this time the glaciers would have flowed out beyond the current coastline on the West Coast, and expanded into the eastern alpine forelands. During the LGM in eastern Fiordland, the glaciers drained onto the inland basins and the ice that flowed through Eglinton Valley would have reached to the township of Manapouri (Figure 2.6; Williams, 1996; Barrell, 2011).

The culmination of the SH LGM is considered to have started c. 18 kya (Suggate and Almond, 2005; Schaefer et al., 2006; Clark et al., 2009; Williams et al., 2009; Barrell, 2011; Vandergoes et al., 2013). Since then, the climate has experienced a number of warmer and cooler periods till temperatures became relatively stable from 6.5 kya to present (Alloway et al., 2007). During the Holocene, interglacial conditions prevailed with two phases of warmth between 11.6-10.8 ka (following the Antarctic Cold Reversal) and 6.8-6.5 ka with one cooler period between, and relatively stable temperatures to present. These warmer and cooler periods prompted vegetation expansion and recession (Alloway et al., 2007), and would have also prompted glacier recession and expansion, shaping the valleys and weakening the geological characteristics of the Eglinton Valley over time.

3.3.2.2 Te Anau Glacier

The Eglinton Valley once held ice contributing to the Te Anau Glacier, one of the largest valley glaciers to form in the Southern Alps (Golledge et al., 2012; Williams et al., 2015). At its largest, *c.* 40 kya, the Te Anau Glacier had accumulated ~600 m of ice above the present Lake Te Anau level (currently at 203 m.a.s.l.) and extended

across the ~20 km wide valley (Williams et al., 2015). The down-valley extent, based on moraine deposits, extended beyond the current Te Anau township to the settlement of Manapouri (Figure 3.4; Suggate, 1990; Williams, 1996; Barrell, 2011). Aurora Cave on the western side of Lake Te Anau holds a record of ice expansion and retreat by way of speleothem growth from as early as MIS 4 (*c.* 71 kya; Williams, 1996) with dates being more refined as dating techniques are improved (Williams et al., 2015). Following the LGM, most of the South Island glaciers, including the Te Anau Glacier, began a rapid retreat leaving behind debris and allowing some valleys to fill with lakes (Suggate and Almond, 2005).

Up-valley of Aurora Cave there is very little known about the retreat history of the Te Anau Glacier. The hummocks found at Knobs Flat (Figure 3.5) are considered to be glacial kames based on their morphological expression (Hayward and Kenny, 1998), however, there is no age control on these features. There is currently no glacial activity within the valley or surrounding tributaries. In many parts of the central Southern Alps there is an extremely detailed chronology of the glacial advances and retreats (see Barrell, 2011, and references therein) as there are many accessible, well-preserved moraine sequences. The same detailed dates do not exist in the Te Anau Valley, despite the moraine sequences bordering the major lakes of the region being mapped (Barrell, 2011).

Figure 3.4: The Eglinton Valley study area (inside white box) and LGM extent of glacial ice outlined in black. Ice extent is adapted from Barrell (2011).

Figure 3.5: Annotated image of the Earl Mountains forming the western boundary of Eglinton Valley. Yellow lines outline the Knobs Flat hummocks that were mapped during field work and are described in Section 5.2.

3.4 Geomorphology of Eglinton Valley

Eglinton Valley is a ~40 km long deglaciated valley with partly-vegetated bedrock walls extending above 2,000 m.a.s.l. The head of the valley is marked by The Divide, a low (532 m.a.s.l.) pass where SH 94 crosses into the Hollyford Valley. Down-valley from The Divide lies Lake Fergus, with Lake Gunn further south. The two lakes are separated by numerous debris flows from the steep western slopes and Lake Gunn is held in place by the large Lake Gunn Landslide (Turnbull, 2000) and two active alluvial fans (Hancox et al., 2013). The entire valley is flanked on the west by the very steep Earl Mountains including Consolation Peak (1,859 m), Disappearing Peaks (1,802 m), Largs Peak (1,707 m), and Mt Eglinton (1,854 m; Figure 3.6). The slightly less precipitous Livingstone Mountains to the east of the valley include David Peaks (2,097 m), Moffat Peak (2,085 m), and Countess Peak (1,829 m; Figure 3.7). The sediment generated from these peaks is transported via scree slopes, alluvial fans, rock falls, and RA's and makes its way into the valley floor below, leaving deposits to be further reworked by fluvial processes.

The Eglinton River (West Branch; and referred to as 'Eglinton River' from herein) is a wandering, gravel-bed river that follows the long-valley trend of the Eglinton Fault through the valley. In 1935, SH 94 was completed, allowing access for hunters. In 1952, Fiordland was designated as a National Park, therefore Eglinton Valley has had little human disturbance except for recreational hunting, maintenance on SH 94, and pest control.

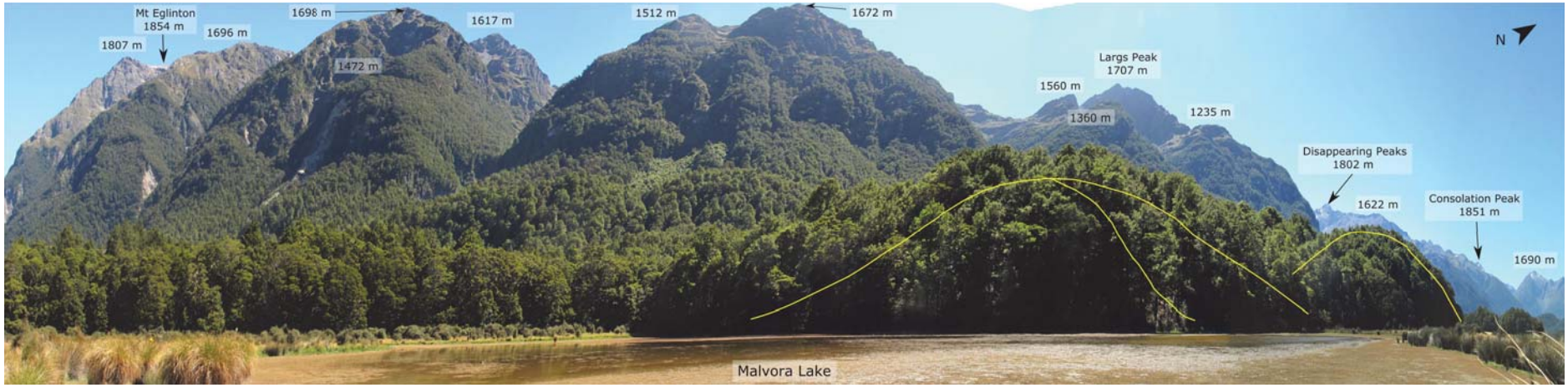

Figure 3.6: Annotated image of the steep Earl Mountains viewed from Malvora Lake. Yellow lines outline two hummocks that were mapped during field work and are described in Section 5.2.

Figure 3.7: Annotated image of the Livingston Mountains viewed from Malvora Lake. Dotted blue lines indicate the tributaries adding water and sediment to the Eglinton River. Knobs Flat Campground is on the far left of the image.

3.5 Site description

An easily-accessible 18 km stretch of Eglinton Valley was chosen to study; from the lower end of Lake Gunn Landslide in the north, to the Mirror Lakes in the south and just above the convergence between the East and West Eglinton Rivers. The floor of Eglinton Valley is currently a wide aggradation floodplain with ≤15 m high conspicuous hummocks dotted throughout the valley from Lake Gunn to the Mirror Lakes. Numerous swampy areas and small, shallow, lakes are scattered throughout the modern floodplain with some also occurring within the trees of the vegetated floodplain.

A number of large, partially-active alluvial fans enter the valley from the eastern streams including the Knobs Flat Fan, Smithys Creek Fan, and Wesney Creek Fan (names given for the purpose of this thesis; Figure 3.8), with a number of these being truncated by the Eglinton River (e.g. Figure 3.9). On the steeper, western side of the valley, the alluvial fans are much more active, identified by fresh clasts widespread throughout the tall vegetation (e.g. the two un-named streams adjacent Deer Flat campground; Figure 3.10) with little-to-no undergrowth present.

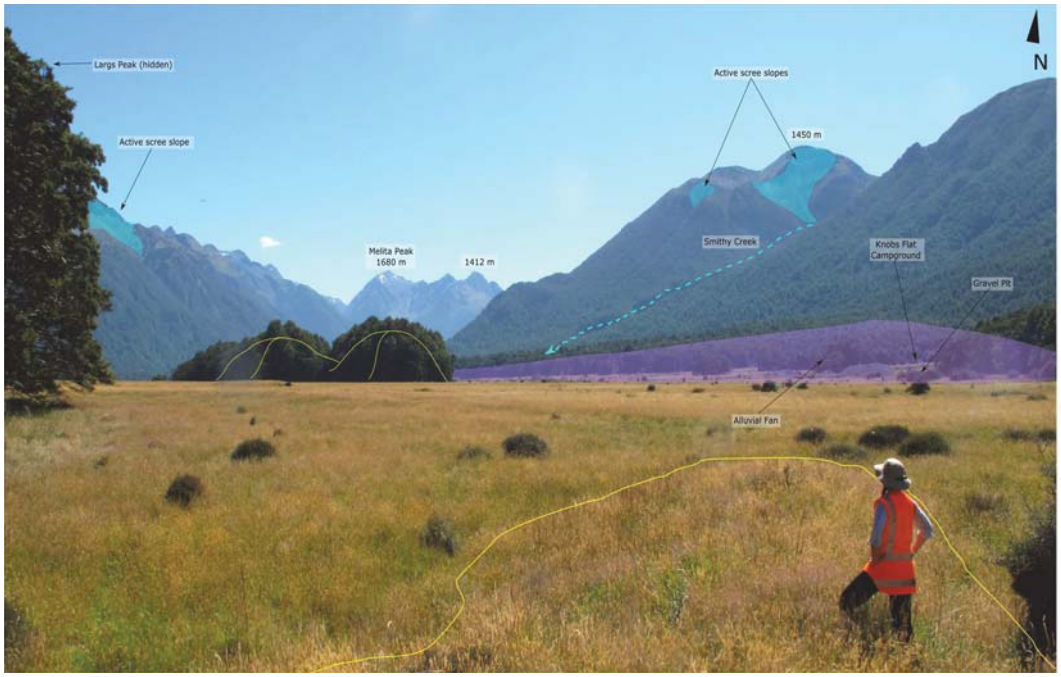

Figure 3.8: Annotated image looking up Eglinton Valley from Malvora Lake. Yellow lines generally outline the Lower Knobs Flat hummocks that were mapped during field work and are described in Section 5.2. The purple fill shows the relative low angle and extent of Knobs Flat Fan. Photo credit: S. McColl.

Figure 3.9: Image of a clear section of the Knobs Flat Fan that has been truncated by the Eglinton River. This shows distinct layers of silt, sand, and cobbles indicating periods of quiescence and more active sedimentation. This section was located just off the right of Figure 3.8. Photo credit: A. Clement.

Figure 3.10: Image of an active fan adjacent to Deer Flat campground on the steeper, western side of Eglinton Valley. Rock hammer shown for scale beside hand-specimen clasts of representative lithologies.

3.6 Previous work

The Fiordland region contains possibly the highest concentration of very large and giant (>100 Mm^3) mass movements in New Zealand, with at least 50 post-glacial prehistoric landslides of these sizes identified proximal to the Alpine Fault and the PSZ (Hancox et al., 2013). However, Lake Gunn Landslide is the only major mass movement in Eglinton Valley that has been mapped and dated. This was undertaken by Hancox et al., (2013) who mapped the deposit area and used radiocarbon dating from three sites within the deposit to devise a minimum age of 7,630 ±52 years BP (note: for simplicity this thesis uses the notation ~7.6 kyrs BP). This has been tentatively correlated with a large earthquake either on the nearby Alpine Fault or the PSZ. They also noted that active alluvial fans at the outlet end of Lake Gunn appear to be constricting the lake and holding it in place. No other alluvial fans in the valley were mapped during their study.

Another study has examined Eglinton Bog sediments to reconstruct the mid- to late-Holocene climatic history of the area. This study identified there may be glacial moraine sequences at Eglinton Flat (Valkengoed, 2011) however no further work was undertaken to confirm this. Other major work in the valley has primarily focused on

mapping the underlying geology, with field mapping being carried out by Grindley (1958) and Williams (1975) and collated by Turnbull (2000). The hummocky topography at Knobs Flat is currently protected as 'glacial kames' in the New Zealand Geopreservation Inventory, however, McColl and Davies (2011) suggested that these hummocks may have been incorrectly interpreted as being glacial in origin. This suggestion was further supported by some preliminary observations of angular sediments found within exposures, that are were deemed more consistent with a mass movement origin (S. McColl, personal communication, June, 2015).

Chapter 4

Methods

4.1 Introduction

The range of methods used in this study aim to distinguish between the different depositional processes responsible for the valley floor deposits in the Eglinton Valley that have been formed during the Late Quaternary. This methodology chapter can be broken into four main sections:

1. Permits and field-site reconnaissance,
2. Data types and collection methods,
3. Sedimentology, and
4. Terrestrial Cosmogenic Nuclide Dating (TCND).

4.2 Permits and reconnaissance

The study area is located entirely within Fiordland National Park, which is managed by the Department of Conservation (DOC). National Parks are protected wilderness areas that host a wide range of New Zealand's distinctive landscapes, ecological systems, and historic features. Public access is granted via strict walking tracks, roads, and hut or camping accommodation. Native flora and fauna are protected, with active monitoring programs gauging many native species. As a result of the conservation values within the study area, a research and collection permit was required from the Minister of Conservation before field work could commence.

A Research and Collection Permit (No. 40188-GEO) was granted for field work within Eglinton Valley over nine days in January-February, 2015, and three days in February 2016. The permit allowed collection of bedrock, landslide deposit samples, and sediment samples. Special conditions of the permit included avoiding all wildlife, thorough cleaning of all equipment to prevent the spread of didymo (*Didymosphenia*

geminata) and other freshwater pests, and final research results be made available to DOC.

4.2.1 Preliminary field investigations

Reconnaissance and preliminary field investigations within the Eglinton Valley study area (Figure 4.1) focused on identifying accessible geomorphic deposits for clast sample collection, as well as visiting known landslide deposits (e.g. Lake Gunn Landslide), and determining possible mass movement source areas as identified on aerial photographs. One day of ground-based investigation included viewing 'The Hillocks', located in the nearby Dart Valley, which is a hummocky landform that has recently been reinterpreted to be RA origin (McColl and Davies, 2011).

Figure 4.1: Field reconnaissance photos: A) Eglinton River. B) Camp site at Knobs Flat. C) View north up Eglinton Valley. D) Knobs Flat. E) 'The Hillocks' in Dart Valley. F) Crossing Eglinton River at Deer Flat. Photos by S. McColl and author.

4.3 Data types and collection methods

4.3.1 GIS mapping

Data was compiled in a geospatial information system (GIS; ArcMAP): Land Information New Zealand (LINZ) data service geospatial layers and DEM's; GNS Science geological data (QMAP); and field-gathered GPS data. Field geomorphological maps were digitized and incorporated into the GIS. The following geospatial datasets were compiled to produce geomorphological maps of the valley:

- LINZ (2014) data:
  - Southland 0.75 m Rural Aerial Photos (2005-2011),
  - River Environment Classification Catchment Order 2 Polygons (2010),
  - River Environment Classification Catchment Order 3 Polygons (2010),
  - River Environment Classification Catchment Order 5 Polygons (2010),
  - NZ Terrain Relief (Topo, 1:50 k),
  - NZ Coastlines (Topo, 1:50 k),
  - NZ Contours Polygons (Topo, 1:50 k),
  - NZ 8 m Digital Elevation Model (DEM; 2012),
  - NZ River Polygons (Topo, 1:50 k),
  - NZ River Centre Lines Polygons (Topo, 1:50 k),
  - NZ Lake Polygons (Topo, 1:50 k), and
  - NZ Road Centre Lines (Electoral, 2016).
- GNS Science 1:250 000 geological map version 1-2 (QMAP; Turnbull, 2000):
  - Geological units,
  - Geological structures: active and inactive faults, and
  - Landslides.
- GPS track data, and
- Field-site waypoints (e.g. TCND locations, microsediment sample sites, and clast analysis sites).

4.3.2 Ground Penetrating Radar

The surface expression of landforms on the valley floor may only present the 'tip of the iceberg'. Hummocky topography that was potentially deposited hundreds to thousands of years ago may have been partially buried by modern sediments, thus giving a false representation of actual size and overall shape and extent. Ground

Penetrating Radar (GPR) is a non-invasive geotechnical tool used to determine subsurface geomorphic features and view soil and rock conditions in high resolution (Davis and Annan, 1989). Areas of application vary greatly; it has been used to successfully map water depth in lakes, bedrock depth, and detect buried pipes and tunnels (Davis and Annan, 1989). More recently, GPR has been successfully used to trace buried RA deposits within a glacier accumulation zone (Dunning et al., 2015).

In this study two GPR lines were run: a ~280 m, 100 MH_z line in a straight line over three hummocks at Knobs Flat (Figure 4.2), and a second ~60 m, 50 MH_z line was run between two hummocks at Deer Flat (Figure 4.3).

Figure 4.2: Location of the ~280 m GPR line (red) across the hummocky deposits (yellow) at Knobs Flat. *Note:* The GPR line continues to the left of the image for another ~30 m.

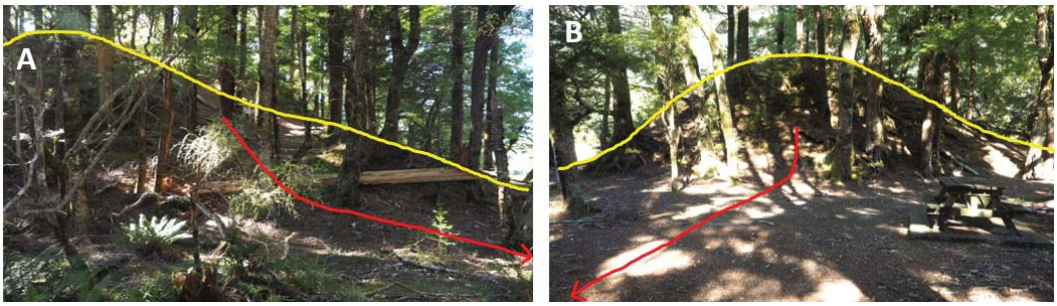

Figure 4.3: General location of the ~60 m GPR line (red) between two hummocks (yellow) at Deer Flat: A) Western hummock that the GPR line started on, and B) the eastern hummock where the GPR line ended. Eglinton river flows from right to left behind these hummocks. *Note:* The GPR line was straight, however the trees and sunlight did not allow for a more accurate image.

4.3.3 Terrestrial Cosmogenic Nuclide sample collection

In order to assess the age of key landforms in Eglinton Valley, samples were collected and processed for TCND. A thick cover of vegetation and soil meant very few boulders were visible and suitable for sampling, and as a result, only six suitable samples were identified within the study area. Only five of these were be collected (Figure 4.4), due to a swollen river preventing access to be regained at one site.

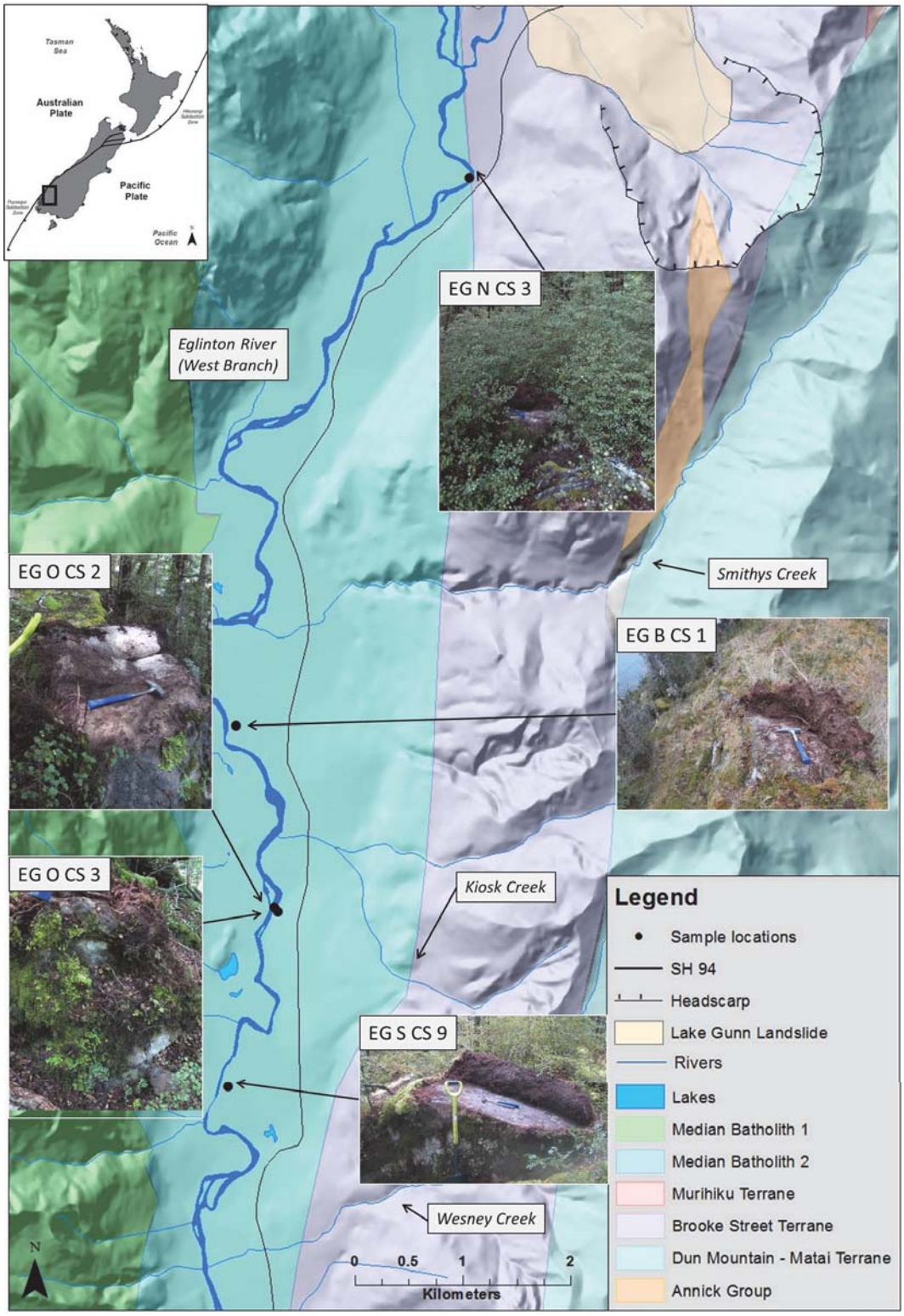

Figure 4.4: Location map of the five cosmogenic samples collected for analysis. Inset photos show boulders selected for TCND. Rock hammer for scale. Note that EG O CS 2 and EG O CS 3 were both located no more than 1 m below the crest of the hummocks. Basemap shows simplified basement geology in the valley (adapted from Turnbull, 2000).

All sample sites were chosen based on a range of criteria:

- Exposed boulders on or near the highest points of deposits were selected to reduce the chances of overturning since deposition and also to minimise the soil formation.
- Boulders at least 1 m diameter were selected as these are most likely to be *in situ*.
- Surface areas with visible fracturing were avoided to reduce contamination of meteoric ^{10}Be.
- Horizontal (or near-horizontal) flat surfaces were selected, while staying a minimum of 15 cm away from boulder edges to reduce complications due to cosmic-ray penetration from multiple angles.

At each of the boulder-sample sites, specific information was recorded:

1. Time, date, and weather,
2. GPS latitude, longitude, and waypoint reference,
3. Approximate height of the boulder (above the floodplain),
4. Approximate boulder size,
5. Average sample size (length, width, and depth),
6. Topographic shielding data (compass bearing and inclination for each horizon break point),
7. Depth of any moss cover,
8. Location sketch, and
9. Notes about the geomorphic significance of the site and general weathering of the boulder.

Approximately 2 kg of rock chips were collected from the upper 2-5 cm of the five exposed boulder surfaces from four hummocks (Figure 4.4) using a cordless 18V DeWALT angle grinder with a diamond impregnated blade along with a chisel and rubber mallet (Figure 4.5). A hand-held Garmin eTrex Vista HCX GPS unit was used to record latitude and longitude. GPS elevations were not used due to the inadequate accuracy of the GPS unit operating in a confined valley and often in vegetated areas. Instead, elevations were estimated from a topographic map.

Figure 4.5: Rock chip collection for TCND using an angle grinder. Photo by S. McColl.

4.4 Sedimentology

The morphology of sedimentary particles is widely accepted to be a key source of information for determining transport and depositional environments within a system (Powers, 1953; Boulton, 1978; Bridgland, 1986; Benn and Ballantyne, 1993). A number of early studies, including Chinn (1975), recognised there was a distinct difference between sub-micron RA sediment and glacial sediment characteristics. This has been further tested and agreed by Reznichenko et al., (2012a) so the same method was applied here.

This section is divided into two main subsections:

1. Hand-specimen sampling and analysis (Subsection 4.4.1): 30 hand-specimen sized clasts were collected from 31 sites and four rivers for provenance analysis (*sensu* Wandres et al., 2004) and determining roundness to deduce possible transport processes and distances (Powers, 1953).

2. Microsediment sampling and analysis (Subsection 4.4.3): Fourteen microsediment samples (i.e. sand and silt) were collected from within ten hummocks in Eglinton Valley and examined using a Scanning Electron Microscope (SEM).

4.4.1 Hand-specimen field sampling

The geology of the valley is a useful tool for provenance analysis of the hummocky topography. Clasts from within the hummocks themselves can be matched with the geology throughout the valley to determine where they originated. Sampling of 30 random clasts was undertaken in Eglinton River (West Branch), three accessible tributaries, and within 31 hummocky deposits (Figures 4.6 and 4.7). The size range for sampling was kept to between 20-125 mm (long axis) as within this range the roundness is considered to be independent of size (Shakesby, 1989; Benn and Ballantyne, 1994). Where possible, clasts were collected from the upper-most parts of the hummocks and retrieved from spade-dug sections to reduce the chance of collecting clasts that may have been deposited subsequent to hummock formation. In many locations clasts were exposed beneath uprooted trees, allowing easy sampling. The river clasts were taken from within the active channel for an accurate representation of the current sediment transport and deposition regime. In the lab the clasts were individually hand-scrubbed to remove soil prior to analysis (Figure 4.8).

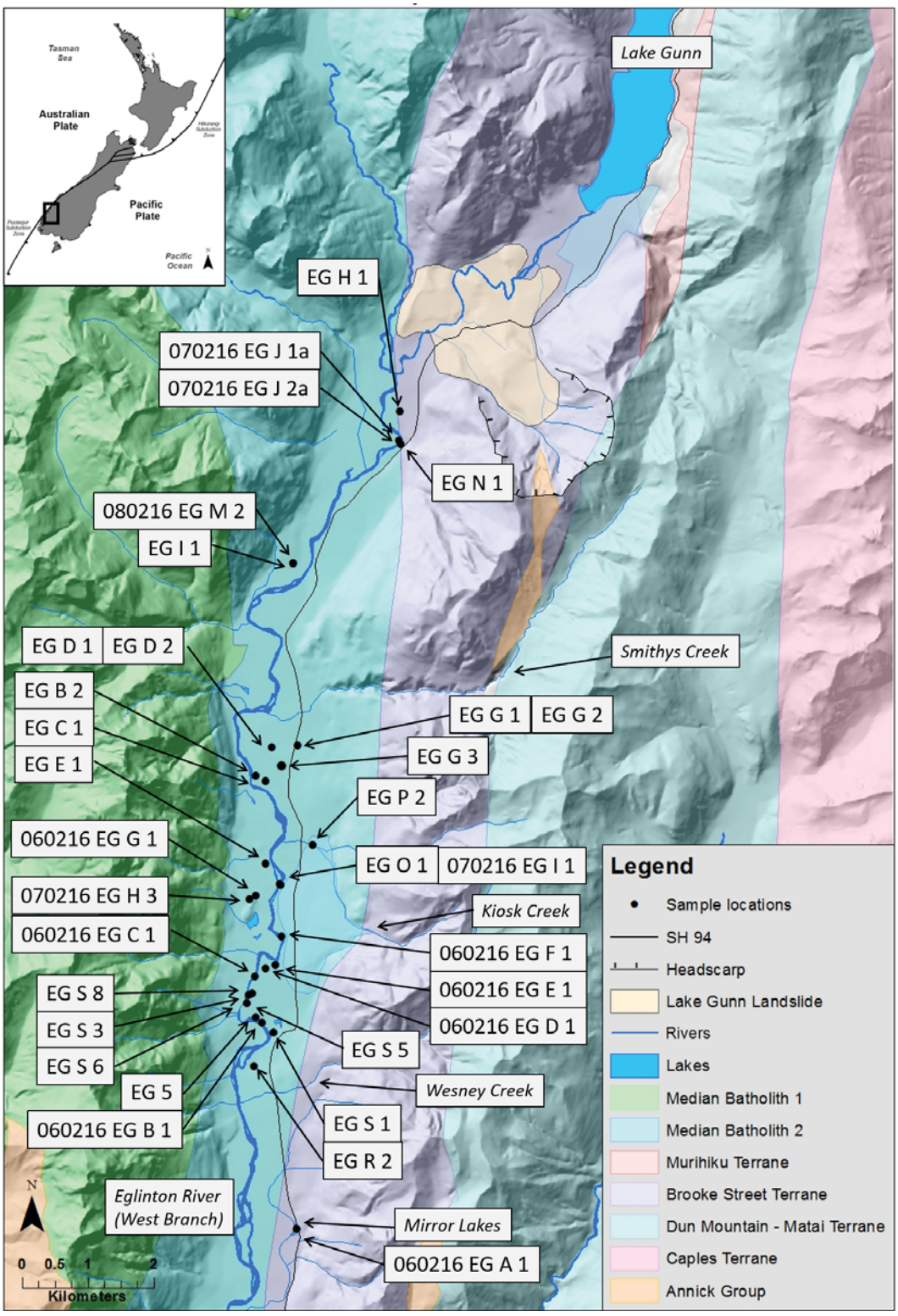

Figure 4.6: Location map of the 31 sites and four rivers: Eglinton River, Smithys Creek, Kiosk Creek, and Wesney Creek, where 30 clasts were collected for roundness measurements and provenance analysis.

Figure 4.7: Field sampling: A) Clast sampling at Wesney Creek. B) Clast sampling within a Middle Deer Flat hummock. Photos by A. Clement and S. McColl respectively.

Figure 4.8: Clast scrubbing and rock-type identification for provenance analysis. Sample shown is from Middle Deer Flat.

4.4.2 Hand-specimen lab analysis

Reconstruction of potential transport pathways for pebbles, cobbles, and boulders can be informed by analysis of the clast roundness, lithology, and inherited features such as striations (Wadell, 1932; Powers, 1953; Barrett, 1980; Hambrey and Ehrmann, 2004).

4.4.2.1 Clast roundness method

Clast roundness was assessed visually by comparing each collected clast with a set of standard images (Figure 4.9; Powers, 1953) and descriptive criteria (Table 4.1) to avoid biased measurements. The Powers (1953) roundness index was chosen as it offers a simple numerical measurement of roundness where the sample is not normally distributed. These results are presented as histograms (in Section 5.4) and the angularity index (referred to as 'AI' in this study to avoid confusion with 'RA' as it is commonly referred to; the percent of angular and very angular clasts within the sample) was calculated. The AI is a quantitative way to identify samples that have been passively transported on a glacier or deposited by a RA (high AI), or, clasts that have been actively transported within/beneath a glacier or fluvially (low AI; Benn and Ballantyne, 1994; Hambrey and Ehrmann, 2004).

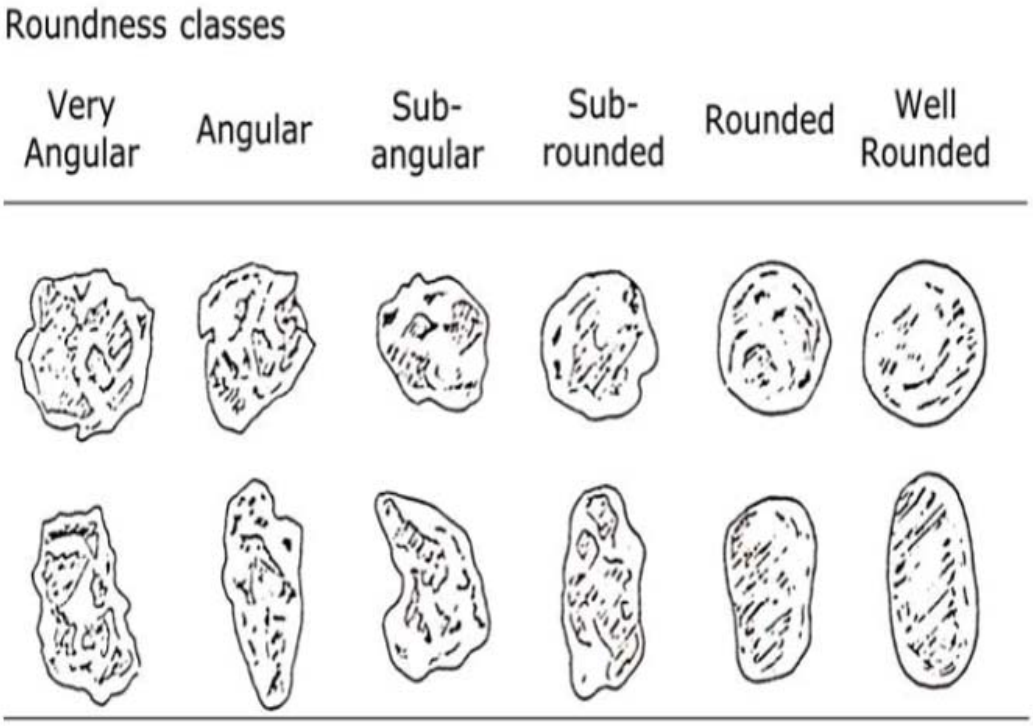

Figure 4.9: Chart for visually estimating roundness and sphericity of clasts (based on Powers, 1953).

Table 4.1: Descriptive criteria for clast roundness categories (Benn, 2004).

Class	Description
Very Angular (VA)	Edges and faces unworn; sharp, delicate protuberances
Angular (A)	Edges and faces unworn
Sub Angular (SA)	Faces unworn, edges worn
Sub Rounded (SR)	Edges and faces worn but clearly distinguishable
Rounded (R)	Edges and faces worn but barely distinguishable
Well Rounded (WR)	No edges or faces distinguishable

4.4.2.2 Provenance analysis method

Provenance analysis was used to identify where the clasts potentially originated from; whether they have come from tributary valleys or valley walls adjacent to the hummocks, or if they may have a wider catchment origin. This was informed by visually assessing the overall lithology of clasts from within the hummocks and rivers while taking into account the calculated AI. The clasts were then compared with previous geological studies from the valley including Grindley (1958), Williams (1978), and Turnbull (2000). Grindley and Williams compiled concise descriptions of the lithologies found throughout Eglinton Valley so were used to confirm the provenance

of all the clasts. The naming conventions in both Grindley and Williams have been revised in Turnbull, and the revised names are used in this study.

4.4.3 Microsediment SEM examination preparation

Examination of sediment in the form of whole grains and polished grain cross-sections under SEM is a relatively novel approach for examining and distinguishing the microsediment characteristics of glacial (low strain) versus RA (high strain) processes (Reznichenko, 2012). Fourteen samples of the fine-grained matrix were collected from within ten hummocks throughout Eglinton Valley (Figure 4.10). Three samples (I, J, and K) were collected from within an exposed section of the Lake Gunn Landslide deposit (Figure 4.11) to see if agglomerates were present or not. An example of the deposits chosen is shown in Figure 4.12 where Samples E, F, G, and N were collected. Following Reznichenko's technique, a number of steps were taken to analyse the microsediment:

1. Sediment samples were sieved to 63 µm and 1000 µm (Figure 4.13A).
2. Samples were subjected to ultrasonic bath treatment for 11 minutes.
3. 30 individual grains were randomly selected from each sample for whole grain SEM analysis of morphology.
4. Approximately 200 grains from each sample were resin-mounted to assess internal grain morphology under SEM.

The collection and lab method was replicated from Reznichenko's novel technique, however, she isolated individual quartz grains (with a Mohs hardness of 7) as they do not weather readily. Within Eglinton Valley, quartz is extremely rare, so every grain was used in the identification resulting in a mixture of mineralogies. As this may have adversely affected the results, care was taken to remove any weathered (to clay) particles and use minerals of relatively high hardness (to reduce the potential effect of weathering features), such as olivines (Moh 6.5 - 7), epidotes (Moh 6 - 7), pyroxenes (Moh 5 - 6.5), and amphiboles (Moh 5-6).

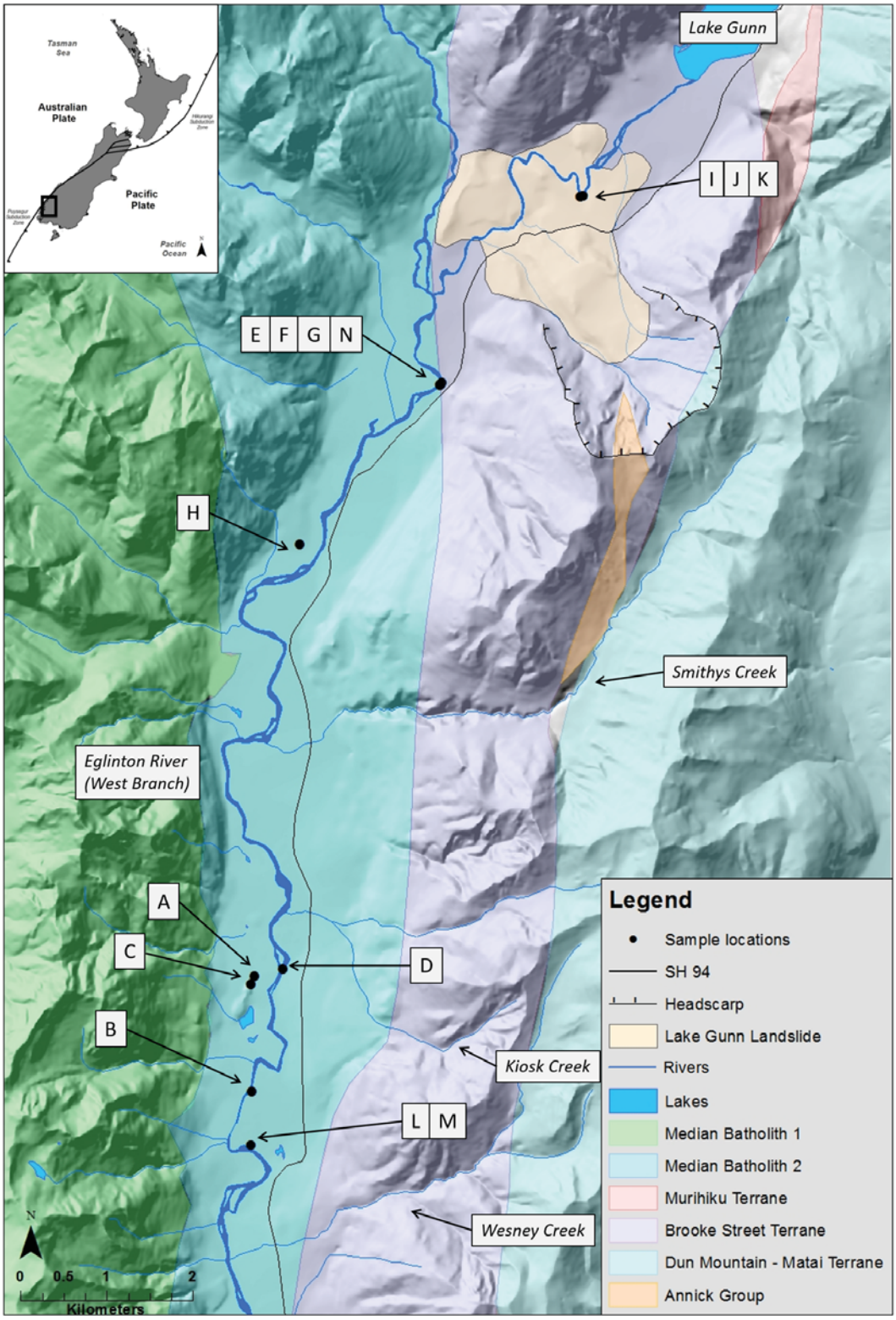

Figure 4.10: Location map of microsediment samples A-N. Geological basemap adapted from (Turnbull, 2000).

Figure 4.11: Sample locations of microsediment from within an exposed section of the Lake Gunn Landslide deposit. Sam for scale, though he is still ~50 m away from the base of the outcrop.

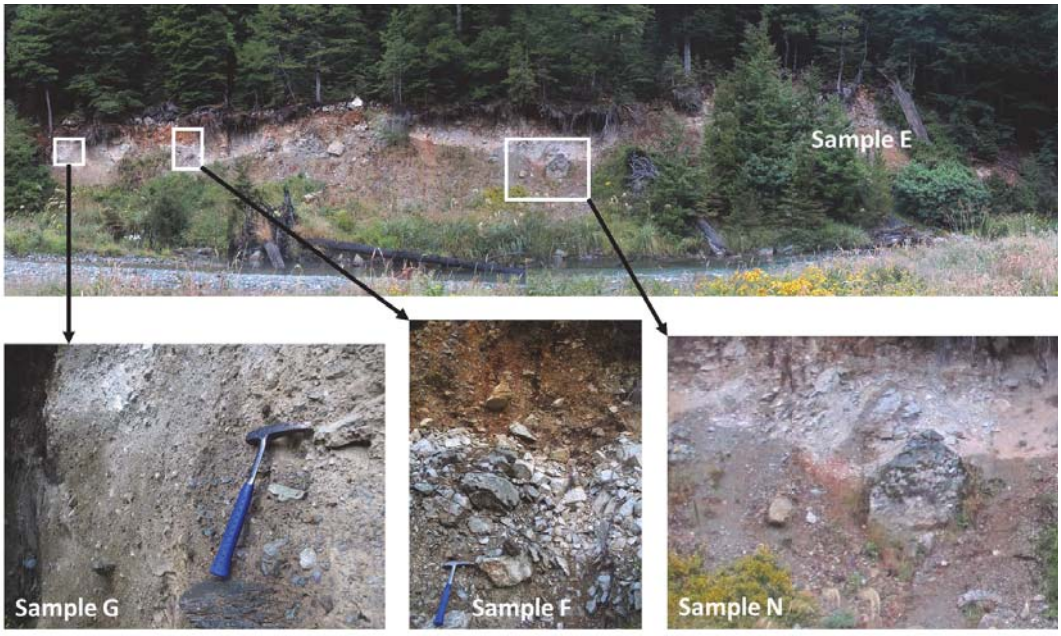

Figure 4.12: Stitched panorama and close-up images of the Eglinton Flat site where microsediment Samples E, F, G, and N were collected.

Figure 4.13: SEM preparation: A) Stacked sieves of 63 µm and 1000 µm. B) Sieved fraction with beakers containing sediment post-ultrasonic treatment of 1 minute (left beaker) and 10 minutes (right beaker).

Under stereomicroscope examination, the sieved samples appeared to be coated in sub-micron grains with very little clean faces or edges. In an attempt to disaggregate these sediments, they were gently rinsed with deionised (DI) water and subjected to an ultrasonic bath for 1 minute to check for any changes, then a further 10 minutes as no changes were observed (Figure 4.13B; *sensu* Reznichenko, 2012). Some samples still appeared to be coated in sub-micron-sized grains after the 11 minutes, however, this was also found in Reznichenko's study so the next steps were carried out instead of further ultrasonic treatment.

4.4.3.1 Whole grains

To view the overall grain morphology and features, 30 coarse (~800 µm - ~1000 µm) grains from each sample were randomly selected by shifting the tray under a microscope and selecting the centre-most grain then repeating 30 times. Each grain was stuck with double-sided tape to custom SEM stubs for analysis of overall grain morphology. The imaging was undertaken by lab technicians in the microscope laboratory at Massey University, using their own procedures.

4.4.3.2 Polished grain cross-sections

To analyse the internal structure (i.e. whether the grains were whole or 'agglomerated') of individual grains they needed to be mounted, cut in half, polished, and finally 30 individual cross-sections photographed by the lab technicians in the microscope laboratory (except samples L-N which only had 6 images as they were originally only going to be used as test samples but later added to the study).
For this process, a two-component epoxy (EpoTek) resin was made. Approximately 200 grains were tipped randomly into mounts made of sawn-off bottle lids stuck

with double-sided tape onto glass slides (Figure 4.14A-B). The resin was carefully poured over to cover the grains, then left to harden for 48 hours (Figure 4.14C). The lids were removed with a saw and the same saw used to remove ~1-1.5 mm of the resin/sediment mix to expose the internal structure of the grains. The surface was hand-polished using a 400, 600, and 1000 silicone carbide grit for 5 minutes on each grit. The ground surface was then polished using a Buehler Minimet 1000 and MetiDi Ultra Diamond Paste for 1.5 hours (1 hour at 6 µm and 30 minutes at 1 µm; Figure 4.14D-E). Imaging was also undertaken by lab technicians in the microscope laboratory at Massey University, using their own procedures.

Figure 4.14: Preparation stages for cross-section SEM analysis. A) Sawn-off bottle lids with double-sided tape on glass slides B) Dry samples inside mounts. C) Resin-filled mounts left to harden. D) Glass slide with lid removed and diamond paste being applied. E) Buehler Minimet 1000 polisher.

4.5 TCND

4.5.1 Terrestrial Cosmogenic Nuclide sample preparation overview

The following sample preparation was conducted to remove the minerals not suitable for analysis and to transform the usable samples into a form suitable for TCND. The five samples collected from large boulders were first analysed for mineralogy and degree of weathering by preparing thin-sections. The rest of each sample then hand-washed and subjected to ultrasonic treatment to remove any organic matter and soil, oven-dried for 24 hours, and crushed using a Fritsch pulverisette at Massey University. Quartz and pyroxene minerals were then magnetically separated for isotopic analysis in the purpose-built laboratories at Victoria University of Wellington (VUW). Two TCN techniques were attempted:

1. The use of fine-grained quartz for ^{10}Be dating in New Zealand (a novel technique), and
2. Extraction of ^{10}Be from pyroxene minerals for dating (an emerging technique).

4.5.2 Thin-section preparation

To determine the mineralogy of the samples, thin-sections were made. Boulder samples were cut into c. 1 cm thick blocks to fit 27x46 mm petrographic slides using a rock saw. A coarse (200 grit) silicone carbide grit was used to roughen one surface of the petrographic slides. A 400 grit was used to smooth the basal surface of each sample block before EpoTek was used to glue the pre-roughened samples to the roughened glass slide. After 24 hours under pressure the blocks were cut close to the slide (~500 µm) and progressively finer grits (400, 600, and 1000 grit) were used to grind the thin-section to ~32 µm (Figure 4.15).

Figure 4.15: Preparation stages of each thin-section from clast to sawn rock to mounted and ground sample on a glass slide.

The five thin sections (EG B CS 1, EG N CS 3, EG O CS 2, EG O CS 3, and EG S CS 9) were observed with a Nikon Eclipse E600 POL microscope fitted with a Nikon DS-U1 digital camera and the images were analysed using NIS Elements with default settings (Figures 4.16-4.21). All except sample EG N CS 3 (which had ~5% micro-quartz) were extremely quartz-poor due to their mafic origin, therefore, a novel method of TCND was chosen to utilise the mafic mineral pyroxene. This involves measuring ^{10}Be in the pyroxene following a technique adapted from Blard et al., (2008) and Collins (2015).

The pyroxene constituent of each sample ranged from 5% - 80%. Plagioclase was the most abundant mineral forming the majority of the groundmass with proportions up to ~70%, while chlorite formed up to ~30% of each sample. Other accessory minerals included olivine, phrenite, epidote, mica, pyrite, and magnetite. The degree of weathering was relatively high in all samples, with many plagioclase minerals altering to clays and iron-staining occurring along grain boundaries (particularly visible in Figure 4.17).

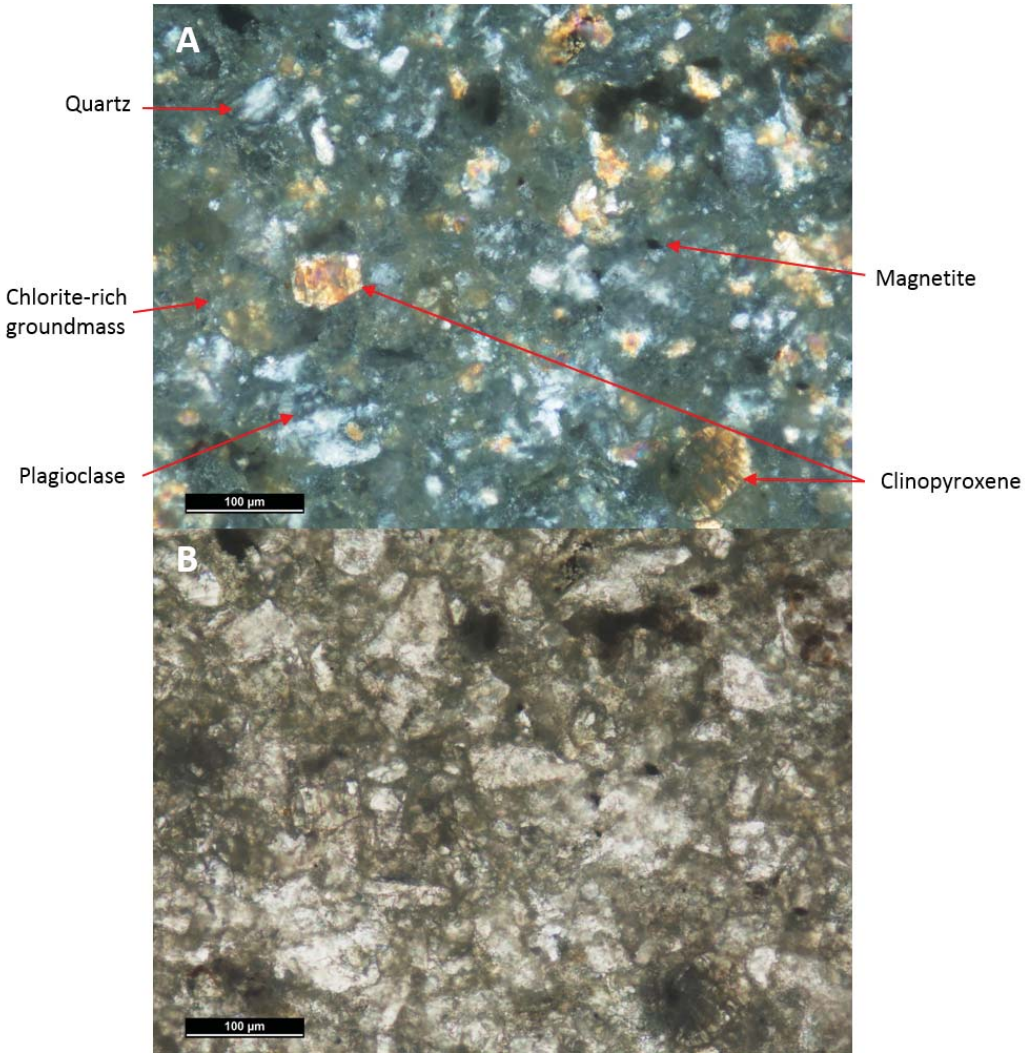

Figure 4.16: Boulder sample EG B CS 1 in cross polarised light (A), and plane polarised light (B). Note this sample is very weathered giving it a mottled and soft appearance.

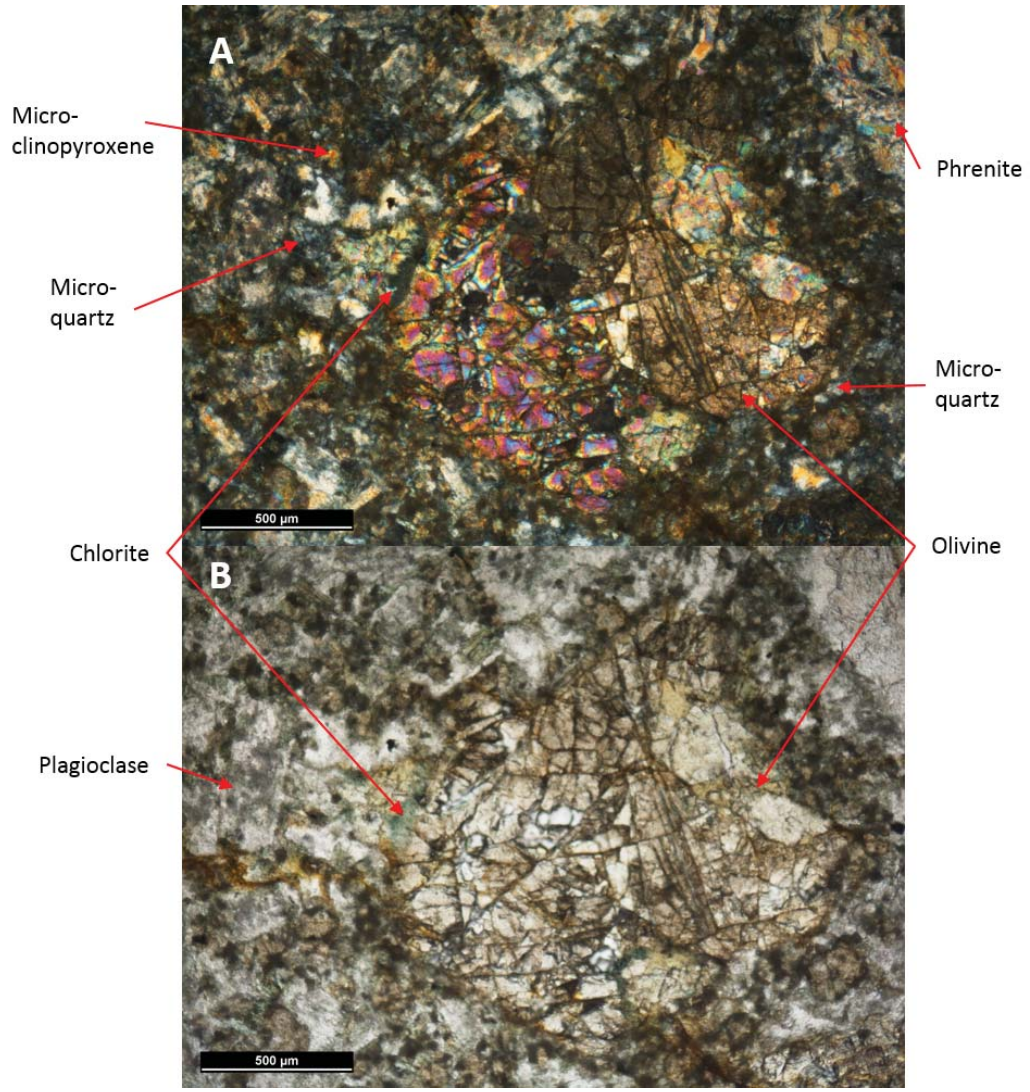

Figure 4.17: Boulder sample EG N CS 3 in cross polarised light (A), and plane polarised light (B). Note the heavy iron staining along fractured boundaries. Minor micro-quartz minerals are evident.

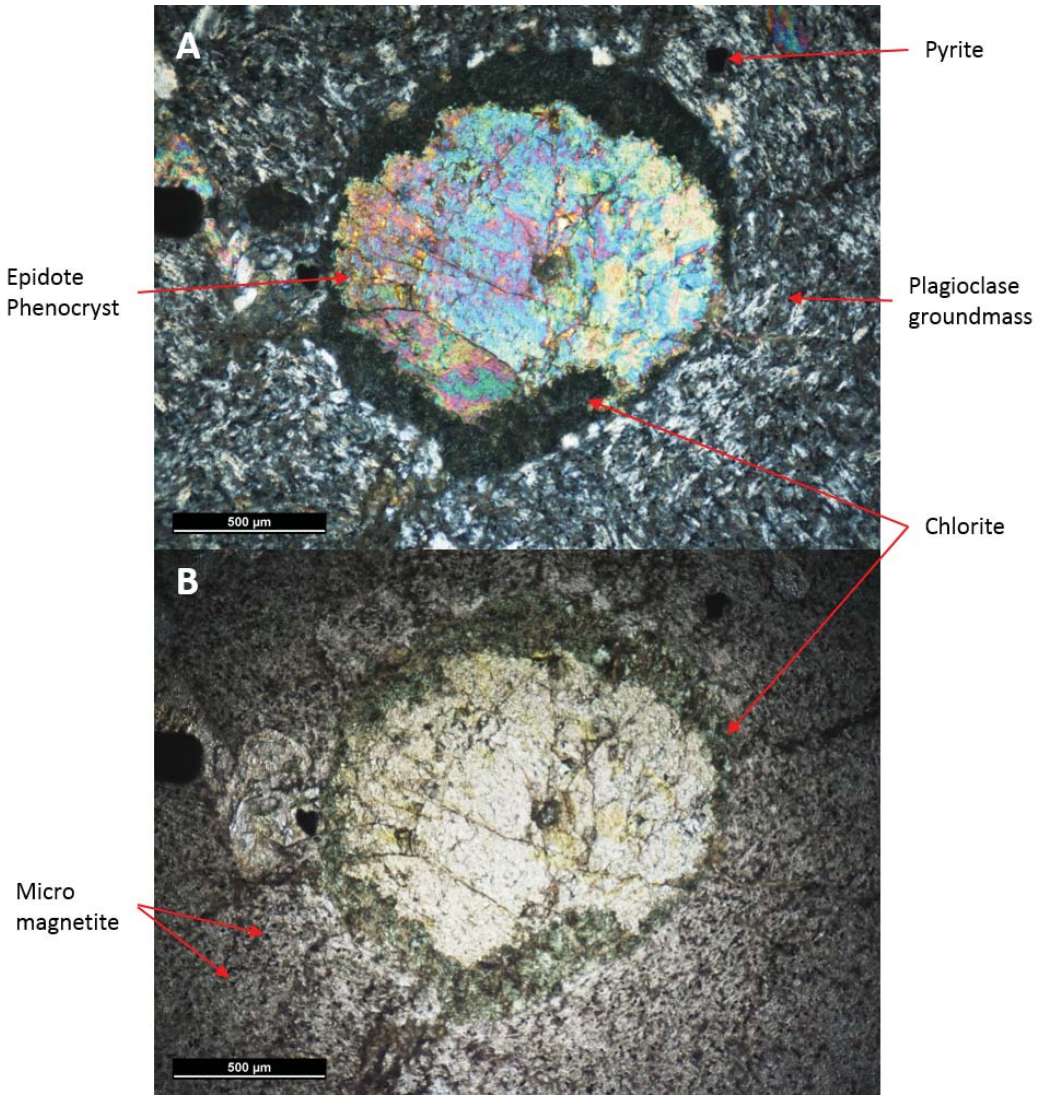

Figure 4.18: Boulder sample EG O CS 2 in cross polarised light (A), and plane polarised light (B). Note the incredibly fine-grained groundmass and zoning of chlorite around the epidote.

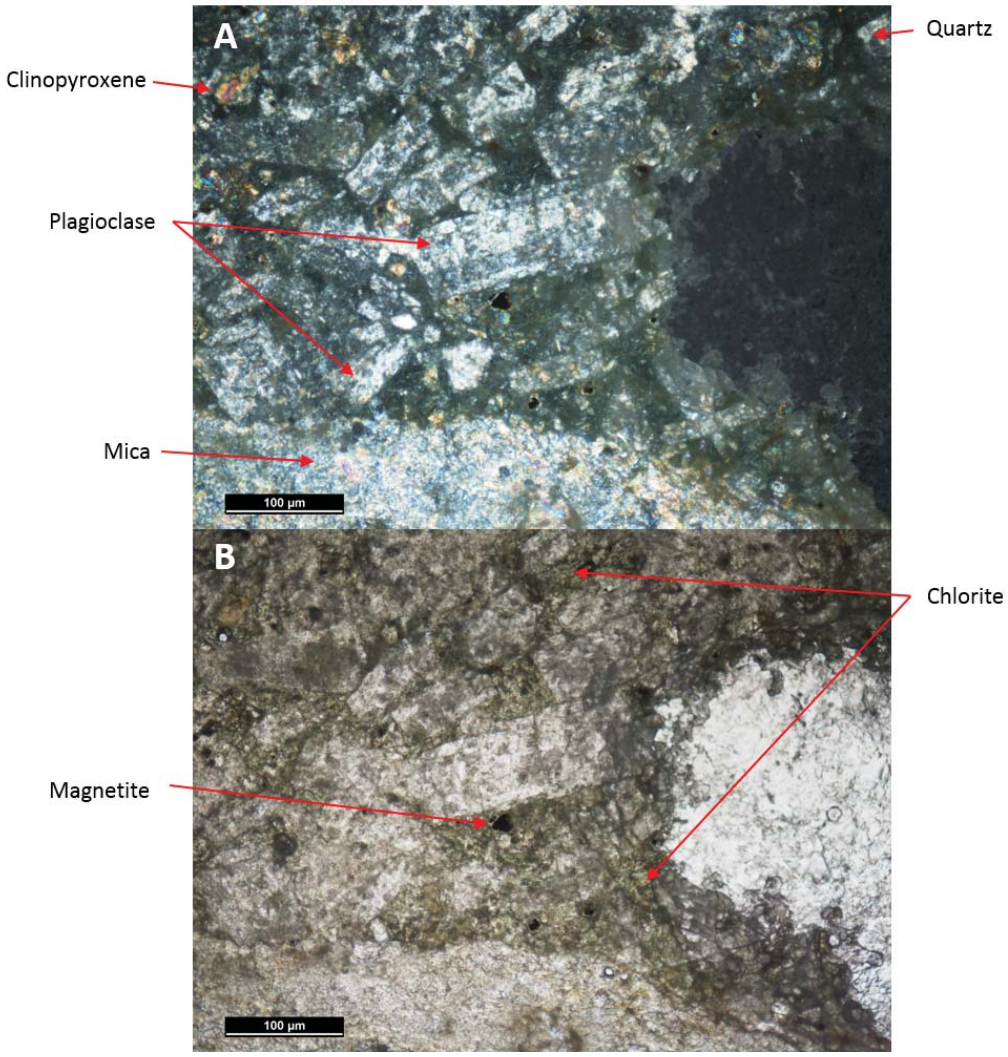

Figure 4.19: Boulder sample EG O CS 3 in cross polarised light (A), and plane polarised light (B). Note this sample is slightly weathered.

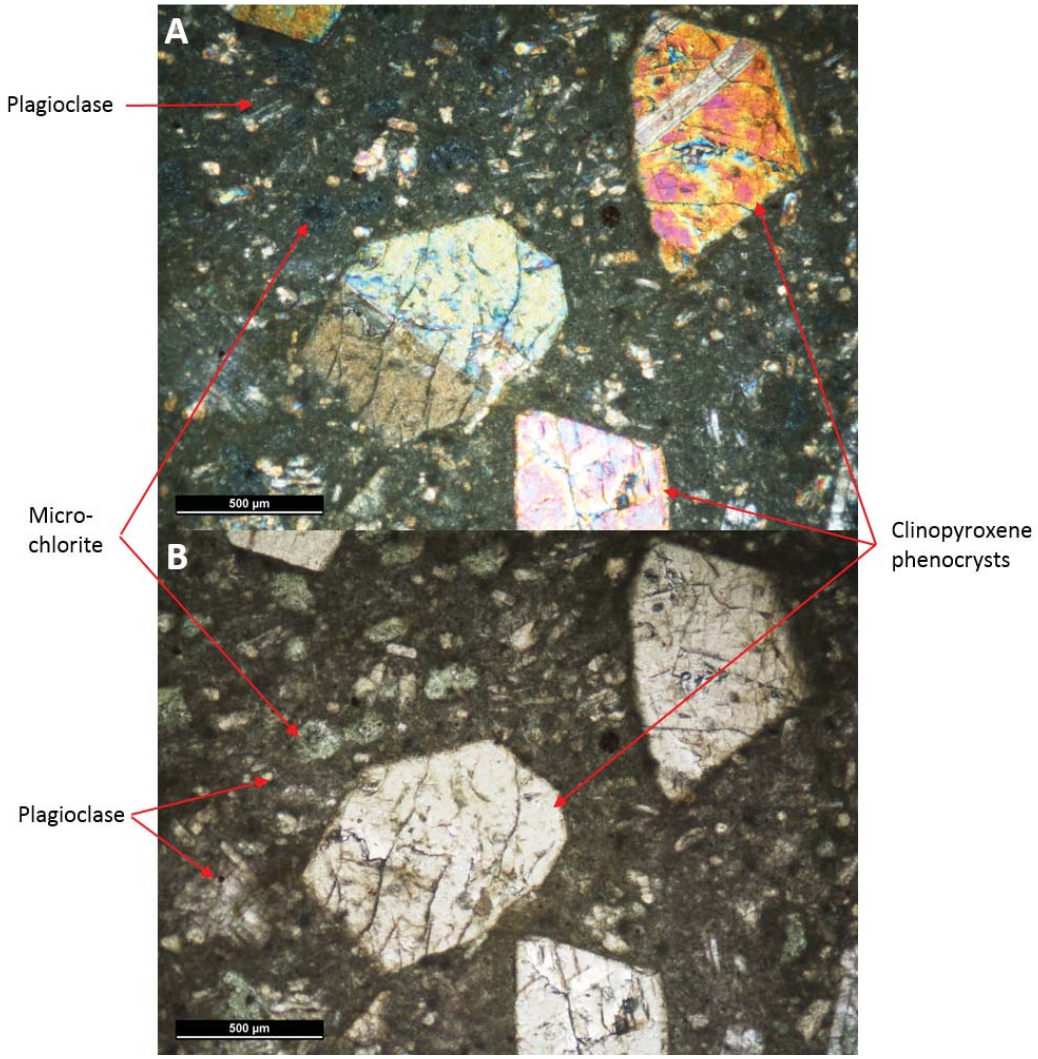

Figure 4.20: Boulder sample EG S CS 9 in cross polarised light (A), and plane polarised light (B).

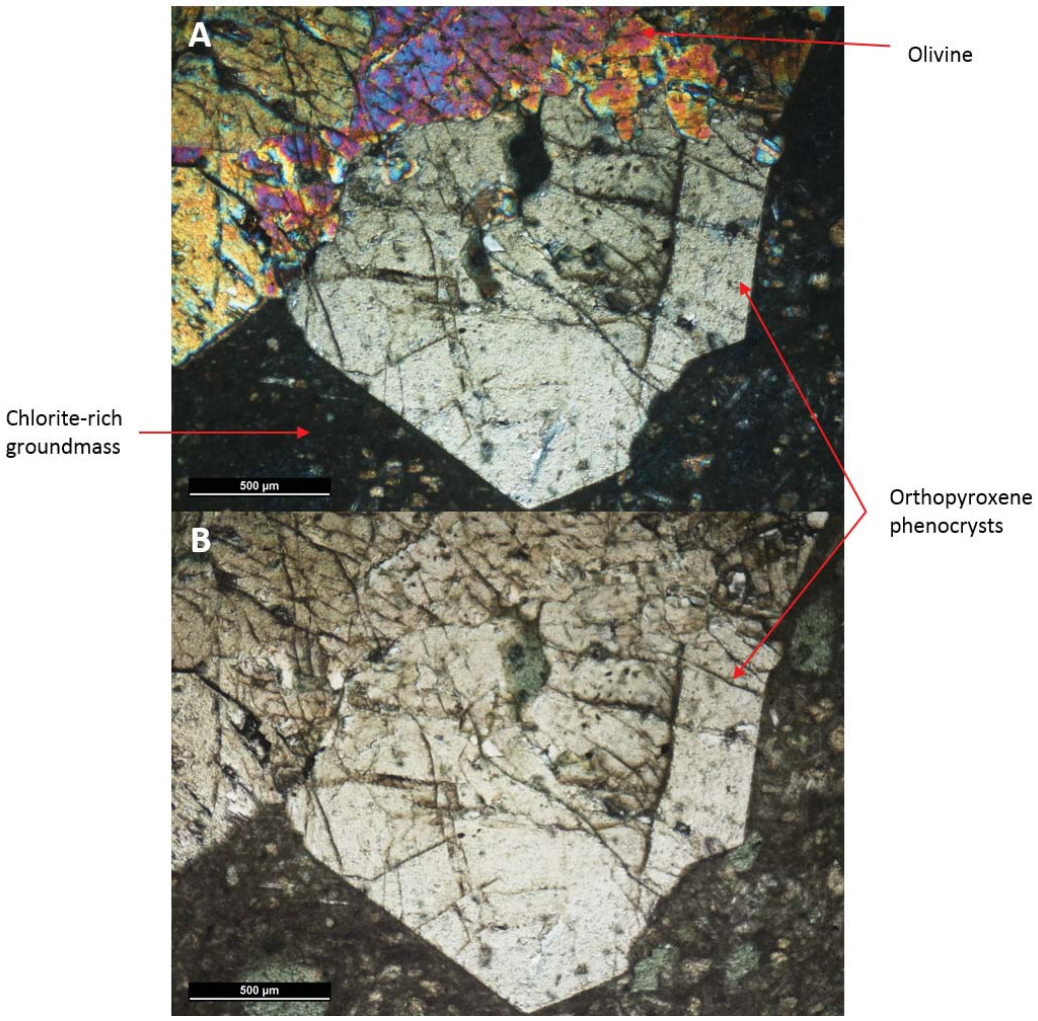

Figure 4.21: A second image of boulder sample EG S CS 9 in cross polarised light (A), and plane polarised light (B).

In sample EG O CS 2, a number of minerals were unidentifiable due to metamorphism and subsequent weathering. These samples were analysed by X-ray Diffraction (XRD) to accurately determine mineralogies (Figure 4.22) with the results revealing no quartz or pyroxene. EG O CS 2 was removed from the study at this point.

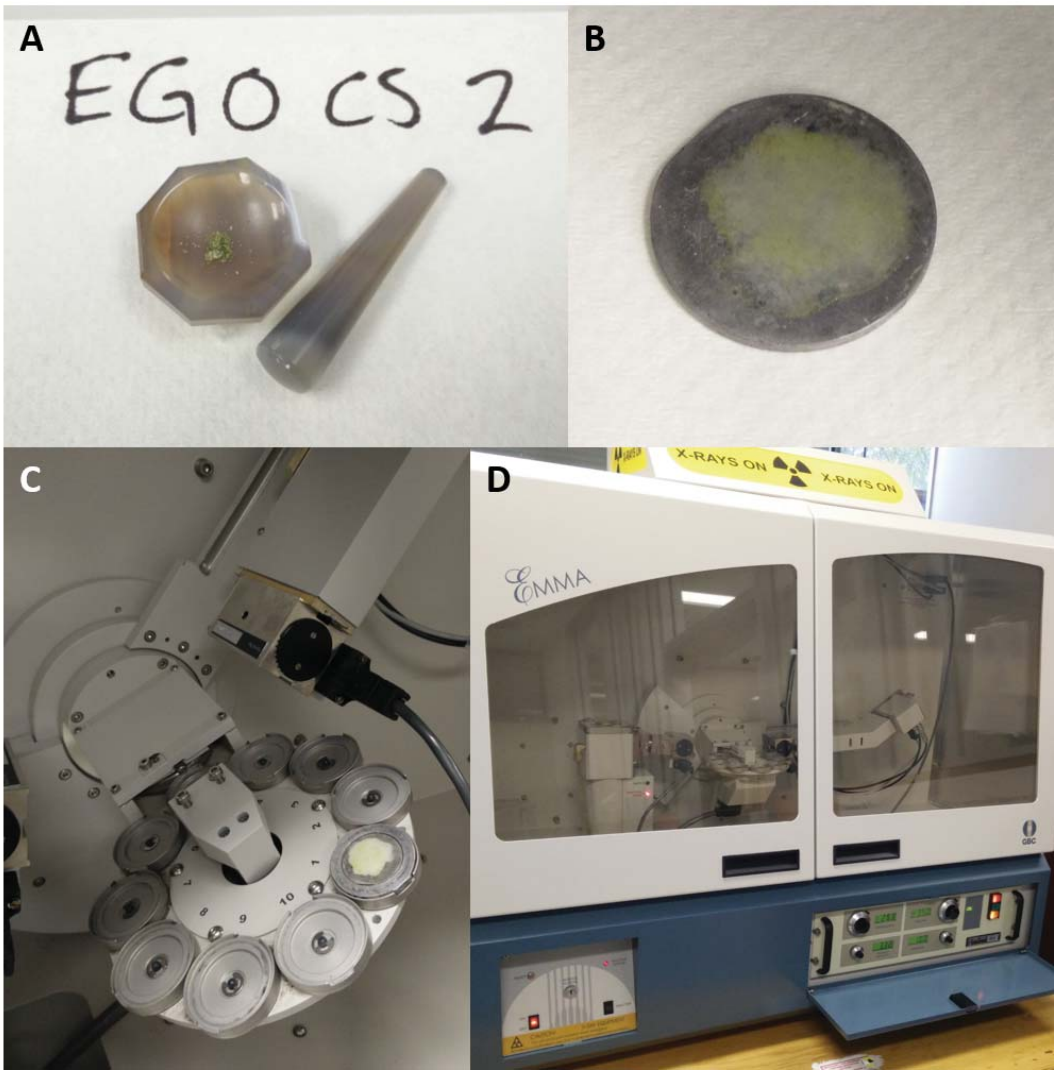

Figure 4.22: Preparation stages of XRD analysis. A) Powdering sample EG O CS 2 using an agate mortar and pestle, B) The powdered sample on a smear slide ready for analysis, C) Smear slide in the XRD machine, D) Benchtop enhanced mini-materials analyser (EMMA) X-Ray Diffractometer.

4.5.3 Mineral separation - magnetic

4.5.3.1 Size preparation - cleaning

The crushed field samples were sieved to >1 mm and <1 mm and the larger fraction (>1 mm) was set aside for possible future analysis if needed. Any particles <32 µm needed to be removed from the <1 mm fraction as this size would not go through the magnetic separator effectively. Separation was done in batches using DI water by putting 1 cm deep samples in a 1 L beaker, stirred briskly, left for three minutes to settle, water poured off and set aside, then repeated till the water ran clear upon stirring each batch (Figure 4.23). Each sample was oven-dried overnight at 50°C.

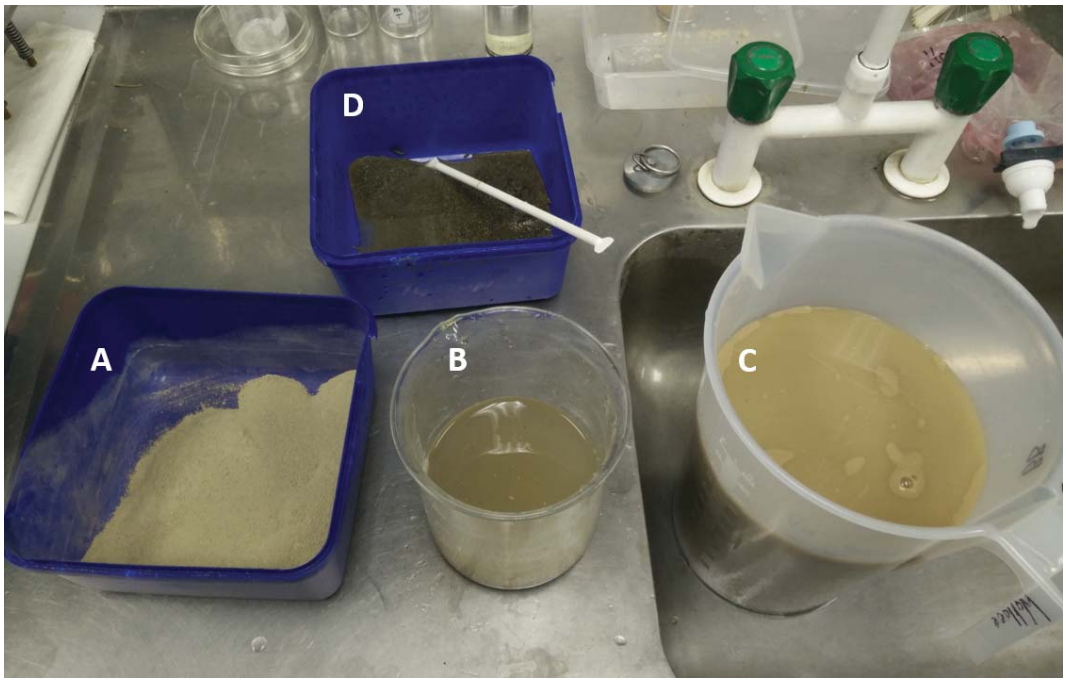

Figure 4.23: Preparation steps for magnetic separation: A) <1 mm fraction of a sample, B) 1 cm deep sample in a beaker with DI water left to settle for three minutes, C) liquid decanted from beaker with <32 µm sediment, D) 1 mm - >32 µm sediment ready for oven-drying and magnetic separation.

4.5.3.2 Pure mineral identification

Initial microscopic inspection of the fine fraction revealed contamination of fine metal shavings (possibly from the angle grinder when collecting them in the field) and also very few clean, separated minerals. Each fine sample was sieved into smaller fractions (1 mm-850 µm, 850-710 µm, 710-500 µm, 500-250 µm, 250-125 µm, 125-63 µm, and <63 µm) to find the size fraction with the purest minerals (i.e. individual grains of one particular mineral) and the least metal contamination. The cleanest size fractions were used for magnetic separation.

4.5.3.3 Hand magnet and Frantz

A hand magnet was carefully moved across all samples to remove the highly magnetic minerals (e.g. magnetite) to reduce the chance of them blocking the magnetic separator (Figure 4.24B). An Isomagnetic Separator (Frantz) was used at VUW to separate the remaining magnetic minerals from each sample (Figure; 4.24A, D; 4.25).

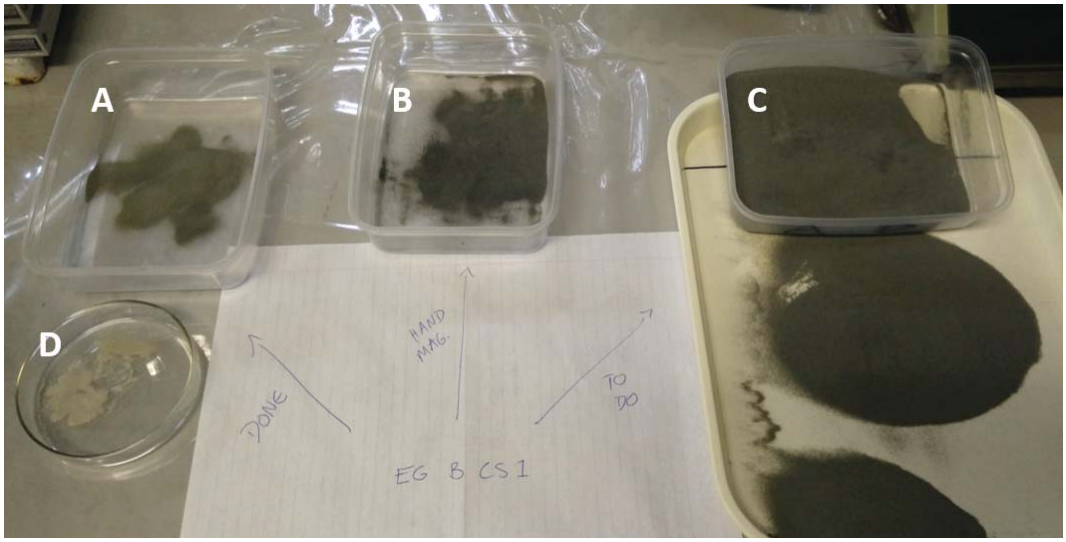

Figure 4.24: Sample EG B CS 1 in the process of being separated by hand magnet and Frantz. A) Magnetic minerals after Frantz separation. B) Highly magnetic minerals removed by hand magnet. C) Original sample. D) Non-magnetic fraction after Frantz separation.

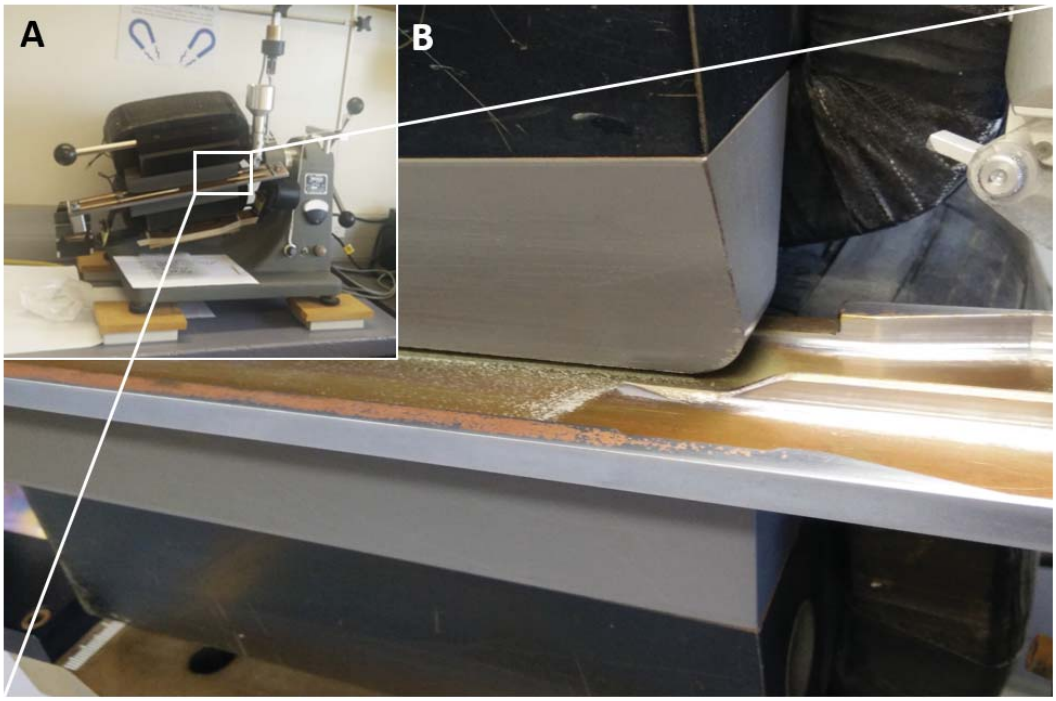

Figure 4.25: Magnetic separation of minerals: A) The Frantz isomagnetic separator, B) A close-up of the non-magnetic minerals (white) being dropped away from the magnet.

Ideal amperage, slide angle (which regulates speed of grains without saltation), and slide tilt (which influences the amount of magnetic grains extracted) were determined by laborious trial and error, based on multiple runs of each sample and using Rosenblum and Brownfield (2000) as a vague guide. Once optimal separator settings were achieved each sample was cycled through the Frantz until no further separation could be observed. In this study, complete separation was achieved after two cycles through the Frantz.

The resulting magnetic fractions (which included the pyroxenes needed for TCN, chlorite, amphiboles, minor magnetite inclusions, and others) were set aside for further magnetic separation prior to beryllium separation chemistry. The non-magnetic fractions (which included quartz and feldspars) were set aside for quartz leaching and beryllium separation.

4.5.4 Pyroxene preparation and ^{10}beryllium separation chemistry

4.5.4.1 Magnetic separation - pyroxene

Further microscopic analysis of the magnetic fraction revealed grains partially bound by clay-sized particles as a result of the crushing process. To remove the fine particles, each sample was subjected to 90-120 minutes (rinsing every five minutes) in an ultrasonic bath, at VUW,with a frequency of 35 kHz, power at 80%, and temperature of 25°C until the water ran clear (Figure 4.26). The samples were then oven-dried at 50°C.

Figure 4.26: The samples undergoing an ultrasonic bath at VUW to disaggregate any attached clay-sized particles.

The magnetic fraction of each sample was once again run through the Frantz at various amperages, slide angles, and slide tilts, in an attempt to extract clean pyroxene minerals. For each sample that had a pyroxene constituent, the pyroxene was found to be non-magnetic at 0.15 amps and magnetic at 0.4 amps (though this is subjective to the specific Frantz being used). This method produced samples with clean pyroxene minerals, but it was not possible to separate out some other minerals that shared the same magnetic susceptibility e.g. chlorite.
Heavy liquid separation, which provides an alternative method for mineral separation was not used because the densities of the major minerals within each sample were too similar for the process to be feasible.

4.5.4.2 Pyroxene cleaning procedure

The four samples that contained pyroxenes were crushed individually using VUW's RockLabs Ring Mill pulverizer to enhance the exposure of contaminated zones (i.e. weathering pits containing meteoric ^{10}Be; *sensu* Blard et al., 2008; Collins, 2015). The following procedure outlines the crushing process:

- Crush each sample for 20 seconds and sieve to $<$90 µm.
- Re-crush any $>$90 µm material for a further 20 seconds and sieve again.

Note: If the first 20 seconds crushed <50% of the sample, increase this crushing time by a few seconds.

- Continue this process till the >90 µm fraction is less than the minimum amount required for the Ring Mill (refer to specific lab instructions for minimum and maximum samples weights).
- Hand crush any leftover >90 µm material with a mortar and pestle and add to the sample.

This procedure resulted in four samples, with different amounts of pyroxene (Table 4.2), ready for chemistry. While the proportion of pyroxene is not crucial for this method (K. Norton, personal communication, August, 2016), it is important to know the mineralogy of the samples.

Table 4.2: Pyroxene constituent of each sample.

Original sample name	Simplified sample name	Approximate amount of pure pyroxene (%)
EG B CS 1	pA	5
EG O CS 3	pB	5
EG N CS 3	pC	20
EG S CS 9	pD	80

4.5.4.3 Pyroxene ^{10}beryllium separation chemistry

This technique is based on Blard et al., (2008) who pioneered the idea of extracting ^{10}Be from pyroxene minerals though had large errors in the results. Collins (2015) successfully dated pyroxene minerals with relatively large errors though had no quartz mineral controls from the same sample. In this study, one sample (EG N CS 3) had both pyroxene and quartz minerals. During the chemistry steps, small adjustments to Collins' methods were made to account for low pyroxene percentages and equipment limitations. These include: adjustments to centrifuge rpm, rinsing with water as opposed to hydroxylammonium-chloride ($NH_2OH.HCl$) in Leach 1 as we did not need to measure the ^{10}Be concentration of the solution, and chemical amounts were adjusted based on sample size. The leaching steps are outlined in 4.5.4.4 and 4.5.4.5. Note that a simplified step-by-step version of the pyroxene leaching process is supplied in Appendix A.

4.5.4.4 Leach 1 - hydroxylammonium-chloride

The following leach steps dissolve any metal oxides and releases grain-absorbed meteoric ^{10}Be without removing the *in situ* ^{10}Be (Blard et al., 2008; Collins, 2015).

Approximately 5 g of each sample was put into 180 ml Savillex beakers of a known weight and total weights recorded. The samples were leached for 12 hours at 95°C in 25 ml of a 0.04M solution of $NH_2OH.HCl$ in 25% acetic acid. After decanting excess solution into a waste container, the sediment samples were transferred into 50 ml centrifuge tubes. These were centrifuged three times for 5 minutes at 3000 rpm, rinsing the supernate into the waste container with ultrapure DI water (MilliQ) each time. The sediment samples were transferred into their original Savillex beakers and dried for two hours on a 100°C hotplate. Once dry, the samples were precisely weighed to determine the mass of material dissolved (Table 4.3).

4.5.4.5 Leach 2 - hydrochloric acid

The remaining sediment was transferred into the original 50 ml centrifuge tubes and topped up to 25 ml with 1M HCl. The tubes were shaken gently on 'hot dog' rollers at 20°C for 24 hours. The samples were centrifuged three times for 5 minutes at 3000 rpm, again rinsing with MilliQ and discarding the supernate each time. The sediment samples were rinsed back into the original 180 ml Savillex beakers and dried overnight in a 70°C oven before being precisely weighed once again (Table 4.3).

Table 4.3: Pyroxene sample weights before and after the chemistry steps and total mass of material dissolved/lost from each sample.

Simplified sample name	Sample weight (g)	Post-leach 1 (g)	Post-leach 2 (g)	Post-HF (g)	Total mass lost (%)
pA	5	4.8964	4.6117	3.675	26.5
pB	5.2	4.8831	4.4066	3.091	40.5577
pC	5.1	4.8685	4.5217	4.2503	16.6608
pD	5	4.7964	4.5173	3.6415	27.17

4.5.4.6 Leach effectiveness

The total mass lost from samples pA-pD was compared with Collins' total mass lost (from her Table 2.1, p. 54) to clarify whether the leach steps had been effective enough to continue with processes without needing to perform a subsequent leach. The mass dissolved here falls within the bounds of Collins' data, therefore is sufficient to continue with the next steps.

The final stages of pyroxene separation were performed by Dr. Kevin Norton at VUW following the hydrofluoric acid dissolution, carrier addition, and column steps proposed by Collins (2015) and Jones (2015).

4.5.5 Quartz preparation and ^{10}Be separation chemistry

4.5.5.1 Quartz separation

The non-magnetic fraction from three of the samples (X, Y, and Z; see Table 4.4 for sample naming convention) were chosen for the leaching process as they had inclusions of feldspar and other light minerals that needed to be removed from the quartz fraction. The other two samples with insufficient quartz for analysis were discarded at this point.

Table 4.4: Quartz sample weights through the chemistry steps.

Original sample name	Simplified sample name	Sample weight (g)	Post-amorphous steps (g)	Post-crystalline steps (g)	Post-aqua regia (g)	Outcome
EG N CS 3	X/Xa	49.3089	46.3437	29.0128	28.2108	Continue
EG O CS 3	Y/Ya	10.4324	9.218	1.8877	0.5915	Removed
EG B CS 1	Z/Za	7.6604	7.1519	0.2909	Removed	-

Note: Individual simplified sample names (e.g. X and Xa) are interchangeable. They were named differently during the chemistry stages for ease of record-keeping.

4.5.5.2 Quartz leaching technique

As the grains were very fine (i.e. 63 µm to 250 µm) there was a high chance of losing most, if not all, of the quartz during this process. In an attempt to combat this, a novel leaching technique is proposed in this study and was adapted from Tessier et al., (1979), Bourles et al., (1989), and Guelke-Stelling and Blanckenburg (2012). The purpose was to remove the meteoric component of ^{10}Be for measurement, while leaving most of the quartz grains with *in situ* ^{10}Be to be measured. The process went as follows:

1. Each sample was added to individual, labeled, 1 L Nalgene lab bottles.
2. *Amorphous oxide-bound beryllium extraction:*
    - 100 ml 0.5M hydrochloric acid (HCl) solution was added to cover sample, (25 ml of 0.6M HCl in 275 ml of milliQ H_2O made 300 ml 0.5M HCl).
    - The Nalgene bottles were agitated gently for 24 hours using a hotdog roller set to cold,
    - Some sediment was rinsed into 50 ml centrifuge tubes with MilliQ water and filled to 75%,

It was not possible to rinse all the sediment into the tubes without over-filling them with water.

- The tubes were centrifuged for 12 minutes at 3500 rpm,
- The supernate was decanted into 380 ml Savillex beakers and sediment left in the tubes,
- More sediment was rinsed into the tubes with MilliQ water,
- The centrifuge step was repeated till no more sediment was left in the bottles. Bottles were rinsed.
- The sediment was rinsed into bowls and dried overnight in a 60°C oven,
- The sediment was precisely weighed (Table 4.4) and returned to the 1 L bottles for use in Step 3 (Figure 4.27),
- The solution was dried on a 110°C hotplate in a fumehood till close to dryness (24 hours),
- The residue was dissolved in ~30 ml (enough to cover generously) of 5M HNO_3 for 2 hours on a hotplate at 80°C,
- After cooling, all the contents were poured/pipetted into 50 ml centrifuge tubes (Figure 4.28) and set aside.

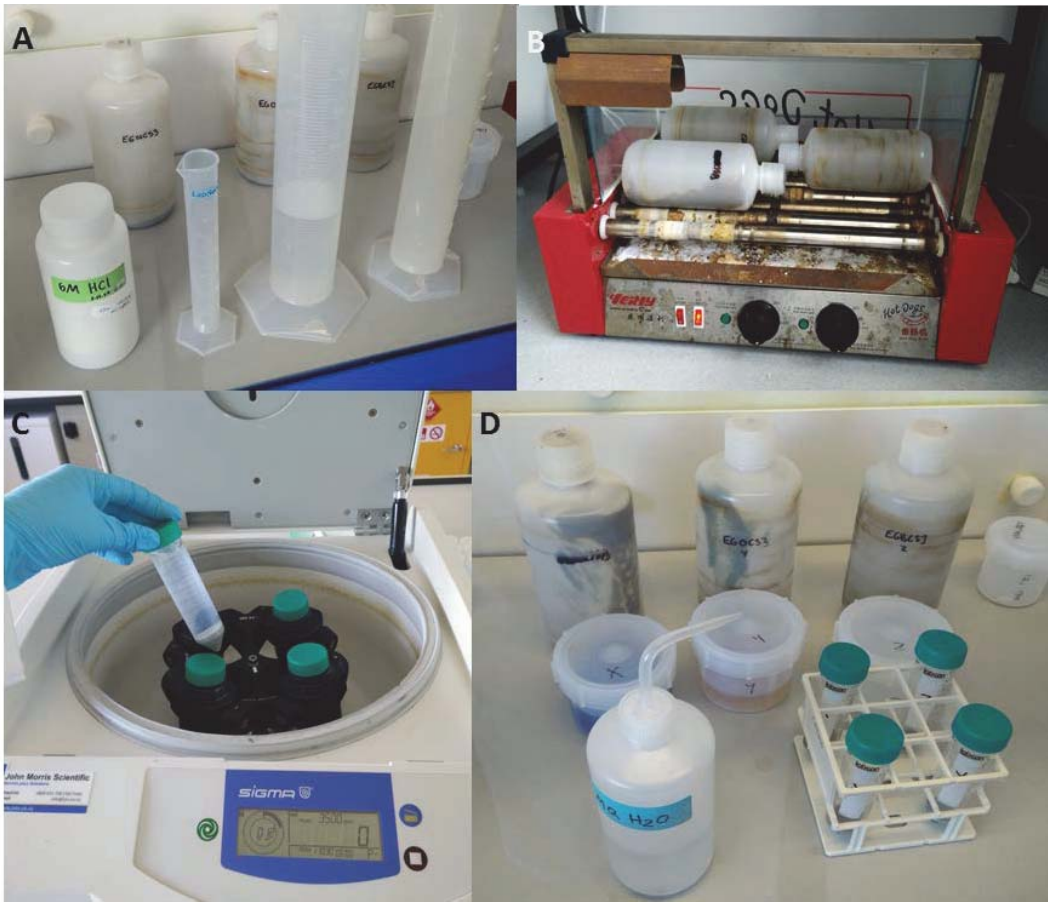

Figure 4.27: Initial leaching steps for amorphous oxide-bound beryllium extraction. A) Making 0.5M HCl solution, B) agitating the samples on cold hotdog rollers, C) samples placed in the centrifuge, and D) sediment returned to the Nalgene bottles and solution ready for drying.

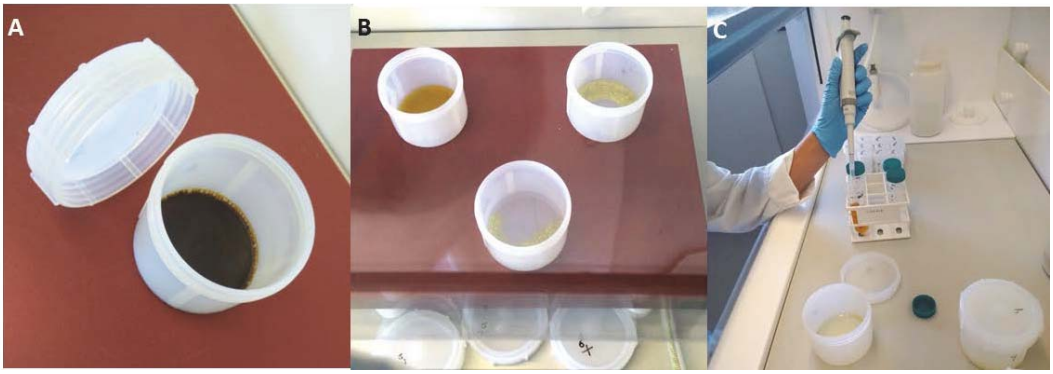

Figure 4.28: Dissolution stage of the amorphous process. A) 5M HNO_3 added to the residue, B) solution drying on an 80°C hotplate, and C) pipetting concentrated solution into centrifuge tubes.

3. *Crystalline oxide-bound beryllium extraction*

- The 1 L bottles with sediment from Step 2 were gathered,
- 30 - 90 ml 1M hydroxylamine-hydrochloride ($NH_2OH.HCl$) solution was added, enough to cover sediment generously,
- The bottles were agitated gently for 4 hours on 80°C hotdog rollers,
- The solution was rinsed into 50 ml centrifuge tubes (same process as Step 2),
- The tubes were centrifuged for 12 minutes at 3500 rpm,
- The supernate was decanted into 380 ml Savillex beakers (reserved for Step 6), and sediment left in the tubes,
- Centrifuge and rinsing steps were repeated till no more sediment was left in the 1 L bottles (Figure 4.29).
- Sediment was rinsed into bowls and dried overnight in a 60°C oven,
- Once dry, the sediment was precisely weighed and returned to the 1 L Nalgene bottles (Table 4.4).

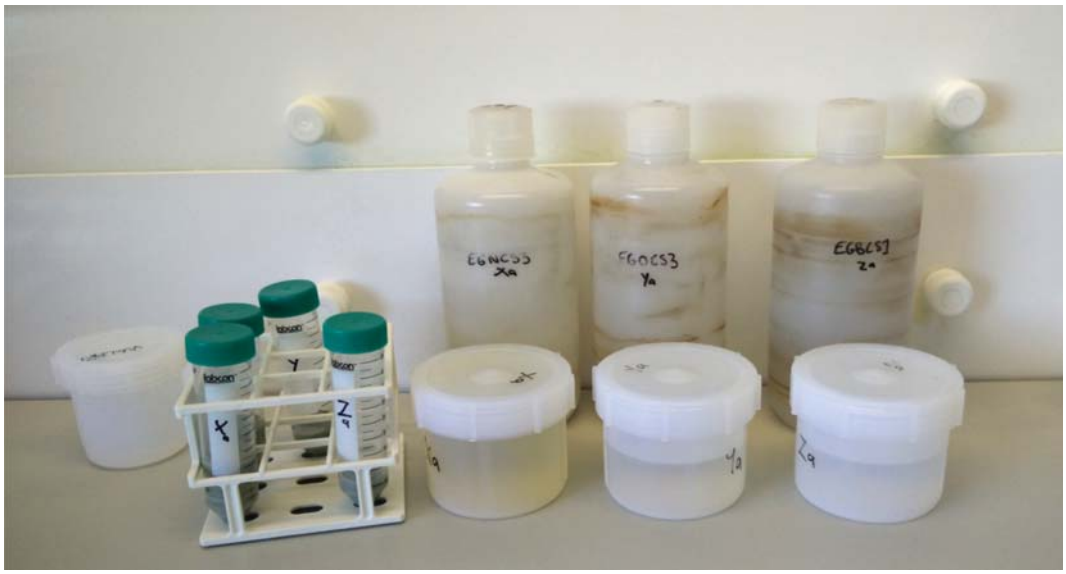

Figure 4.29: Initial steps for crystalline oxide-bound beryllium extraction. Centrifuge tubes with entire sediment samples following centrifuging, Savillex beakers with 1M hydroxylamine-hydrochloride solution and MilliQ water from rinsing, and empty Nalgene bottles.

4. *Hydrofluoric acid leach*

   - 250 ml of 5% Hydrofluoric acid (HF) was added to the 1 L bottles with sediment in them,
   - Bottles were agitated gently for 24 hours on 60°C hotdog rollers,
   - The supernate was tipped into HF waste containers and rinsed with MilliQ water 4 times,
   - The sediment was rinsed into bowls and dried overnight in a 60°C oven (Figure 4.30),
   - The 380 ml Savillex beakers were precisely weighed and sediment tipped into them (Table 4.4).

     Note: At this point sample Z/Za was reduced to $<$1 g, therefore was removed from the experiment.

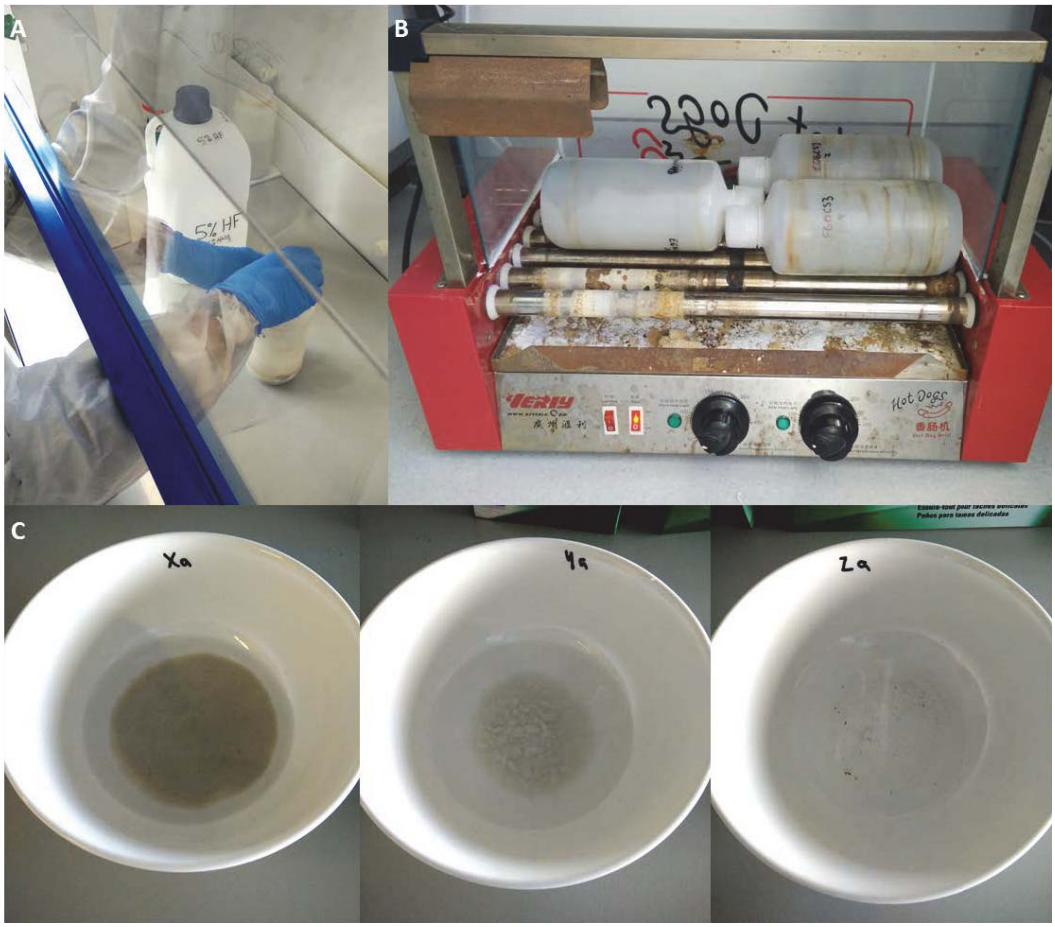

Figure 4.30: Steps taken to extract meteoric ^{10}Be from the quartz-rich sediment. A) Adding 5% HF, B) agitating on 60°C hotdog rollers, and C) rinsed sediment. Note that in C), Za is removed at this point.

5. *Aqua regia*

- The aqua regia was prepared by mixing 3:1 concentrated HCl and HNO_3 (respectively) in a graduated beaker (enough for the it to cover the sediment by approx. 5 mm),
- The aqua regia was added to the 380 ml Savillex beakers containing the sediment from Step 4,
- The beakers were gently swirled to combine and placed on a 120°C hotplate for 30 minutes,

  Note: Brown gas formed during this process.
- The lids were put on the beakers and left on the hotplate for 1 hour,
- The beakers were removed from hotplate, lids loosened, and left to cool for 1 hour,
- the beakers were rinsed 4-5 times with MilliQ water, leaving the sediment in the beakers,
- The sediment was dried overnight on a 60°C hotplate,
- The beakers and sediment were precisely weighed (Table 4.4).

6. *Hydroxylamine-hydrochloride solution removal:*

- The 380 ml Savillex beakers with supernate from Step 3 were gathered,
- 20 ml of concentrated Nitric acid (HNO_3) and 20 ml 30% Hydrogen peroxide (H_2O_2) were slowly hand-poured (respectively) into the beakers,

  Note: A strong reaction occurred during this step.
- The solution was left to cool/settle for half an hour,
- The solution was dried completely on a 70°C hotplate over 24 hours,
- 10 ml conc. HNO_3 followed by 10 ml H_2O_2 was very slowly hand-poured to reduce the reaction intensity,
- The solution was left to cool/settle for half an hour and dried once again on a 70°C hotplate (Figure 4.31),
- The above two steps (of adding the acid and drying) was repeated five times till the solution was nearly clear.

The final stages of quartz separation were performed by Dr. Kevin Norton at VUW following the standard quartz/^{10}Be procedure as described in Gosse and Phillips (2001).

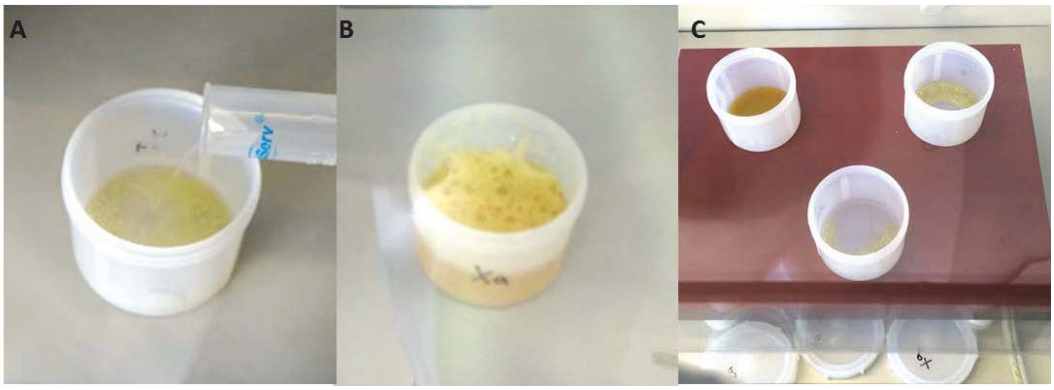

Figure 4.31: Removal of hydroxylamine-hydrochloride from the solution prepared in Figure 4.29. A) Addition of HNO_3 and H_2O_2, B) the reaction taking place, and C) the solution drying down on a 70°C hotplate.

4.5.5.3 ^{10}Be measurements

For reasons beyond anyone's control, all pyroxene and quartz samples were contaminated with dust while undergoing the final stage of preparation at VUW, resulting in unusable samples. The time-frame to prepare a completely fresh batch of samples for AMS measurement greatly exceeds the time-frame for this thesis submission, therefore will not be attempted until after submission, in 2017.

Chapter 5

Results

5.1 Introduction

The following sections describe the morphology of the features within the valley, both above and below the modern floodplain. The internal sedimentology of a number of the deposits throughout the valley is examined and initial inferences on the origin of the hummocks are made. The presence of paleo-lake sediments, discovered during field work, is introduced. The ages of the hummocks throughout the valley are touched on. The modern morphology of Eglinton Valley is likely to have formed from a combination of glacial, fluvial, and mass movement processes. All locations referred to within this section are shown in Figure 5.1.

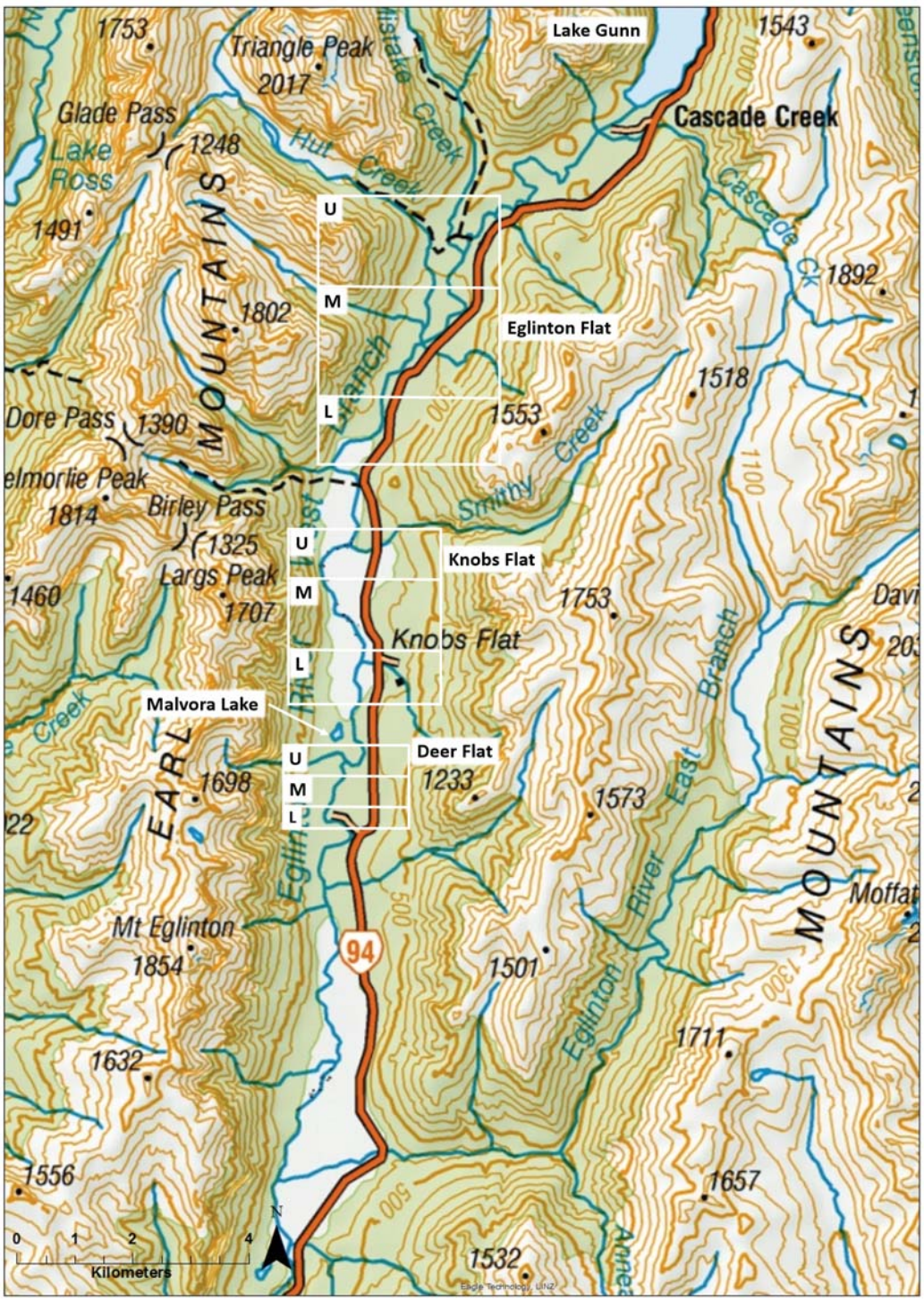

Figure 5.1: Geographical locations that the study area has been divided into. U: Upper, M: Middle, and L: Lower. Topographic basemap from LINZ.

5.2 Hummock morphology - surface expressions

A prominent feature of Eglinton Valley is the various forms of hummocky topography scattered throughout. Some are relatively conical, some elongate (both parallel and perpendicular to the valley), some egg-shaped (when viewed from above), a few (at Deer Flat and Lower Knobs Flat) appear to radiate out from a point, and others have no apparent simple shape to them (as outlined in Figure 2.2 and field examples shown in Figure 5.2).

The heavily vegetated hummocks at the Upper Deer Flat, Malvora Lake, and Lower Knobs Flat (see Figure 5.1 for these locations), exhibit some minor compressional ridges, and are partially radiating away from inferred RA source areas on an adjacent slope of the Earl Mountains. They are also large (up to ~20 m above the floodplain), have steep (40°- 50°) sides in most directions, and the upper surfaces of all of them appear to be undulating with ~1-5 m deep channels running parallel to the main valley. Other hummocks (e.g. Upper Knobs Flat hummocks) are not as high and do not have ridges or troughs. They also do not appear to radiate from anywhere. These hummocks, and others in the valley, have been/still are being truncated by the Eglinton River resulting in potentially a different morphology to when they was first deposited. This is evident from typically one side of these hummocks being steeper than the other sides. The aggrading floodplain has also partially buried the hummocks (see Subsection 5.3), hiding the actual depth and extent of the initial deposits; making it difficult to estimate volumes.

Figure 5.2: Various photos of some hummocks in Eglinton Valley. A) South-western face of a Middle Knobs Flat hummock (clast sample EG C 1), note the steeper right-hand side, photo credit S. McColl. B) Looking North from Malvora Lake (hidden behind vegetation on lower-left of image), towards the Lower Knobs Flat hummocks (clast samples EG E 1). C) Alastair for scale, on top of a conical hummock under trees beside Kiosk Creek (clast sample EG M 1). D) A Middle Deer Flat hummock exposed by the Eglinton River (clast sample EG 5, microsediment samples L and M). E) View due west along the ~280 m GPR line looking towards an elongate, parallel (to the valley), hummock. F) View Southeast towards the conical hummock at Middle Knobs Flat where cosmo sample EG B CS 1, and clast sample EG B 2 were taken.

5.3 Hummock morphology - subsurface

The depth and extent of the hummocks beneath the modern floodplain in Eglinton Valley can be partly identified in the radargrams presented in Figures 5.3 and 5.4. Both radargrams show stratified fine-grained sediments between each of the hummocks with the degree of stratification becoming less with depth. Boundaries can be identified where the hummocks extend below the floodplain, however, it is not possible to see whether the hummocks are joined at depth due to attenuation of the radar signal at depth where such features would be expected to be seen. The radargrams also show that the hummocks are made of different material to that of the adjacent floodplain. The numerous hyperbolas (convex arch-shapes) within the hummocks indicate coarser, probably bouldery, material which is unlikely to be of fluvial origin given the size of the material in the modern floodplain. At Upper Knobs Flat, the ground surface between the two eastern hummocks is slightly higher when compared to the left side (note that the image is 2x vertically exaggerated; Figure 5.3). The more elevated topography is thought to be part of the Knobs Flat alluvial fan which enters the valley at this location (highlighted in Figure 3.9 and discussed further in Section 6.3.4.

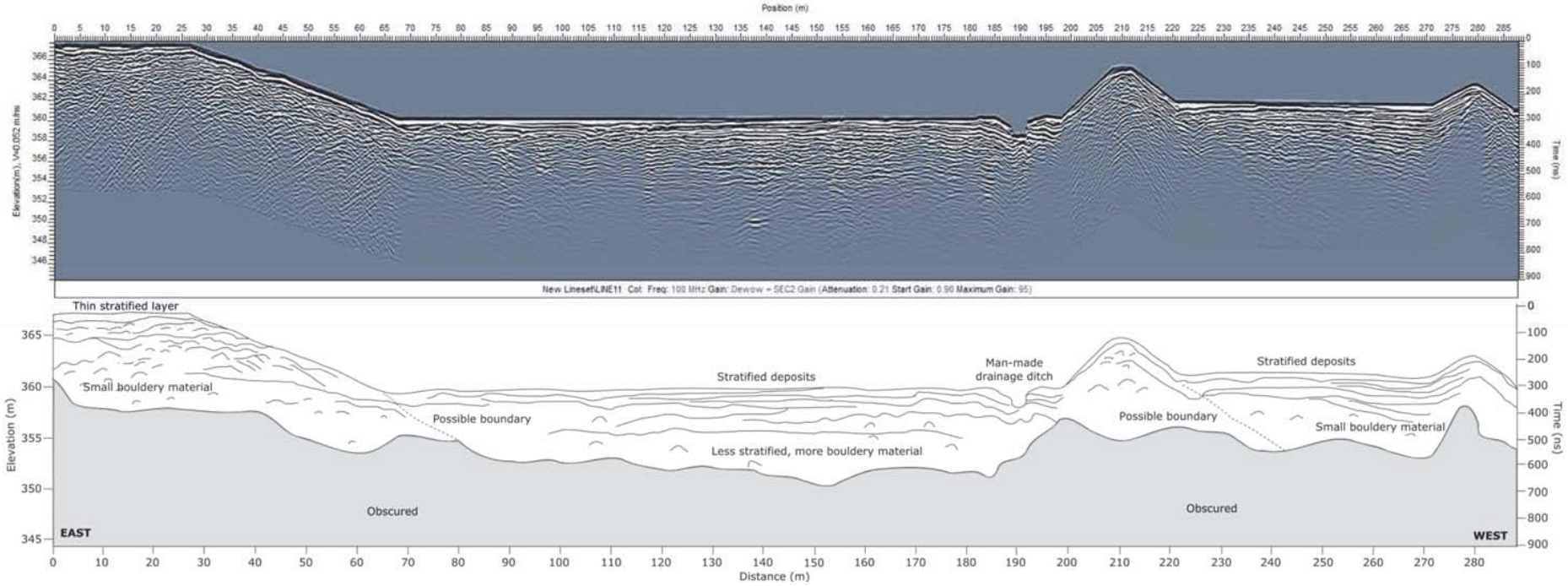

Figure 5.3: Raw data radargram and schematic of the ~280 m, 100 MHz line at Upper Knobs Flat. Note: This is 2x vertically exaggerated for better visualization. The floodplain has potentially built up around the the hummocks, with possible boundaries identified (dotted lines) in two locations. The large eastern hummock has many small hyperbolas indicating gravel- to small boulder-sized material forming it. Note: internal sedimentology of this particular hummock is discussed in Section 5.4.

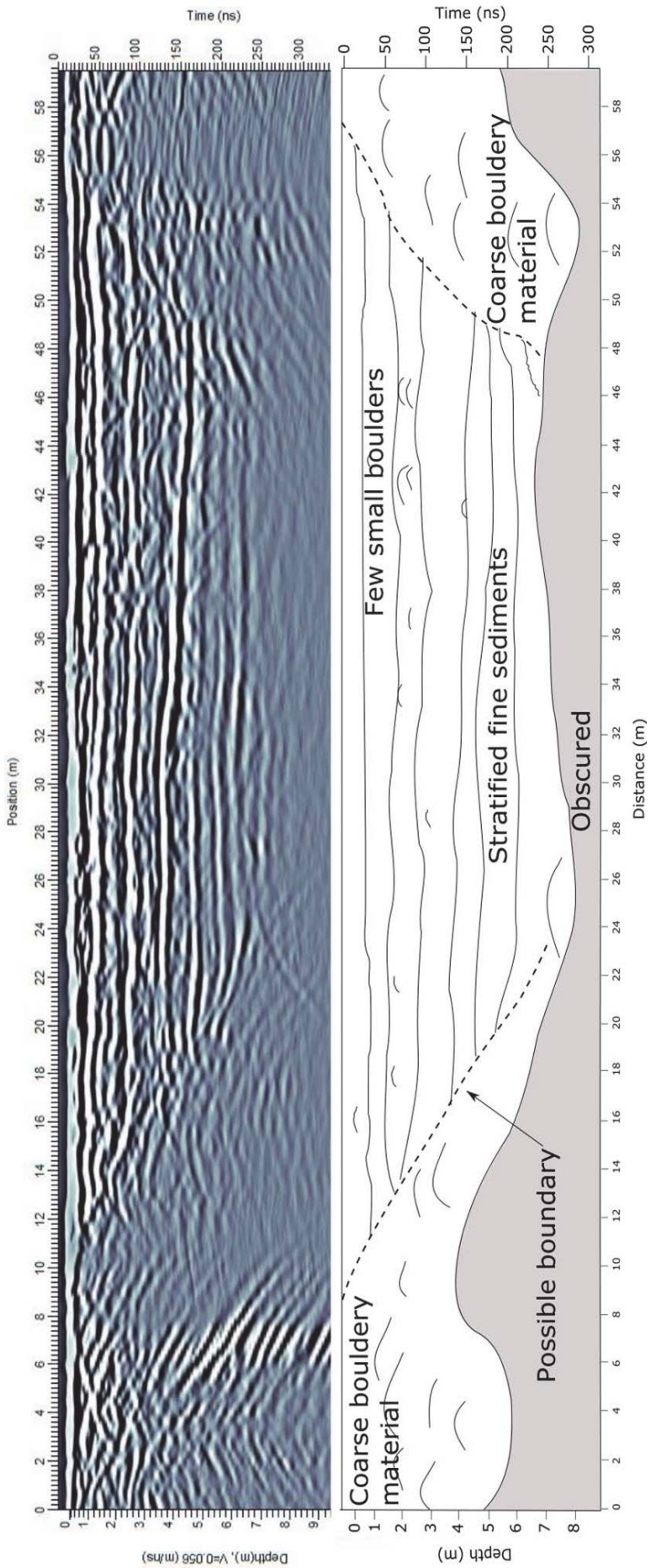

Figure 5.4: Raw data radargram and schematic showing the 60 m, 50 MHz GPR line that was run between two hummocks at Lower Deer Flat. very-fine grained sediments have built up around the hummocks, indicating the hummocks are much larger than the surface expressions. The data is obscured below ~7 m due to radar attenuation. Note: this has not been topographically adjusted as the ~1 m rise at each end is negligible to affect interpretation.

5.4 Sedimentology of the hummocks

5.4.1 Clast analysis - angularity index

While the angularity index (AI) alone can not be directly linked to a specific transport process, it can help to inform the likely processes responsible for transportation and deposition of the sediments. The majority of the sites throughout the valley have AI's over 50 (50% or more of the sample is very angular and/or angular) indicating possible mass movement (e.g. rock fall or RA) and/or supraglacial transport processes. Roundness histograms for all clast sample locations are shown in Figures 5.5 - 5.8. Those with AI less than 50 appear to be clustered together at the Upper Knobs Flat hummocks where five sites there have low AI indicating a fluvial, subglacial, or englacial transport pathway. The other low AI samples were collected from the Mirror Lakes road cutting site (060216 EG A 1), the periphery of Wesney Creek Fan (EG R 2), one site from Middle Deer Flat (EG S 8), the Kiosk Creek clasts (EG P 2), and two of three samples from Upper Eglinton Flat (70216 EG J 1a and EG H 1).

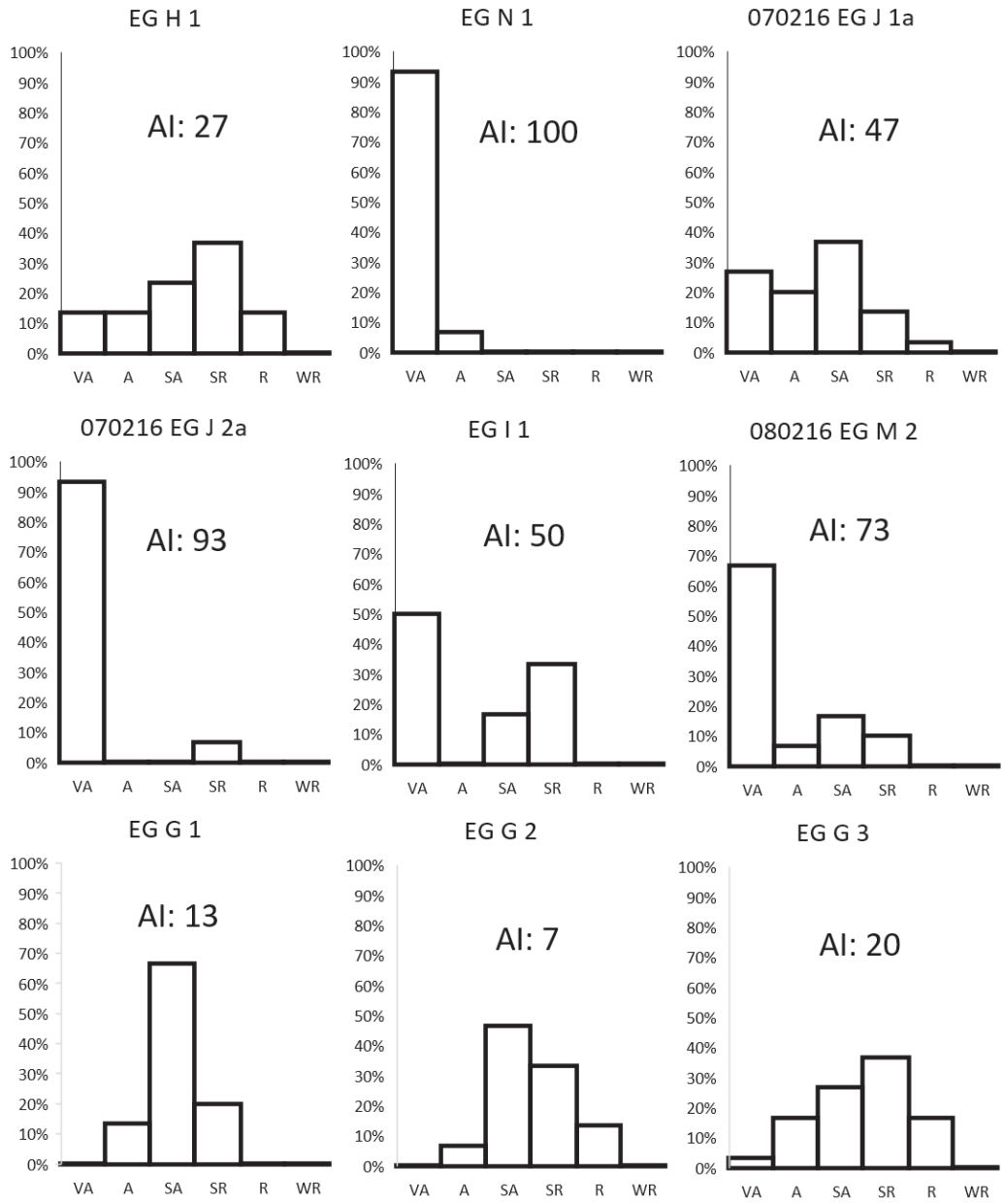

Figure 5.5: Roundness histograms for clast sample locations from Upper Eglinton Flat down to Upper Knobs Flat. AI: The higher the number, the higher the percentage of the sample has angular and very angular clasts which can help deduce transport pathways. Abbreviations: *VA* = very angular; *A* = angular; *SA* = sub-angular; *SR* = sub-rounded; *R* = rounded; *WR* = well rounded.

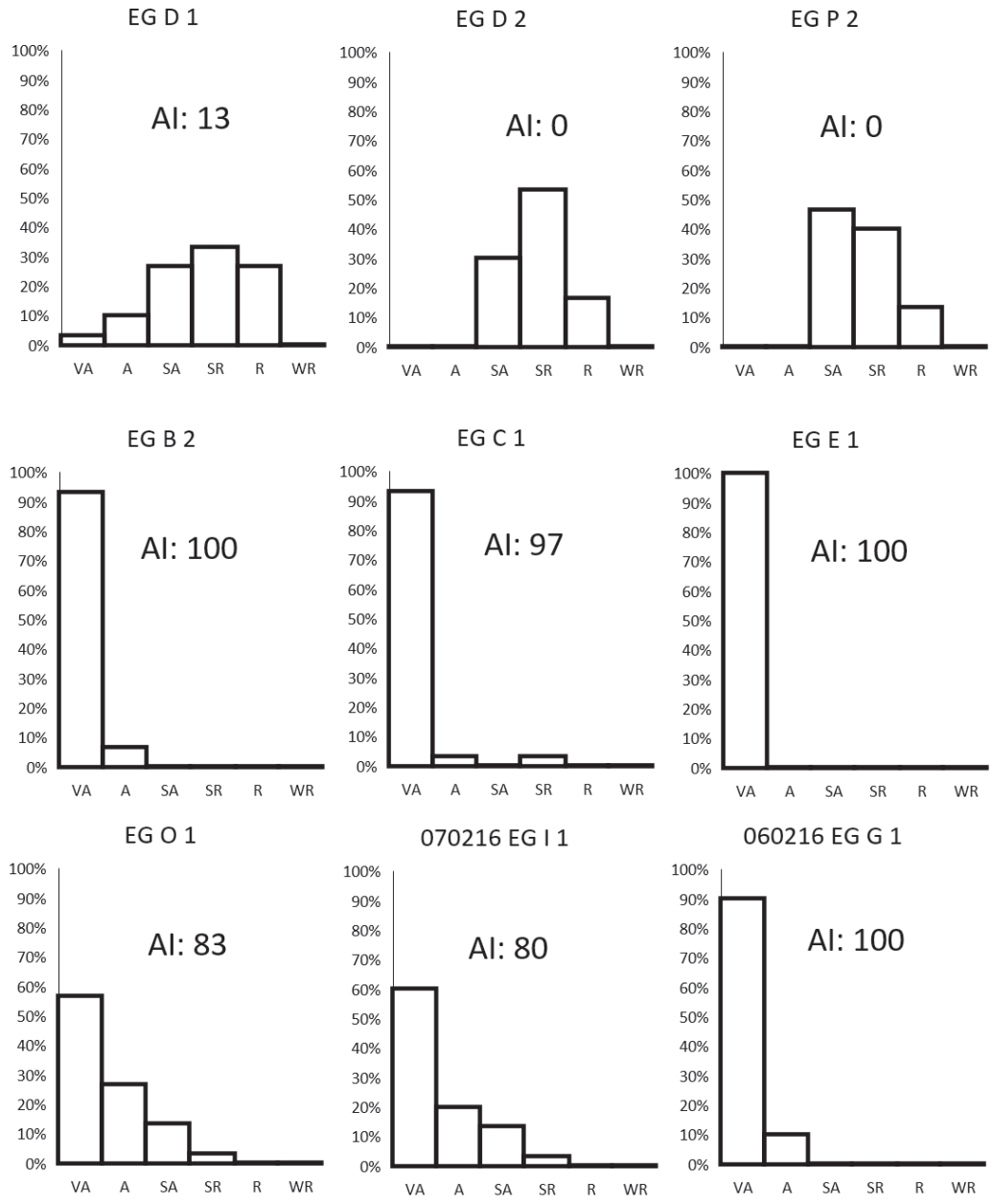

Figure 5.6: Roundness histograms for clast sample locations from the Middle Knobs Flat down to Malvora Lake hummocks.

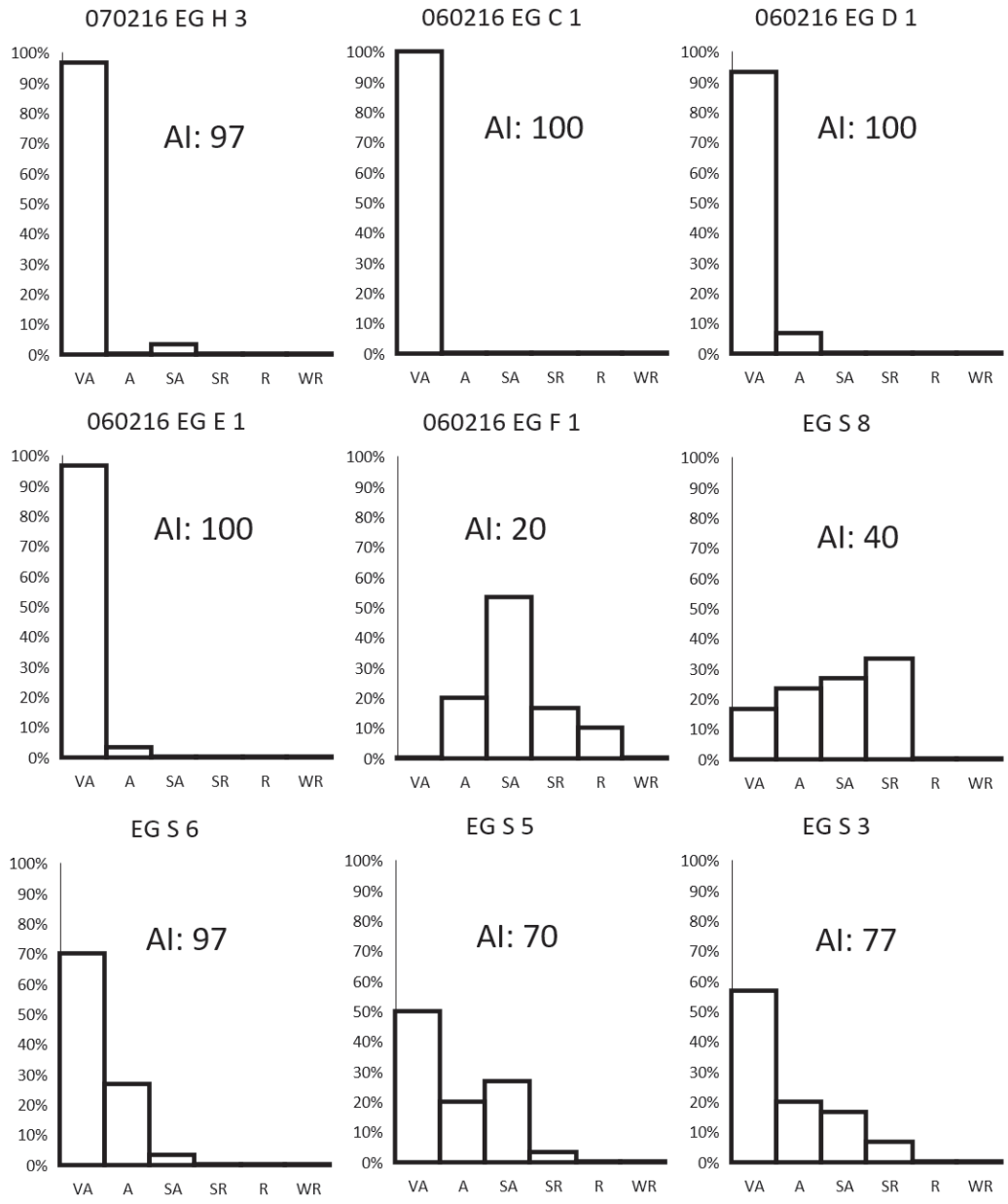

Figure 5.7: Roundness histograms for clast sample locations from Malvora Lake hummocks to Middle Deer Flat.

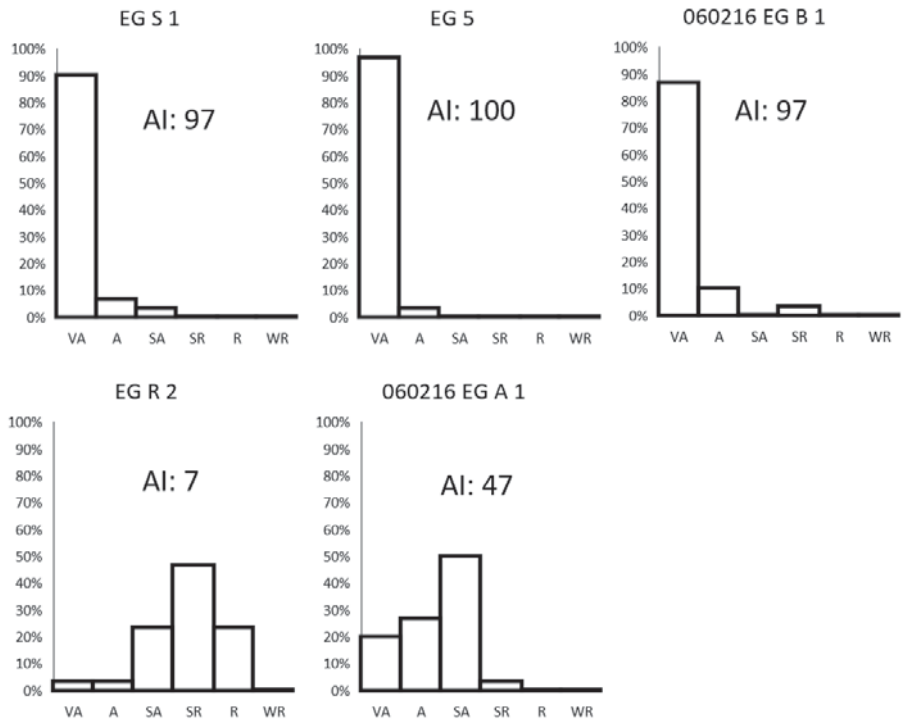

Figure 5.8: Roundness histograms for clast sample locations from Lower Deer Flat to Mirror Lakes.

5.4.2 Microsedimentology

SEM examination of 30 individual whole grains and 30 grain cross-sections from the 14 sites (sites A-N in Figure 4.10) reveals two differing types of overall morphology:

1. Agglomerated grains.
2. Clean grains.

The presence of both grain types supports the hypothesis that the assessed hummocks may have been formed by RA, or a mixture of RA and glacial processes, though none were found to be entirely absent of agglomerated grains. The two morphologies are apparent in Sample A from one of the Malvora Lake hummocks (Figure 5.9). The top left cross-section image shows an 'agglomeration' of many finer grains making up the centre-most grain indicating a possible RA origin. The top right cross-section image is formed by just one grain which is characteristic of glacial deposits (Reznichenko, 2012). The bottom two images show the same characteristics but as whole grains. Where only agglomerated grains are found in a sample, it can be inferred that the deposit has likely been formed by RA processes (e.g. Sample C from one of the Malvora Lake hummocks).

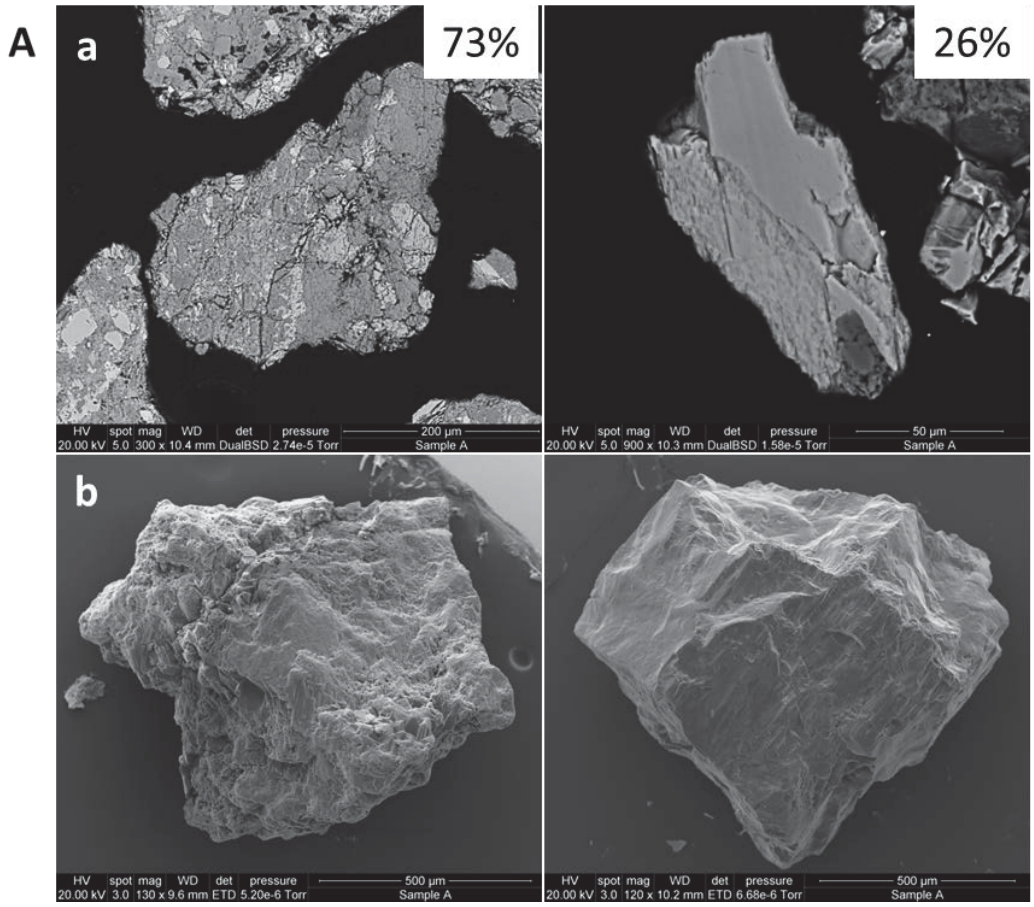

Figure 5.9: Examples of stereomicroscopic examination of sediment between 50 µm and 500 µm from site A - the Malvora Lake hummocks. a) SEM micrographs of the polished grains showing an 'agglomerated' grain on the left and a 'non-agglomerated' grain on the right. The percentage on each cross-section image denotes the percentage of that particular morphology from the 30 sampled grains. b) The SEM image on the left exhibits a rough grain that is heavily coated with agglomerates of finer particles, while the right hand image shows a relatively clean grain.

Where both whole and agglomerated grain types are found (e.g. Samples A, B, D-N; Figures 5.9, 5.10, 5.12 - 5.22), it can be inferred that a combination of RA and non-RA sediment transport processes may be responsible for the formation of the hummocky topography at that location. The relative proportions of agglomerated grains versus non-agglomerated grains can be used to crudely estimate the relative proportions of the processes responsible. The cross-section images for each sample were used to calculate the overall percentage of the two morphology types. The results are displayed as a percentage in Figures 5.9 - 5.22. Samples A and B had a higher proportion of agglomerated grains indicating mostly RA origin, while samples D, H, J, K, and M had higher proportions of clean grains indicating more of a non-RA influence. Samples E, F, G, I, L, and N all exhibited approximately 50% of each type.

Note: The following SEM images are displayed as 'agglomerate' particles in the left column and clean grains in the right column.

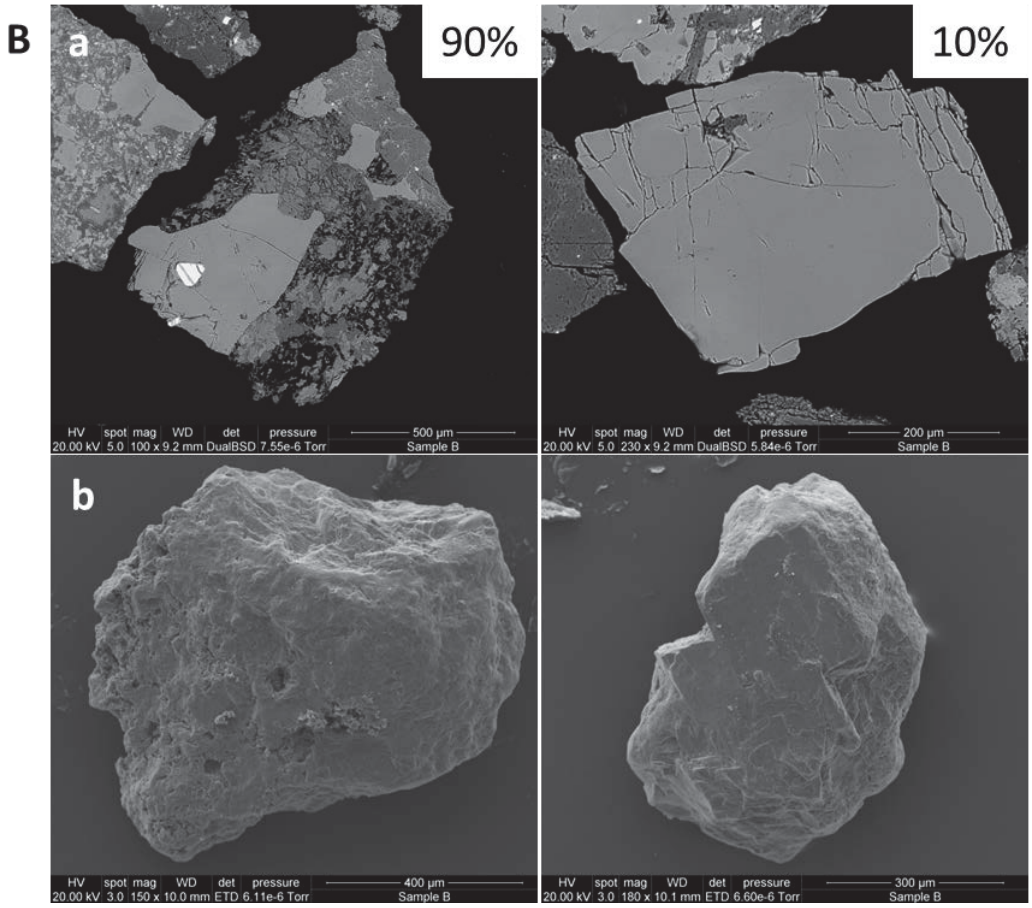

Figure 5.10: Examples of stereomicroscopic examination of sediment between 200 µm and 500 µm from site B - a Middle Deer Flat hummock. a) SEM micrographs of the polished grains from site B. Note the much higher percentage of agglomerated grains in this sample. b) SEM images of the whole grains.

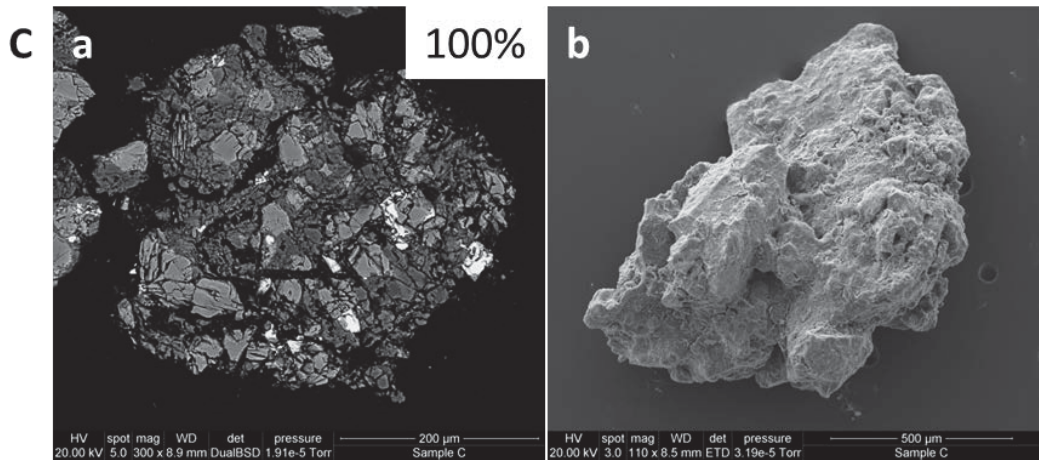

Figure 5.11: Examples of stereomicroscopic examination of sediment between 200 µm and 500 µm from site C - the Malvora Lake hummocks. a) SEM micrograph of a polished grain from site C. Note the entire sample was formed of agglomerates. b) SEM image of a representative whole grain.

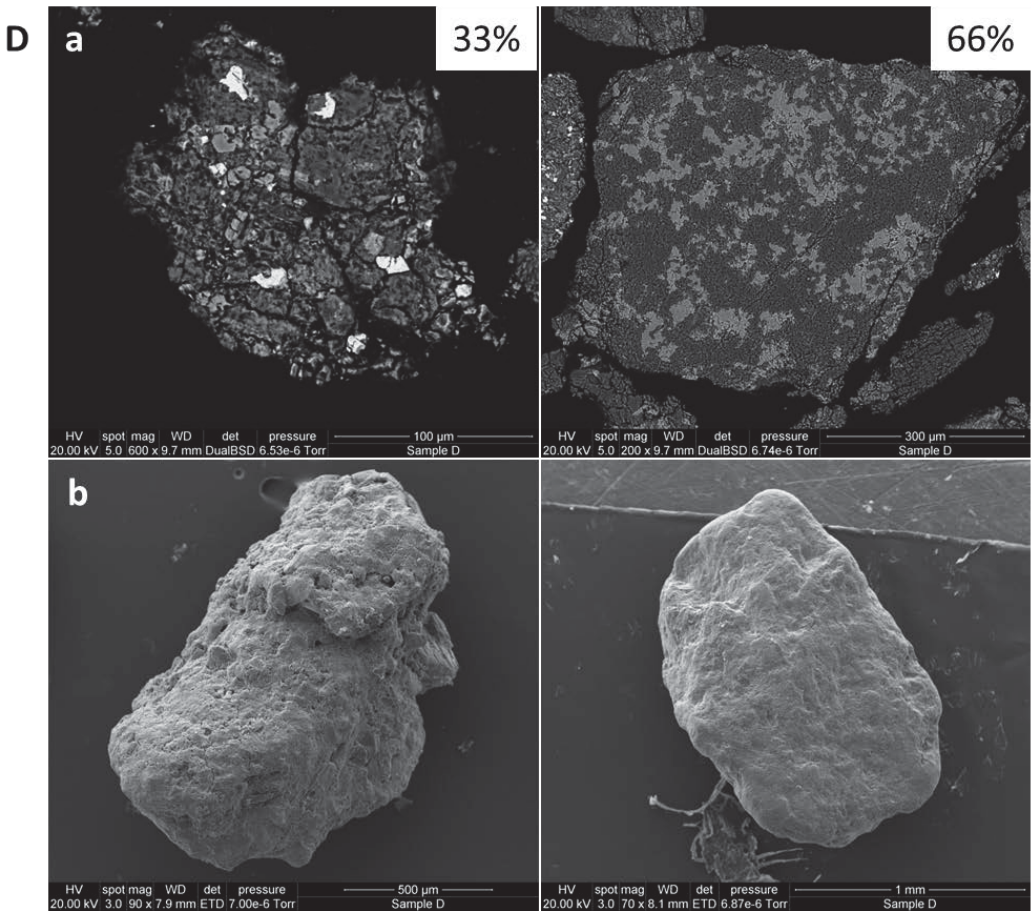

Figure 5.12: Examples of stereomicroscopic examination of sediment between 100 µm and 1 mm from site D - Kiosk Creek Fan. Note the higher percentage of glacial grains in this sample. a) SEM micrographs of the polished grains. b) SEM images of the whole grains. Note the secondary weathering apparent in the lower right grain shown by rounded edges and non-smooth surface.

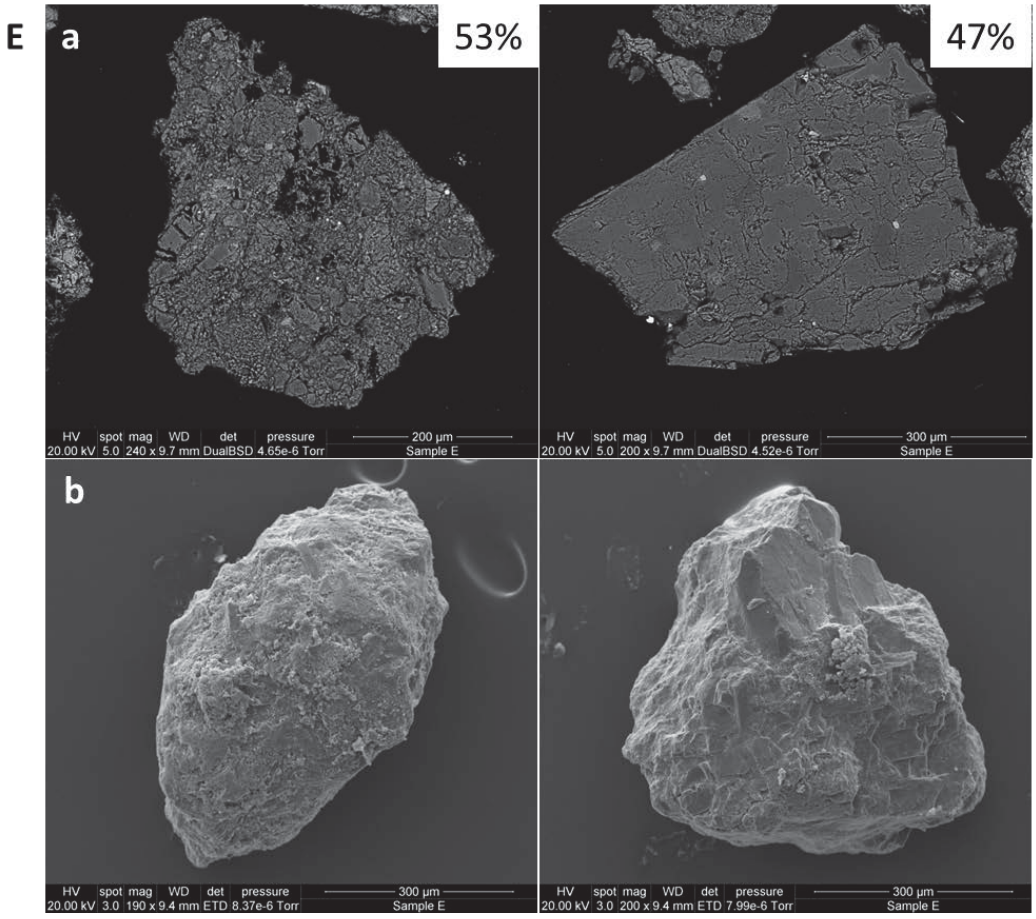

Figure 5.13: Examples of stereomicroscopic examination of sediment between 200 µm and 300 µm from site E - Upper Eglinton Flat. Note the similar percentage of both grain types. a) SEM micrographs of the polished grains. b) SEM images of the whole grains.

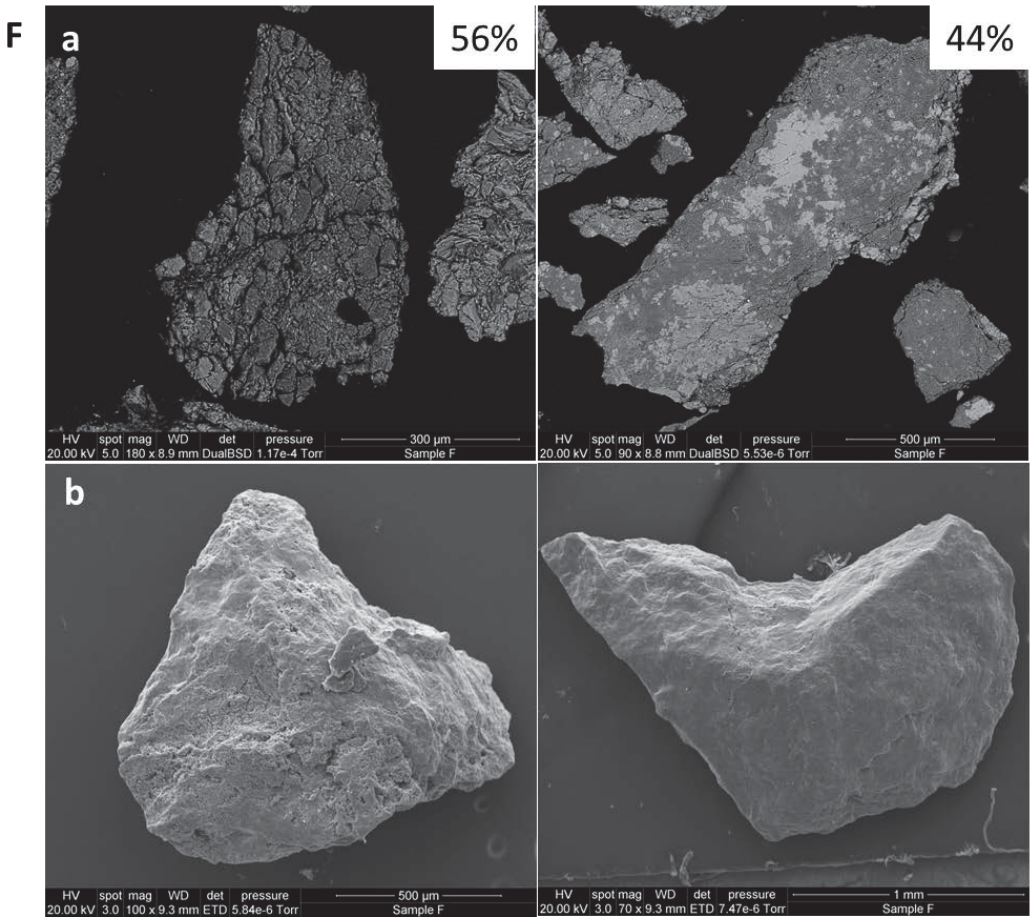

Figure 5.14: Examples of stereomicroscopic examination of sediment between 300 µm and 1 mm from site F - Upper Eglinton Flat. Note the similar percentage of both grain types. a) SEM micrographs of the polished grains. b) SEM images of the whole grains.

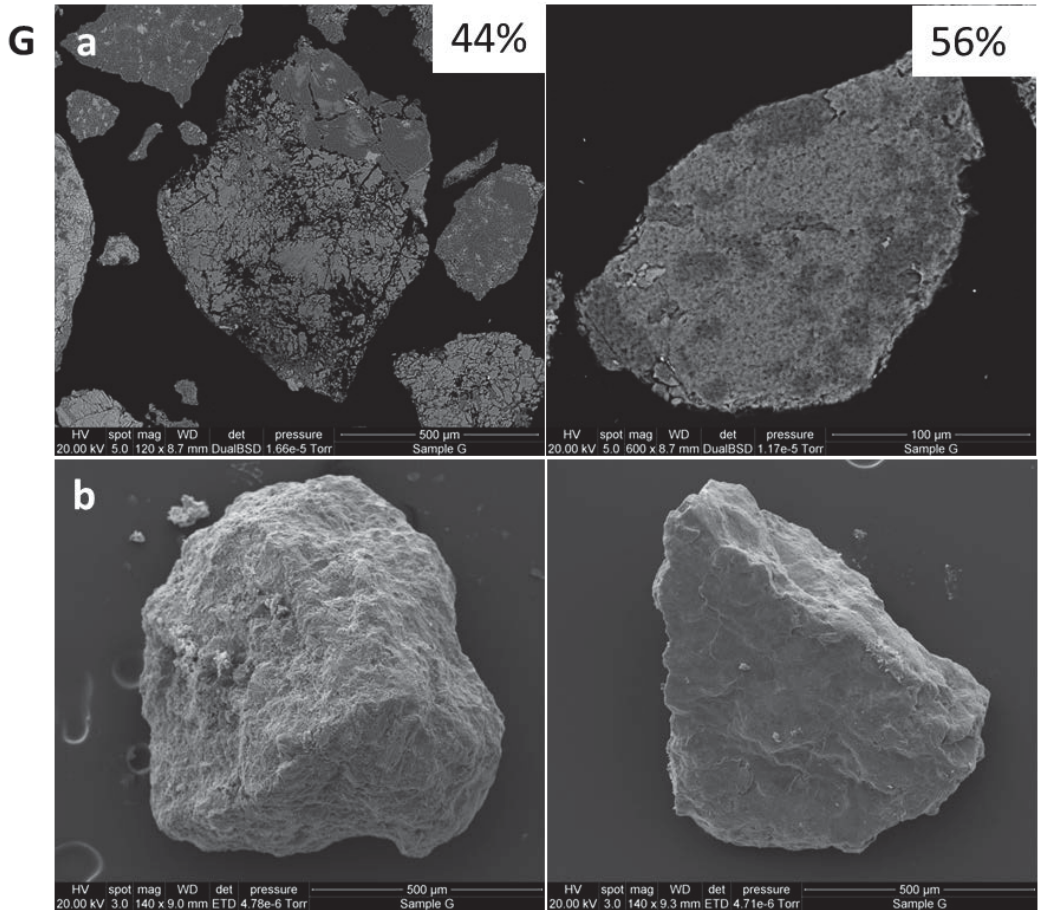

Figure 5.15: Examples of stereomicroscopic examination of sediment between 100 µm and 500 µm from site G - Upper Eglinton Flat. Note the similar percentage of grain types. a) SEM micrographs of the polished grains. b) SEM images of the whole grains.

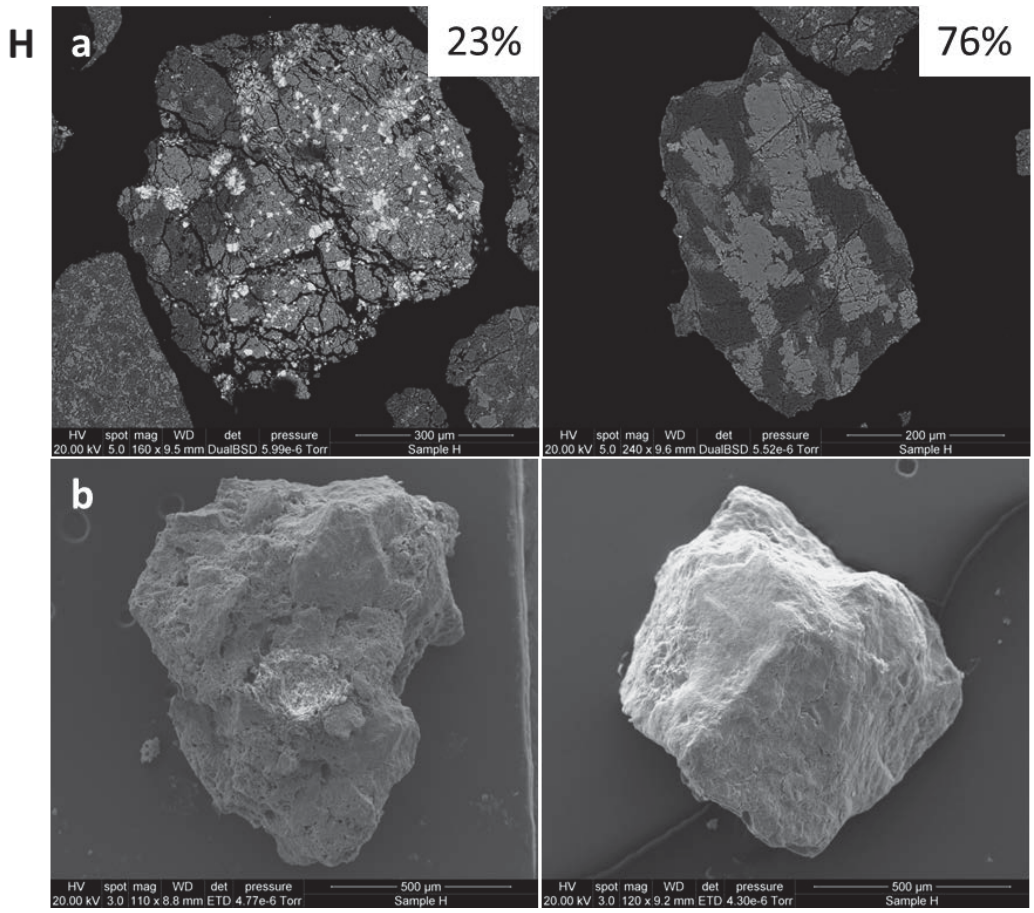

Figure 5.16: Examples of stereomicroscopic examination of sediment between 200 µm and 500 µm from site H - Lower Eglinton Flat. Note the much higher percentage of glacial grains in this sample. a) SEM micrographs of the polished grains. b) SEM images of the whole grains.

In the Lake Gunn Landslide, the percentage of agglomerates found in the samples was not 100% (Figures 5.17 - 5.19) which suggests agglomerates may not always be found in every location within a deposit. 90 individual, <1 mm grains, from within the distal deposits of the Lake Gunn Landslide deposit (Figure 4.11; samples I, J, and K) were observed under SEM while a further 90 grain cross-sections (from the same sample sites) were also observed. Between 26% and 50% of these samples appeared to be agglomerations of some degree, in comparison to sample C from the Malvora Lake hummock (for example) which had 100% agglomerated grains.

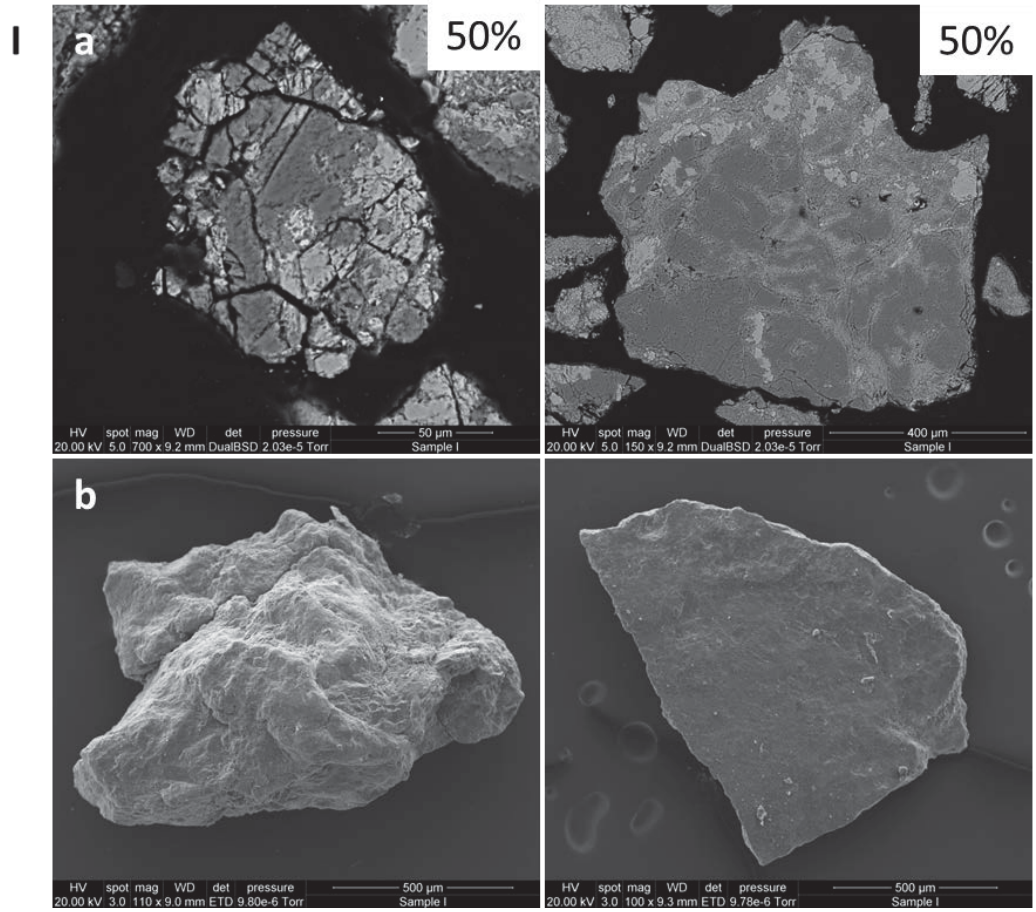

Figure 5.17: Examples of stereomicroscopic examination of sediment between 50 µm and 500 µm from site I - Lake Gunn Landslide. Note the similar percentage of grain types. a) SEM micrographs of the polished grains. b) SEM images of the whole grains.

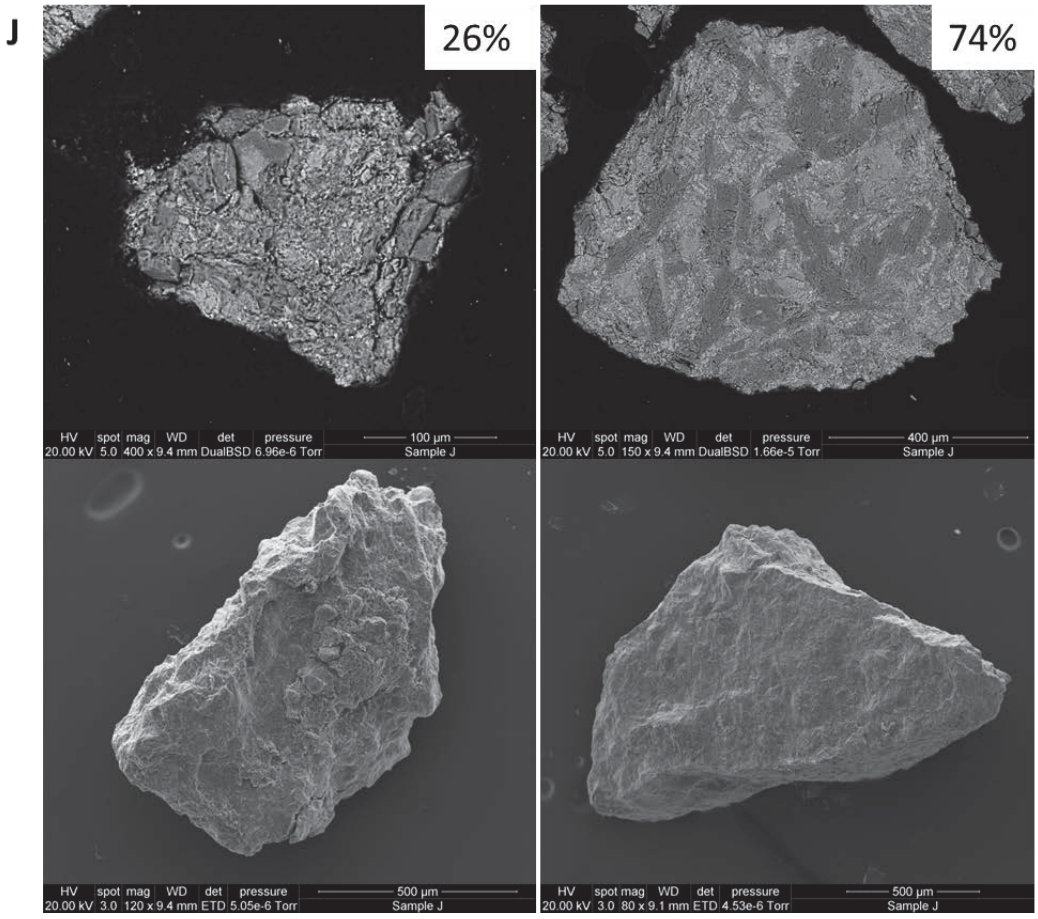

Figure 5.18: Examples of stereomicroscopic examination of sediment between 100 µm and 500 µm from site J - Lake Gunn Landslide. Note the much higher percentage of glacial grains in this sample. a) SEM micrographs of the polished grains. b) SEM images of the whole grains.

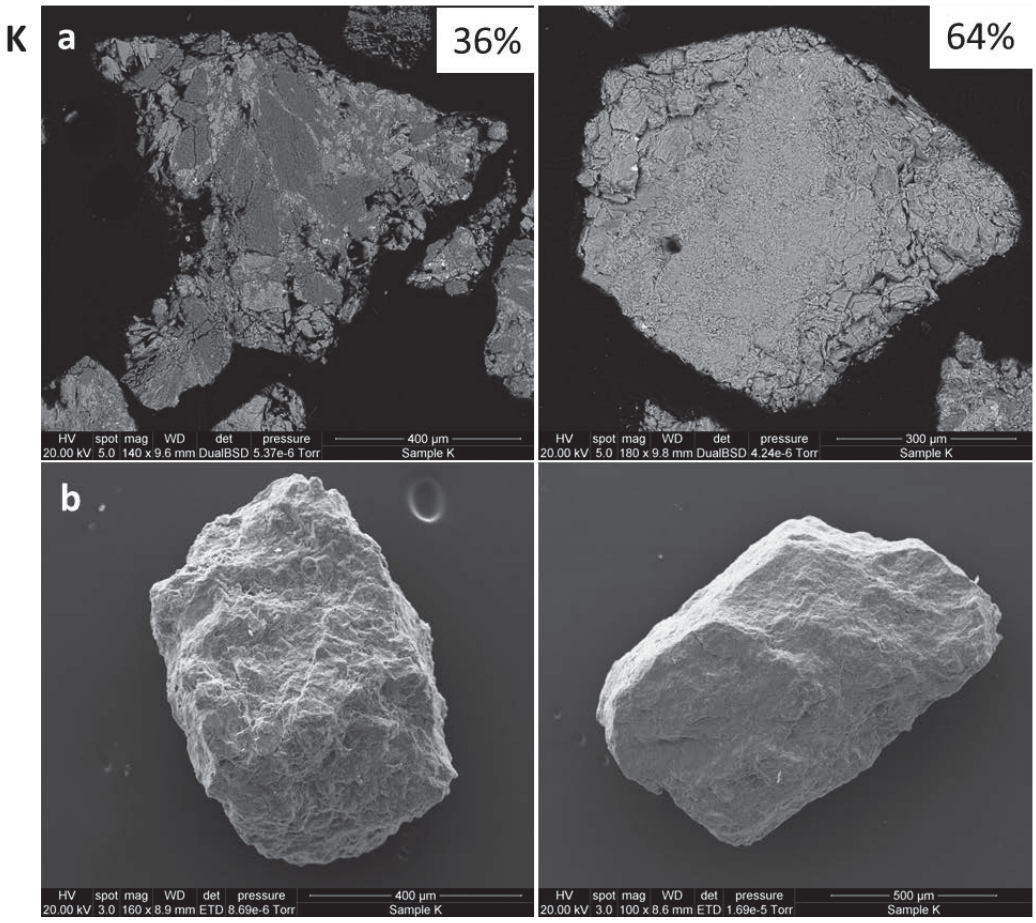

Figure 5.19: Examples of stereomicroscopic examination of sediment between 300 µm and 500 µm from site K - Lake Gunn Landslide. Note the much higher percentage of glacial grains in this sample. a) SEM micrographs of the polished grains. b) SEM images of the whole grains.

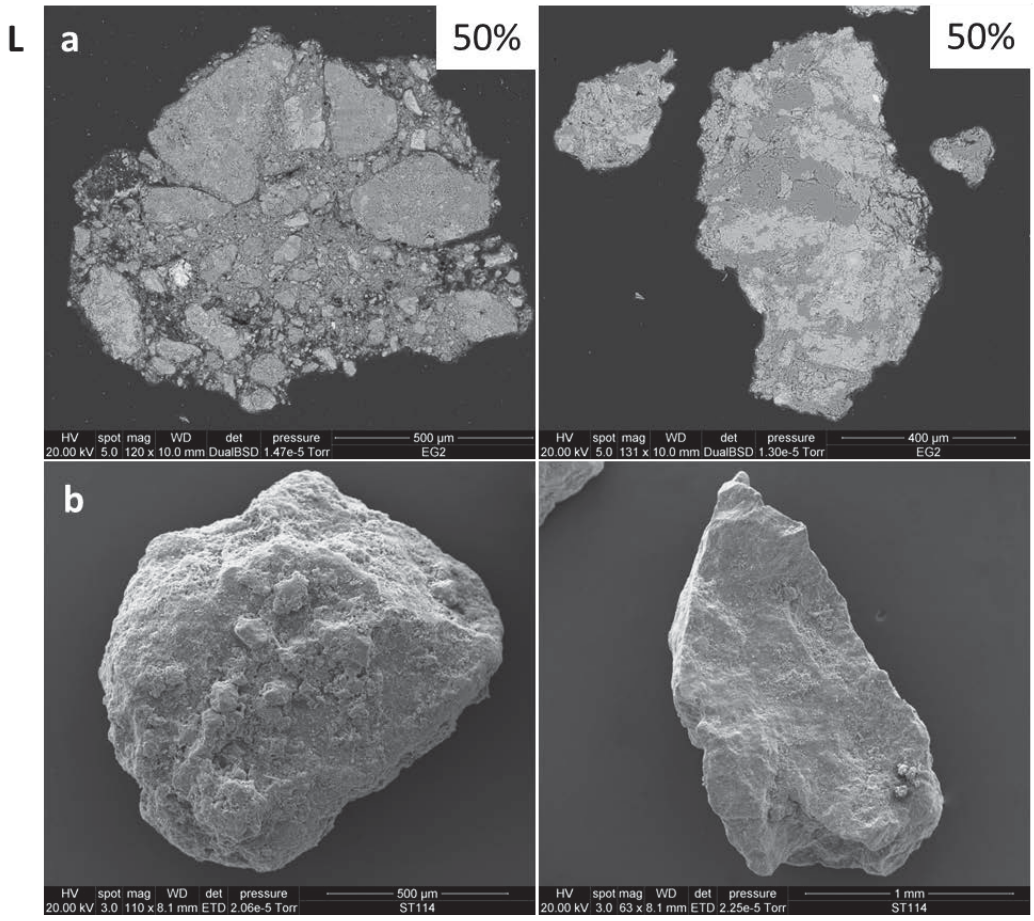

Figure 5.20: Examples of stereomicroscopic examination of sediment between 400 µm and 1 mm from site L - Lower Deer Flat. Note the similar percentage of grain types. a) SEM micrographs of the polished grains. b) SEM images of the whole grains.

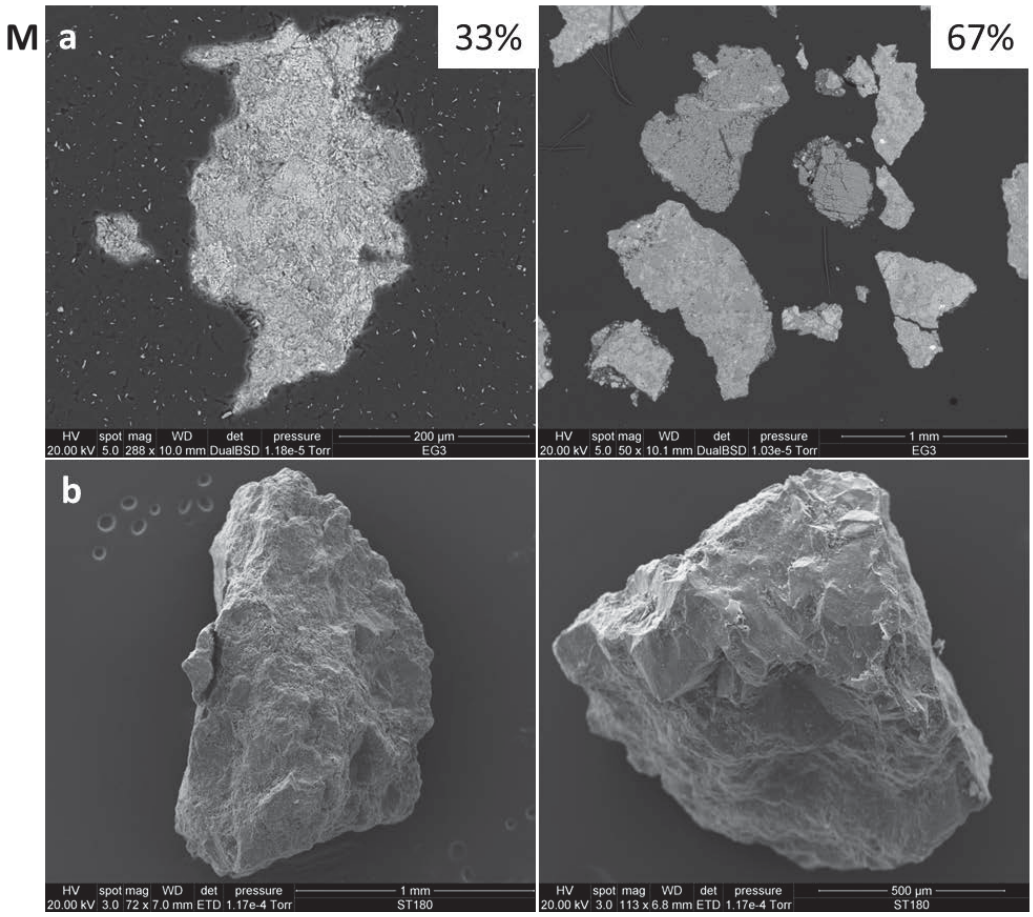

Figure 5.21: Examples of stereomicroscopic examination of sediment between 200 µm and 1 mm from site M - Lower Deer Flat. Note the much higher percentage of glacial grains in this sample. a) SEM micrographs of the polished grains. b) SEM images of the whole grains.

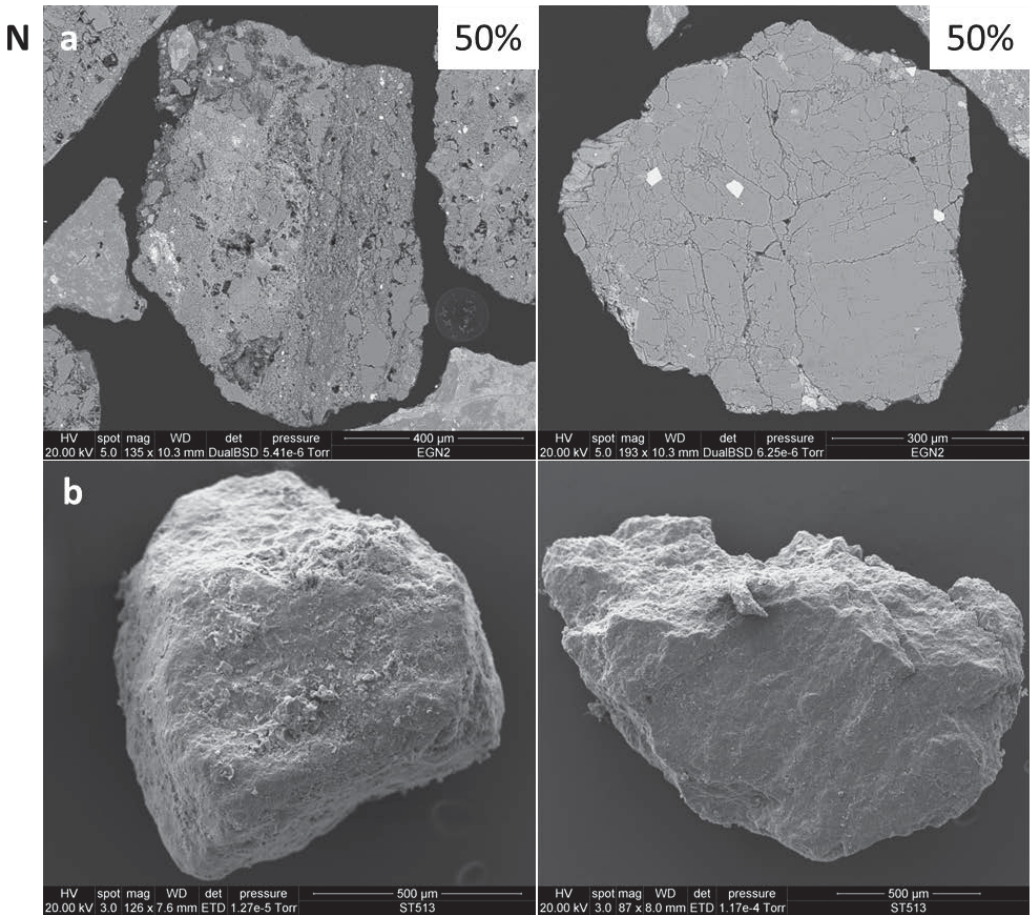

Figure 5.22: Examples of stereomicroscopic examination of sediment between 300 µm and 500 µm from site N - Upper Eglinton Flat. Note the similar percentage of grain types. a) SEM micrographs of the polished grains. b) SEM images of the whole grains.

5.4.2.1 Microtextures

Microtextures are evident on a number of the imaged grains indicating secondary weathering which may relate to time following deposition. For example, in Samples D and I (Figures 5.12b and 5.17), the lower right hand grain is not coated with finer particles, nor does it have smooth, clean faces, which could be a sign of chemical or physical weathering post-deposition (*sensu* Reznichenko, 2012). A number of grains in this study may also exhibit silica precipitation (e.g. samples H and I; Figure 5.23) which is thought to only occur where the grain has been subjected to a fluvial environment (Tiwari et al., 2004). It is important to note that microtextures alone can not be used to differentiate depositional processes as patterns such as conchoidal fractures and rounded edges can be found in fluvial, glacial, and RA environments (Sharp and Gomez, 1986; Tiwari et al., 2004; Reznichenko, 2012).

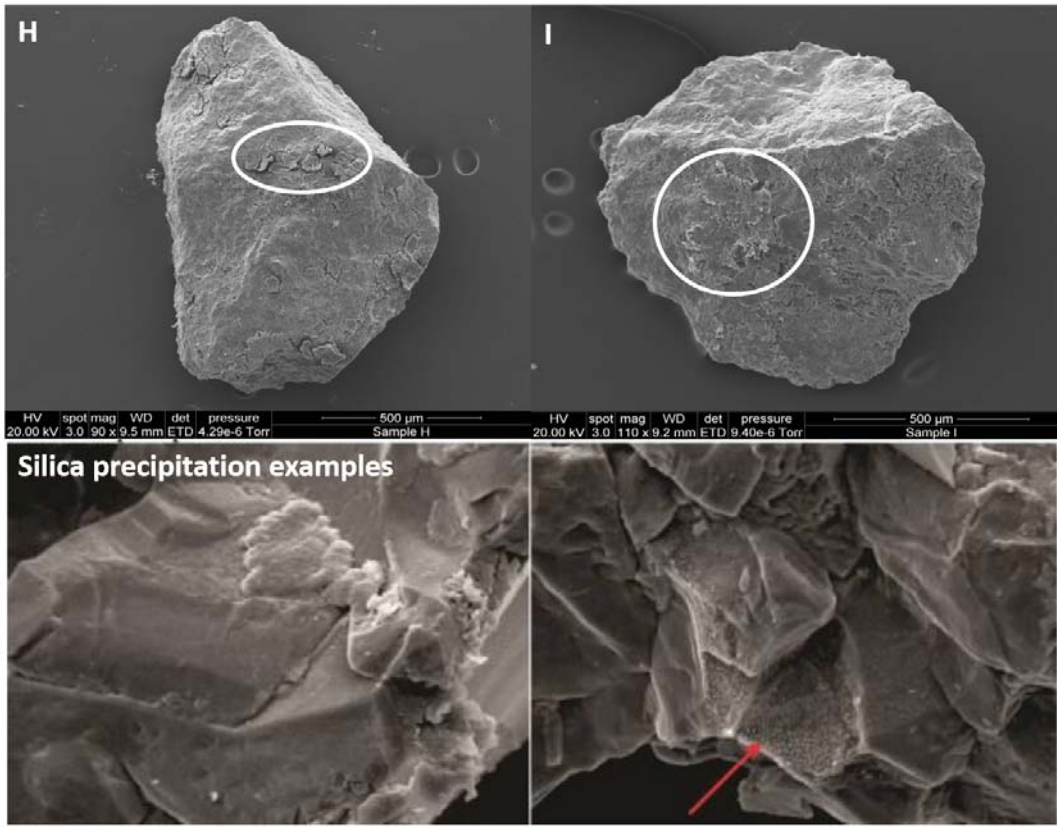

Figure 5.23: Possible silica precipitation on Samples H and I (inside white circles) potentially indicating post-depositional modification in a fluvial environment (Tiwari et al., 2004). The lower two images are examples of silica precipitation from Reznichenko (2012).

It is equally important to note that, in Eglinton Valley, quartz is extremely rare, so all minerals from the samples were used in the identification of agglomerates and microtextures, instead of selecting only quartz as Reznichenko did.

5.5 Lacustrine deposits

Lake deposits are generally formed of fine-grained sediments, indicative of a low-energy depositional environment although many sedimentary structures such as turbidites, wave-ripples, and foresets can be found within lake deposits (Reading, 2009). Coarser material may be found nearer the lake margins where sediment may be actively adding to the lake, or where the deltas are active. During field work, two stratigraphic sections of fine sandy silt were discovered (Figure 5.24). The abrupt sharp contacts with the rounded cobbles below and the distinct lack of sedimentary structures within the silt, suggests these deposits may be paleo-lake sediments. These findings are further discussed in Section 6.3.6.

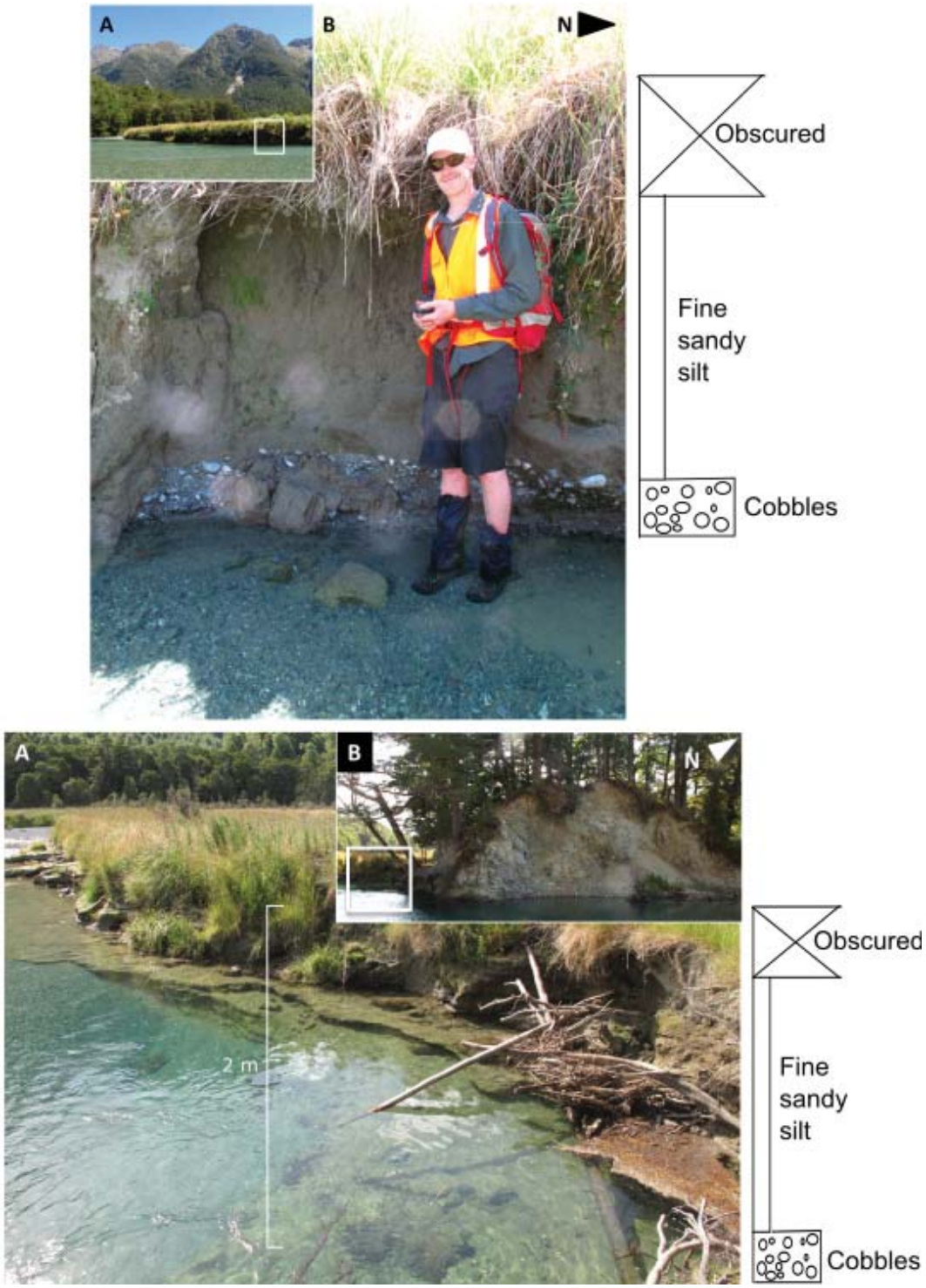

Figure 5.24: Two field sites and stratigraphic columns of where two possible lake sediment sections were found. Adjacent to Malvora Lake (top image) and at the Lower Deer Flat hummocks (lower image). Note the cobbles are clast supported indicating fluvial origin.

5.6 Provenance analysis

This section outlines the results of the provenance analysis and is divided into three subsections: alluvial fans, angular clasts, and rounded-angular clasts. Many of the deposits contain homogeneous, sub- to very-angular clasts that represent the lithologies of the directly adjacent slopes and Eglinton River tributaries. Other deposits contain heterogeneous, sub-rounded to sub-angular clasts indicating larger travel distances from within the wider Eglinton Valley.

5.6.1 Alluvial fans

By analysing the AI together with the clast lithologies, a number of raised surfaces (some currently being truncated by Eglinton River) are confirmed to be the distal reaches of alluvial fans extending out of the eastern ranges. These include the low AI Knobs Flat Fan (samples EG G 1, EG G 2, and EG G 3), relatively low AI Kiosk Creek Fan (samples EG P 2, EG O 1, 070216 EG I 1, and 060216 EG F 1), and low AI Wesney Creek Fan (sample EG R 2). The clasts analysed at these locations consist of rounded to sub-angular clasts with some sample lithologies being heterogeneous and other samples homogeneous. This is to be expected for deposits originating from the eastern ranges as the short streams pass through both the Brooke Street Terrane and the Dun Mountain-Matai Terrane. One sample collected from a road cutting of a fan surface at Mirror Lakes (060216 EG A 1) was steeper than is typical for other alluvial fans in the valley (at ~12-15°)which indicates it was formed by a more rapid debris avalanche-type emplacement (Costa, 1984; Blair and McPherson, 1994) from the short, steep catchment directly above the Mirror Lakes.

5.6.2 Angular clasts

Some clusters of hummocks are made of lithologically homogeneous angular to very-angular clasts that are comparable lithologies to the adjacent valley walls indicating they have only traveled from the valley wall to the valley floor. These include: one hummock at Middle Knobs Flat (samples EG B 2 and EG C 1) and one hummock at Lower Knobs Flat (sample EG E 1) containing clasts of the same lithology as the adjacent Earl Mountains; the hummocks at Upper, Middle, and Lower Deer Flat (also containing Earl Mountain lithologies; samples 060216 EG E 1, 060216 EG D 1, 060216 EG C 1, EG S 8, EG S 3, EG S 5, EG S 6, EG 5, 060216 EG B 1, and EG S 1); and the Malvora Lake hummocks (samples 060216 EG G 1 and 070216 EG H 3).

5.6.3 Rounded - angular clasts

Other deposits contain a range of rounded to very-angular clasts, with homogeneous and heterogeneous lithologies that appear to have traveled from farther up the valley. These are considered to be deposited by glacial processes but may have RA clasts incorporated. These include the Upper Eglinton Flat deposit containing samples

070216 EG J 1a, 070216 EG J 2a, and EG N 1; sample EG H 1; the deposit across the river from Eglinton Flat containing samples 080216 EG M 2 and EG I 1; and the Upper Knobs Flat deposit containing samples EG D 1 and EG D 2.

The clasts from Eglinton River were collected (from the active channel near Deer Flat) to compare lithologies and AI with the hummock clasts in the valley. The river clasts were rounded to sub-angular, there was no sand present in the river, they were all approximately between 4 - 10 cm diameter, and a wide range of lithologies from all over the catchment.

5.7 Hummock ages

Due to unfortunate circumstances beyond the authors control, it was not possible to have TCN ages measured. While this is a key tool in determining the timing of the depositional events involved, other inferences can be made in the mean-time. The high degree of soil development on the hummocks suggests the hummocks are >700 years old.

Chapter 6

Discussion

6.1 Introduction

The purpose of the discussion is to draw together and interpret the observations and results presented. This chapter provides new insights into the geomorphic evolution of the Eglinton Valley during the Holocene, and raises issues and ideas for future research.

6.2 Geomorphology of Eglinton Valley

The results of this study are synthesised in the following three geomorphic maps (that are also included on the supplementary flash drive as the original map size is A2): Figure 6.1 showing the entire Eglinton Valley study site, Figure 6.2 showing the Upper Eglinton Valley, and Figure 6.3 showing the middle Eglinton Valley. Note these are all discussed, in detail, in the following sections.

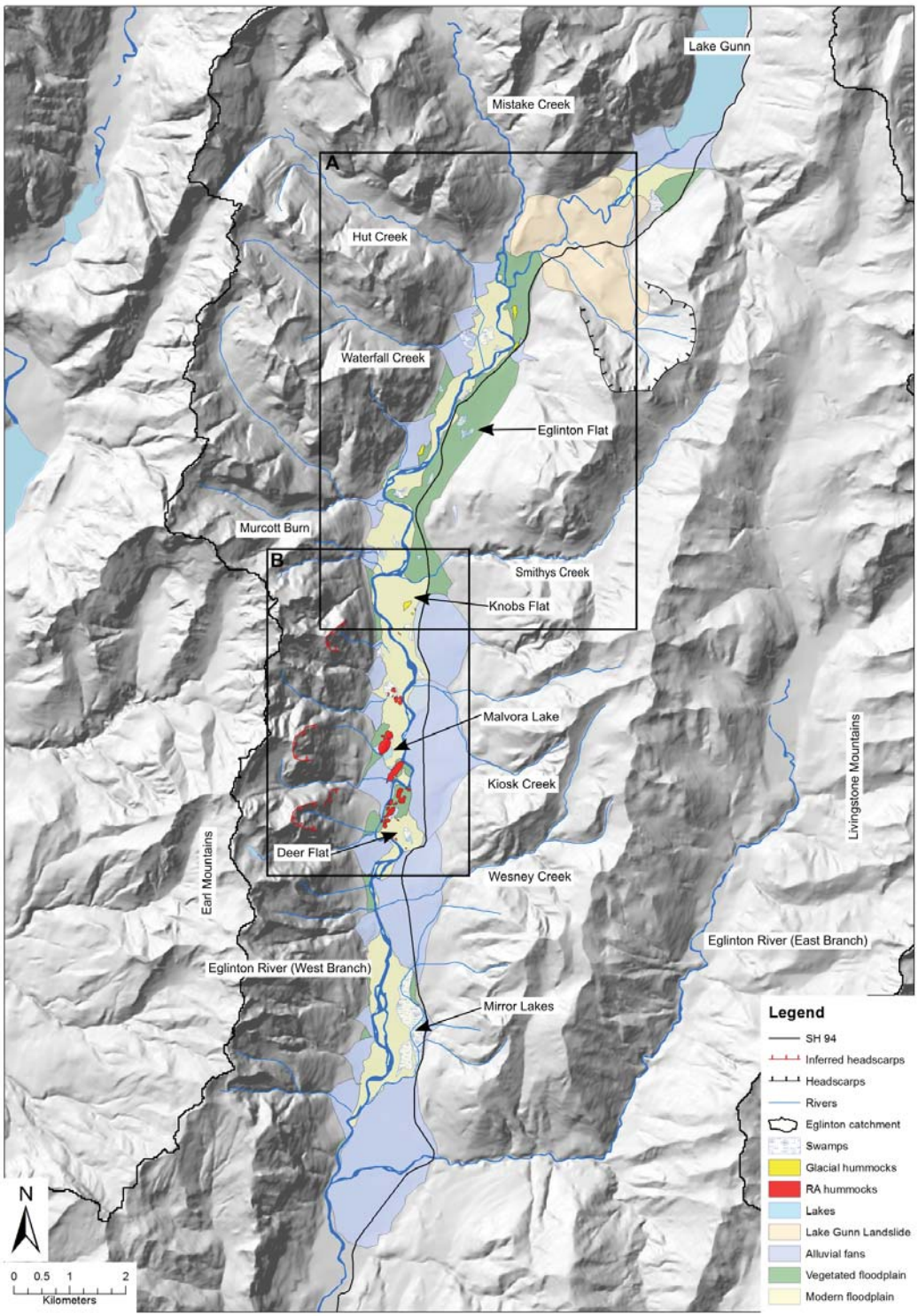

Figure 6.1: Geomorphic map of Eglinton Valley. The study area for this research was from Mirror Lakes to Lake Gunn Landslide. Inset A is the Upper Eglinton Valley study area and expanded in Figure 6.2. Inset B covers Middle Eglinton Valley and is expanded in Figure 6.3.

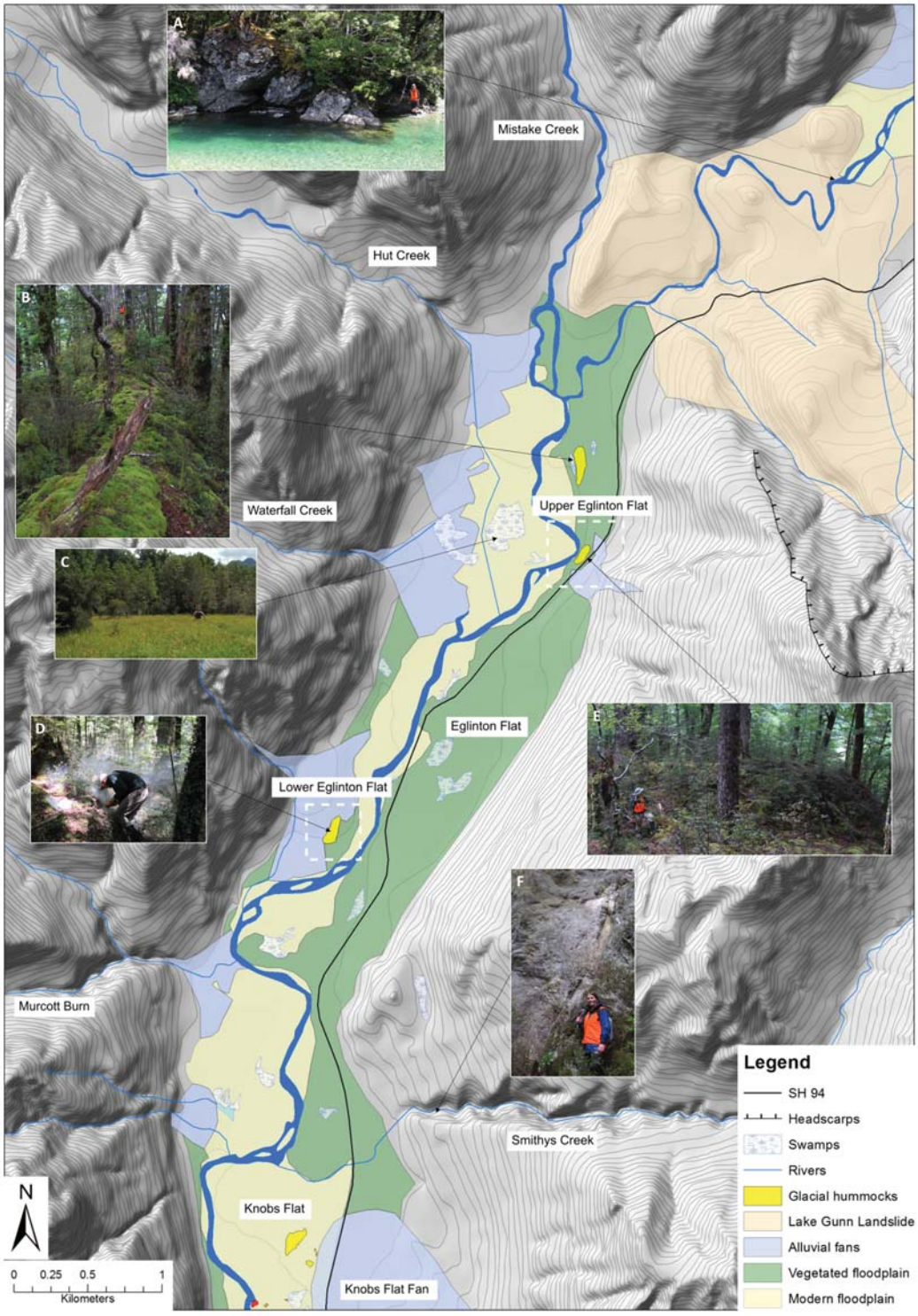

Figure 6.2: Geomorphic map of Upper Eglinton Valley. A) Large boulders deposited by the Lake Gunn Landslide resting in the Eglinton River. B) Elongate ridge of the moraine. C) Swamp with A. Clement for scale. D) Sam collecting TCND samples from the top of the Lower Eglinton Flat moraine. E) A. Clement for scale against the ridge of the moraine. F) Author for scale beside a fault shear zone in Smithys Creek.

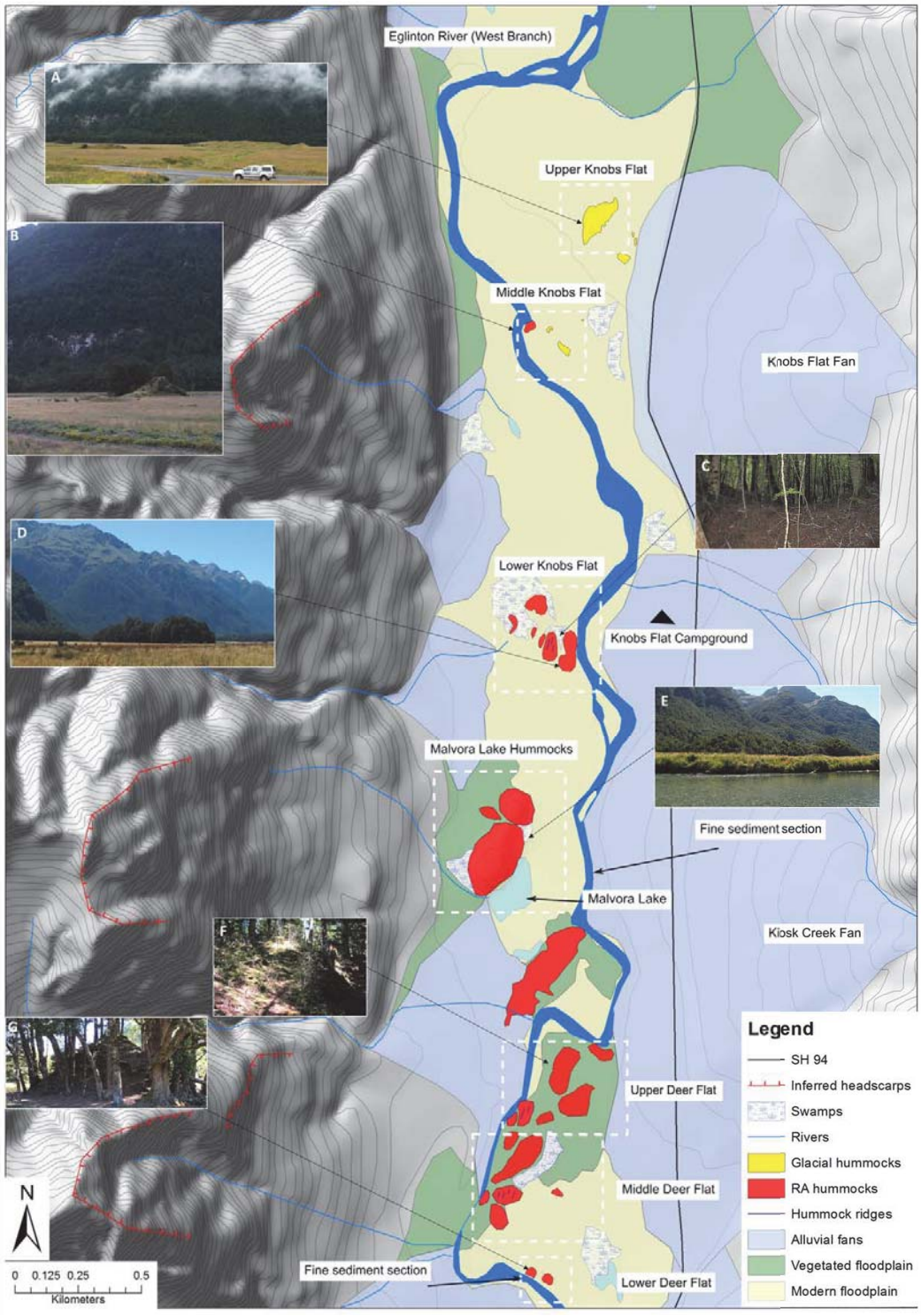

Figure 6.3: Geomorphic map of Middle Eglinton Valley. A) Toyota Hilux for scale at Upper Knobs Flat. B) Middle Knobs Flat RA hummock. C) Ridges on a Lower Knobs Flat RA hummock. D) The Lower Knobs Flat hummocks. E) Malvora Lake hummocks. F) Large RA hummock at Upper Deer Flat with S. McColl for scale in top right. G) One of the two hummocks at Lower Deer Flat.

6.3 Geomorphic evolution of Eglinton Valley

Eglinton Valley has been developed in an active tectonic setting and has previously been affected by glaciations. These tectonic and glacigenic processes continue to influence the mass movement and fluvial processes that are currently conditioning the present day geomorphology of the valley.
Eglinton Valley was glaciated as far as the township of Manapouri, some 50 km down valley from the study area (Figure 3.4), and the ice began to retreat following the LGM (~18 kyrs BP). While there is no direct information as to when the glaciers were completely removed from Eglinton Valley, it is proposed here that this occurred at least 7.6 kya (minimum age of Lake Gunn Landslide; Hancox et al., 2013). Lake Gunn Landslide does not appear to have been substantially remodified by a glacier and this is further backed up by Hancox et al., (2013) who suggests the landslide may have fallen into a lake, based on a chaotic relationship between landslide debris and soft, grey silt found in an exposed river cutting.

6.3.1 Bedrock valley shape

Over tens of thousands of years the differing lithologies on opposite sides of Eglinton Valley allowed glacial, tectonic, mass movement, and fluvial processes to erode and adjust each side of the valley in different ways. The western Earl Mountains are formed of well indurated, igneous and volcanic rocks, allowing this side of the valley to exhibit much steeper (~50-60°) and more stable slopes, however, they appear more blocky than the shallower (~40-50°) eastern slopes which are composed of weaker sandstones, siltstones, and minor igneous rocks. The eastern Livingston Mountains has much smoother topography as the glacial processes were able to grind away the spurs effectively (Figure 6.1). Once the Te Anau Glacier retreated, the entire Eglinton Valley would have been a classic parabolic-shaped valley, primed for further fluvial and mass movement processes to occur.

6.3.2 Paraglacial response of the valley

Major slope failures, alluvial fans, and infilled valleys are widespread throughout the entire Southern Alps and can be indicative of post-glacial topographical adjustment (McColl, 2012). The effect of glaciers on slope stability is well documented with slope failures occurring during glaciations (Smith, 2001; Ambrosi and Crosta, 2006; McColl, 2012; Reznichenko, 2012), during glacial retreat (Haeberli et al., 2002; Fischer et al., 2006), and thousands of years after the landscape has become ice-free (Hancox and Perrin, 2009; Ivy-Ochs et al., 2009; McColl, 2012).

This study has identified several mass movement deposits within the valley that conform to these patterns. The Lake Gunn Landslide and the large, active alluvial fans from Kiosk and Wesney Creeks have probably occurred following deglaciation

(outlined in blue in Figure 6.1). The lithological differences between the eastern and western mountains has likely influenced the size of alluvial fans, with much more erodible sediments being able to form larger fans in the Livingston Mountains. Some of the hummocky deposits that were analysed internally appear to be a mixture of RA and glacial sediments (e.g. Upper and Lower Eglinton Flat deposits shown in Figure 6.2), indicating that the slope failures forming those may have occurred during glaciations and/or glacial retreat. Other analysed hummocky deposits within the valley appear to be formed purely of RA derived sediments (i.e. there is no visible evidence of glacially derived sediments; e.g. Malvora Lake Hummocks in Figure 6.3) indicating that they most likely occurred following glacier retreat.

Although no absolute ages are known for these hummocky deposit events, multiple phases of mass movement activity appear to have affected the Eglinton Valley which conforms to a paraglacial response concept. In particular, there appears to be no evidence of very recent mass movement deposits which supports that these earlier slope failures happened in response to deglaciation and that some of these slopes have become more stable over the longer term.

6.3.3 Origins of the hummocky deposits by location

This study has identified a number of hummocky deposits, primarily in Upper Eglinton Valley that, based on internal sedimentology, overall morphology, and location within the valley, are considered to be moraine. This study has also identified previously unrecognised RA deposits, in particular, at Lower Knobs Flat, Malvora Lake, and Deer Flat.

6.3.3.1 Recessional moraine

Although precise age control on the retreat history of the Te Anau Glacier is not available, morphological indications can be used to estimate the retreat rate of the glacier. During a slow recession larger moraines are expected, given enough available sediment which is common in the Southern Alps. At the foot of Eglinton Valley, where it enters Te Anau Valley (and outside of the study area), there appears to be a large recessional moraine, spanning the width of Eglinton Valley with hummocky topography up to ~100 m above the modern floodplain (Figure 6.4). The geology of this feature has been mapped as undifferentiated Quaternary till which support the moraine theory, and also includes minor mudstone and sandstone of the Waiau Group (Turnbull, 2000) which predominantly outcrops in the Te Anau Basin. This study tentatively suggests this moraine may be indicative of the culmination of the ACR *c.* 13 kya (Putnam et al., 2010).

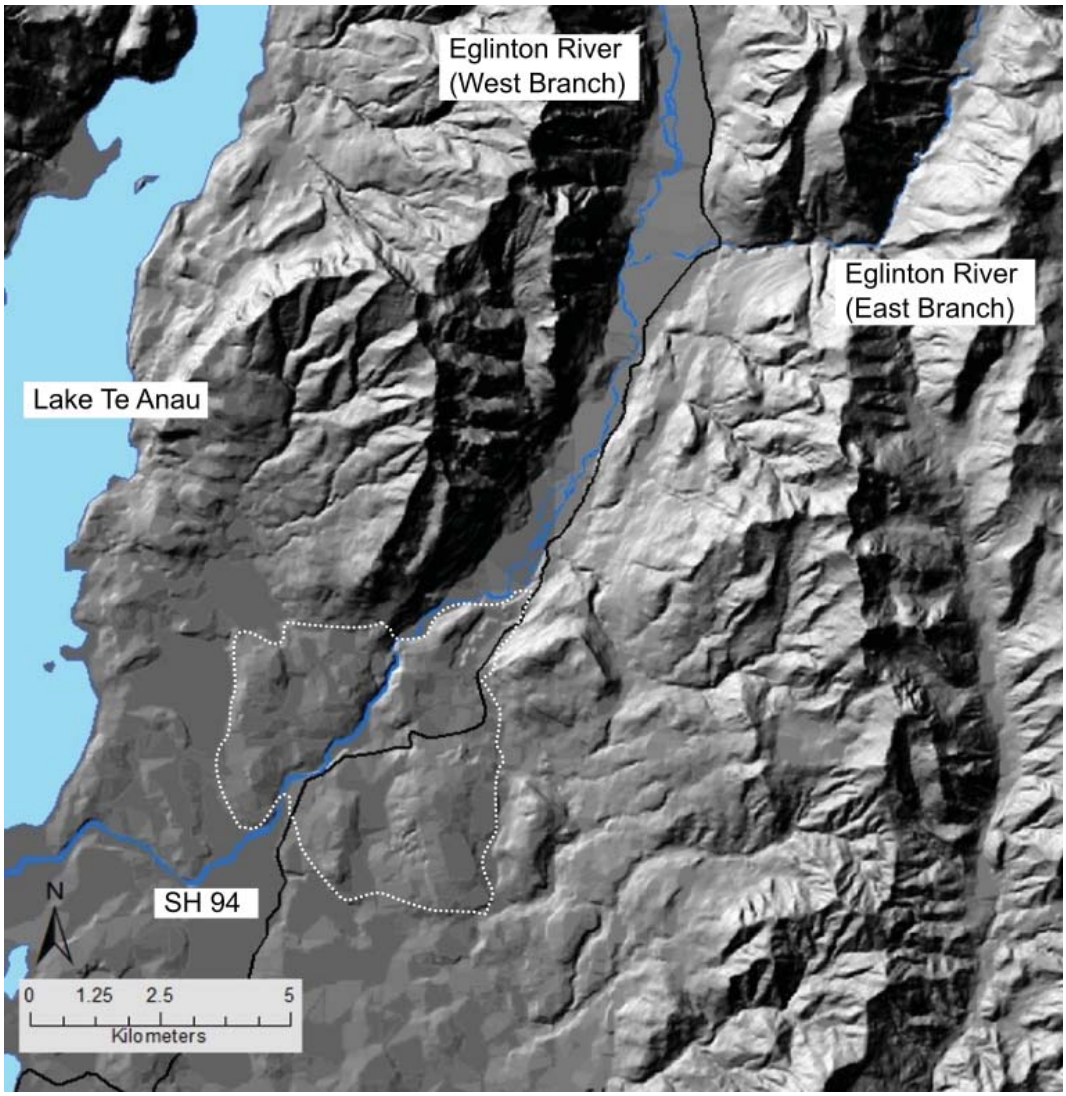

Figure 6.4: Map of Lower Eglinton Valley and Lake Te Anau. White dotted line outlines a potential recessional moraine at the foot of Eglinton Valley. Basemap NZ Terrain Relief from (LINZ, 2014).

6.3.3.2 Eglinton Flat deposits

The heavily vegetated hummocky topography found at Upper and Lower Eglinton Flat is considered to be moraine that was deposited more than 7.6 kya but no later than 13 kya, based on the inference that the Lake Gunn Landslide occurred following glacier retreat from this location. Upper Eglinton Flat lies in the upper reaches of the study area (Figure 6.1). South of this lies Eglinton Flat, with the *c.* 5 kyrs Eglinton Bog nestled among an undulating series of low (<14 m high) ridges that have previously been suggested to be of glacial origin (Valkengoed, 2011). Across the river and a little further south is Lower Eglinton Flat.

This current study did not investigate Valkengoed's deposits though it did explore similar morphological features in Upper Eglinton Flat and across the river, at Lower Eglinton Flat (Figure 6.2 B, D, E). The studied deposits are all considered to be moraine as the clast shape and lithology, geomorphic analysis, and agglomerate identification all provide evidence of glacially transported sediments. The clasts measured are a mixture of sub-angular to very angular and the agglomerate percentage in most samples was ~50% (Table 6.1), indicating that there is RA sourced material (transported from further up the valley) mixed within glacial till. The lithologies are a mixture. In particular, sample EG H 1, included clasts from the Murihiku Terrane, which outcrops on the eastern shore of Lake Gunn (Figure 3.2). The mixture of microsediment is visible in Figure 4.12 that shows close-ups of the internal structure of one of the exposed ridges where there is fine-grained glacial till interwoven with angular clasts.

Table 6.1: Hand specimen and microsediment analysis collected from two hummocks at Upper Eglinton Flat and one at Lower Eglinton Flat. Note that the higher the AI, the more angular the sample is.

Sample name	Angularity Index (AI)	Agglomerate (%)	Lithology
Hand specimen			
Upper Eglinton Flat			
EG H 1	27	-	Dun Mountain, Caples, Murihiku
EG N 1	100	-	Brooke Street
070216 EG J 1a	47	-	Median Batholith 2, Brooke Street
070216 EG J 2a	93	-	Median Batholith 2, Brooke Street
Lower Eglinton Flat			
080216 EG M 2	73	-	Brooke Street
EG I 1	50	-	Brooke Street
Agglomerates			
Upper Eglinton Flat			
E	-	53	-
F	-	56	-
G	-	44	-
N	-	50	-
Lower Eglinton Flat			
H	-	23	-

6.3.3.3 Knobs Flat deposits

The data suggests that the hummocks at Upper and Middle Knobs Flat are of glacial origin with one stand-alone hummock in Middle Knobs Flat being a RA deposit (Figure 6.3 A, B). The hummocks at Lower Knobs Flat are considered to be of RA origin. All of the Upper and Middle Knobs Flat hummocks (except the RA deposit) are relatively low profile (e.g. extending no more than 5 m above the floodplain) and are generally aligned with the long axis leading down the valley (Figure 6.5). A number of these hummocks have a relatively steep side (~30-40°) indicating potential modification by the Eglinton River as it wound its way through the hummocks in the past. Morphological evidence viewed on the GPR radargram (Figure 5.3) of fine-grained slack-water deposits found within the floodplain suggests it has built up post-Lake Gunn Landslide formation (further discussed in Subsection 6.3.6. The floodplain now obscures the full size, extent, and original deposit morphology of the Knobs Flat hummocks and this study has been able to determine that two of the Upper Knobs Flat hummocks extend at least 5 m below the modern floodplain (Figure 5.3) but fails to identify any exact depth of lateral extent below the surface.

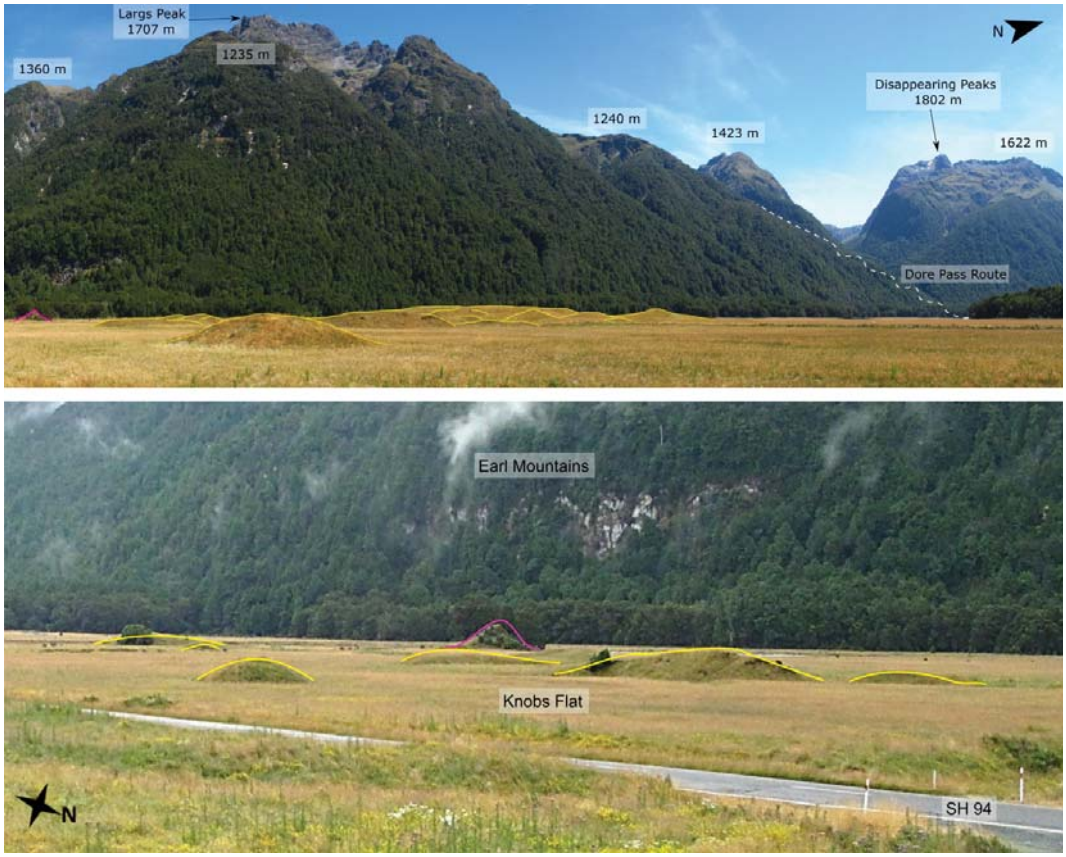

Figure 6.5: The hummocks at Upper Knobs Flat (top) and Middle Knobs Flat (bottom). Yellow lines outline the glacially derived hummocks while the purple line outlines the singular RA deposit. Note: the lower left-most hummock in each image is the same hummock.

It may be of interest to perform GPR on the smaller Middle Knobs Flat hummocks in an attempt to determine their spatial extent below the surface. This would give an insight as to whether they are small individual deposits or one large deposit as this difference can be used to determine how long a glacier may have had to pause at this location to deposit the sediments involved. This information could then be used to help broaden the knowledge of the climatic patterns within the Eglinton Valley over time.

The very low AI and mixed lithologies of the samples (EG D 1 and EG D 2; Table 6.2) collected from within the largest, sprawling Upper Knobs Flat hummock (outlined in yellow in the top-centre image of Figure 6.5) indicates transportation from at least 30 km farther up-valley. Sample EG D 2 is mostly composed of Caples lithologies (with some Median Batholith 2 included). The closest outcrop of Caples is ~30 km north of Knobs Flat, where the Alisa Mountains reach near the valley floor in the Hollyford Valley. The Hollyford Valley is within a different watershed, with the Hollyford River draining to the West Coast, however, The Divide (the pass between the Eglinton Valley and the Hollyford Valley) is only 532 m.a.s.l. This suggests that the Te Anau Glacier did not originate within the Eglinton Valley, instead, it was much larger and acted more like an ice cap (i.e. Was sufficiently large enough to flow over topography between catchments as shown in Figure 2.6) when the climate was at its coolest.

Table 6.2: Eight hand specimen samples collected from hummocks throughout Knobs Flat including Knobs Flat Fan. Note that the higher the AI, the more angular the sample is.

Sample name	Angularity Index (AI)	Lithology
Knobs Flat Fan		
EG G 1	13	Brooke Street
EG G 2	7	Brooke Street/Dun Mountain - Matai
EG G 3	20	Brooke Street
Upper Knobs Flat		
EG D 1	13	Median Batholith 2
EG D 2	0	Caples
Middle Knobs Flat		
EG B 2	100	Median Batholith 1
EG C 1	97	Median Batholith 1
Lower Knobs Flat		
EG E 1	100	Median Batholith 1

The data suggests the hummock outlined in purple in Figure 6.5 in Middle Knobs Flat is probably derived from a RA. It has very high AI's, is same lithology as the adjacent Earl Mountains (Table 6.2), and its morphology differs markedly to the other hummocks at Knobs Flat. It stands approximately 10 m above the current river level, has a relatively sharp ridge along the top, extends perpendicular to the main valley, has a small ~1 m high 'tail' trailing 8 m to the east, and contains very large boulders (one of which was selected for TCND). These features all indicate this hummock has formed through a different process to the other Upper and Middle Knobs Flat hummocks. The internal structure shows a large jigsaw-fractured clast with many other angular clasts (Figure 6.6) which is highly-indicative of a fast emplacement and commonly found in RA deposits (Davies et al., 1999). Performing GPR over and around this hummock may be able to determine any subsurface morphology indicating possible radiating of the deposit away from the Earl Mountains. In addition, analysing microsediment from within the hummock to see if agglomerates are present would help determine whether it was emplaced by a RA or different mass movement process.

Figure 6.6: Internal structure of the RA-derived hummock at Middle Knobs Flat. The solid white line indicates the approximate outline of a largely intact boulder, while the dotted lines outline angular, jigsaw-fractured clasts that were more than likely part of the original boulder. The fine, light-brown material on top is soil that measured approximately 1 m deep. A5-sized field notebook for scale.

The cluster of hummocks at Lower Knobs Flat are very prominent, conical features on the floodplain (and outlined in Figure 3.8) and appear to be RA deposits (Figure 6.3 D). One of these hummocks has a series of small undulating ridges running parallel to the main valley that are considered compressional ridges that can

occur as a RA slows prior to deposition. Soil and vegetation was very well established on these hummocks, limiting sample availability. Clast sample EG E 1 was all very angular and the same lithology as the adjacent Earl Mountains. As only one sample was able to be collected, it is inferred that the other hummocks in very close vicinity (Figure 6.3) are formed of the same material.

6.3.3.4 Deer Flat and Malvora Lake hummocks

The hummocky topography at Deer Flat is radiating away from the Earl Mountains and the visible deposits spread (north-south) approximately 1 km (Figure 6.3. The largest hummocks found throughout the entire study area are located here. The overall AI is very high (in particular at Upper and Lower Deer Flat; Table 6.3), indicating either a short travel distance by mass movement, or passive transportation within the glacial system. However, the samples collected from Middle Deer Flat (and in particular EG S 8; see Table 6.3) have slightly lower AI's which could be explained by a number of processes. These include active transport within a glacier, fluvial rounding, or the clasts could be more easily weathered due to their lithology. Without access to a decent exposure of the internal sedimentological structure (e.g. to identify any possible fluvial sorting), it is difficult to rule out fluvial or glacial rounding. However, the majority of sample EG S 8 was tuffaceous sandstone, a soft and readily-erodible rock type (outlined in Section 3.2), that may have occurred as an isolated outcrop on the hillslope above. This study suggests the rounding is a product of post-depositional modification (i.e. weathering) and that the Upper, Middle, and Lower Deer Flat deposits are all from the same RA event.

Table 6.3: Ten hand specimen samples collected from hummocks throughout Deer Flat and two from the nearby Malvora Lake hummocks. Note that the higher the AI, the more angular the sample is.

Sample name	Angularity Index (AI)	Lithology
Upper Deer Flat		
060216 EG E 1	100	Median Batholith 1
060216 EG D 1	100	Median Batholith 1
060216 EG C 1	100	Median Batholith 1
Middle Deer Flat		
EG S 8	40	Median Batholith 1
EG S 3	77	Median Batholith 1
EG S 6	97	Median Batholith 1
EG S 5	70	Median Batholith 1
Lower Deer Flat		
EG S 1	97	Median Batholith 1
EG 5	100	Median Batholith 1
060216 EG B 1	97	Median Batholith 1
Malvora Lake hummocks		
060216 EG G 1	80	Median Batholith 1
070216 EG H 3	100	Median Batholith 1

The overall lithology of all of the clasts analysed at Deer Flat and Malvora Lake is Median Batholith 1; the principal rock type of the Earl Mountains directly adjacent to the deposits. Median Batholith 1 makes up the entire western mountain range in this location so it is entirely possible that the clasts within these hummocks could have originated from anywhere along the Earl Mountains. However, there is strong evidence to suggest that these hummocks have originated from a slope failure from the slopes immediately adjacent. This evidence includes the very high AI's measured, the overall radiating morphology of the hummocks (described in Section 5.2), and the identification of potential failure zones on the adjacent slopes (Figure 6.3).

The large (<50 m high) hummocks at Malvora Lake could also be an extension of the radiating Deer Flat RA deposit as they appear to radiate away from the same source point. However, another source area can be seen on the hillslope directly adjacent to them (Figure 6.3 E). As the lithology is the same it is difficult to determine

which of these scenarios can explain the formation of the Malvora Lake hummocks. This was the only location in the entire valley where agglomerated particles made up 100% of the microsediment analysed. This, along with the very high AI, overall morphology, and similar lithology to the adjacent hillslope undoubtedly suggests a RA origin for these hummocks. The large elongate hummock between Malvora Lake and Upper Deer Flat (shown in Figure 6.3) is proposed to also be RA deposit as it is strikingly similar in morphology to the Malvora Lake and Deer Flat hummocks. No clast or microsediment samples were collected due to thick soil development.

The largest and most visible exposure of the internal structure of the hummocks in Eglinton Valley is found at Lower Deer Flat (Figure 6.3 G) where the Eglinton River has exposed a large section. Figure 6.7 highlights a textbook example of jigsaw fractured boulders within a fine-grained matrix. The internal structure and morphology of this conical hummock, and the morphologically similar hummock next to it, features all seven features used in distinguishing a RA deposit from another form of deposit (see Subsection 2.2.3.3 for a more detailed description). Fragmented clasts are visible, source-rock structures can be seen, the lithology is monolithic, the clasts are all angular to very angular, agglomerates are identified in the microsediment, the photo appears to show a slight presence of a coarse carapace, and a source scar can be identified on the adjacent hillslope.

Figure 6.7: Internal structure of the RA-derived hummock at Deer Flat. The solid lines indicate the approximate outline of largely intact boulders, while the dotted lines outline angular, jigsaw-fractured clasts that were more than likely part of the original boulder. Dotted red lines indicate possible shear zones and Red stars show location of microsediment samples L and M.

While these factors undoubtedly suggest that the Lower Deer Flat hummocks are a RA deposit, the percentage of agglomerated particles in the two samples collected from within one of the hummocks initially suggests otherwise. Sample L is formed of 50% agglomerate and 50% clean grains, while sample M is formed of 33% agglomerate and 67% clean grains. This leads to the predicament of 'what percent of a microsediment sample will exhibit agglomerates if it is purely RA derived?'. This question is currently untested in the literature, and, all other clast and morphological data from these particular hummocks suggests a RA origin. Therefore, this study confirms that a microsediment sample does not need to be 100% agglomerated grains for it to be purely RA derived. This is further elaborated on in Section 6.4.

The internal clast structure of the Lower Deer Flat hummock is very similar to the Knobs Flat hummock. The difference lies in the soil formation. Knobs Flat hummock has approximately 1 m of soil on top of the fractured boulder (shown in Figure 6.6). There is a possibility this soil has slumped down, however, it is still a large amount of soil to build up over time. The Lower Deer Flat hummock, however, only had ~30 cm of soil on top (Figure 6.7), suggesting it is younger than the Knobs Flat hummock.

6.3.4 Alluvial fan formation

A number of alluvial fans have built up within the Eglinton Valley (Figure 6.1). The retreat of the Te Anau Glacier has provided accommodation space for sediment from the tributaries to be stored in Eglinton Valley. This is commonly seen globally (Ryder, 1971; Ballantyne, 1995; Harvey, 2002) though the length of time that a fan will continue aggrading is dependent on the up-valley sediment and water availability. Many studies highlight the key point that paraglacial alluvial fans generally cease aggradation within a few millennia of deglaciation and are then subject to fan-head incision (e.g. Ryder, 1971; Ballantyne, 2002). Addressing the mapped alluvial fans within Eglinton Valley (notably Knobs Flat, Kiosk, and Wesney fans; Figure 6.1), there was no fan-head incision or terraces cut within the fans, as would be expected in a setting like this. This study suggests the current alluvial fans were initiated following deglaciation, ceased forming at least a few hundred years ago (based on being well vegetated), and are now acting as fluvial and sediment transport pathways as opposed to actively aggrading or degrading.

Down-valley, and beyond the study area, the East Branch of the Eglinton River flows into the main valley through an incised gorge and has a major alluvial fan associated with it (Figure 6.1). The fan is raised ~30 m above the modern West Branch (of Eglinton River) floodplain and is where the major tourist buses stop for a view up the Eglinton Valley. Where the East Branch exits the gorge, and SH 94 crosses the river, there are five visible, grassy, terraces, each between 0.5 and 1 m

high, with ongoing incision occurring in the confined active channel. This is different to the alluvial fans mapped in this study, indicating that there is another geomorphic control on this fan that differs from the others up-valley.

This study favours the explanation that the within-valley difference in alluvial fan behaviour is due to water (un)availability influencing stream power. Water must be available to erode the fans and to transport sediment, where stream power is high enough (Harvey, 2002). There are no flow gauges on any of the streams or rivers in the study area, however, during the two field visits in summer time (when it is much drier and hotter), a number of key points were noted. The East Branch is not as large as the main West Branch, however the large catchment area and high discharge suggests it flows year-round. The active channel on Knobs Flat Fan was dry on both visits, even during the 2015 rain storm (Figure 6.8), therefore no incision or aggradation can occur unless a higher magnitude rain event occurs. A man-made drainage ditch has been built leading away from this fan, dug under the road, and directed out through Knobs Flat, probably to drain the fan and prevent road flooding during heavy rain which is not uncommon in Fiordland. Wesney Creek was in flood during the 2015 field visit, with boulders (clasts $<$40 cm diameter) being tumbled down the channel, however was barely a dribble during the 2016 visit (no photo taken). Kiosk Creek was very small with only enough stream power to transport pebbles. Pebbles $<$5 cm in diameter were actively being transported during the 2015 visit. Kiosk Creek was not visited in 2016.

Figure 6.8: Various images taken in 2015 of the active channels of the Eglinton Valley tributaries. Images show Knobs Flat Fan and the man-made drainage ditch, Wesney Creek during normal flow and in flood (note: the normal flow image was taken above the bridge, higher up the fan, and the flood image was taken below the bridge, near the Eglinton River confluence), Kiosk Creek, and in the Smithys Creek gorge (note: the bedrock image was taken 15 m upstream from the image showing the stream).

6.3.4.1 Alluvial fan size variability

The across-valley difference in lithology, coupled with the size of tributary catchments, has had an effect on the size and distribution of the alluvial fans throughout the valley. The Livingston Mountain catchments (east) are larger than the Earl Mountain (west) catchments. This, along with more erodible sediments in the Livingston Mountains, has allowed the formation of alluvial fans up to five times larger than the Earl fans protruding onto the modern floodplain and holding the Eglinton River closer to the true right of the valley (Figure 6.1).

Within the Livingston Mountain catchments there is considerable variability in the size of the fans being produced. For example, the Smithys Creek catchment is ~16 km^2, and the Wesney Creek catchment is half the size at ~8 km^2. Both catchments share similar relief and incise the same lithologies, however, Smithys Creek has no apparent alluvial fan associated with it while Wesney Creek has the largest mapped fan in the study area. The size of clasts measured differ between both catchments, with Smithys Creek having the majority of the clasts less than half the size of the clasts in Wesney Creek (Figure 6.9). Smithys Creek once had enough stream power to incise the gorge, however, this does not appear to be actively incising today. The gorge incision and small clasts found within Smithys Creek suggests that there is now less available sediment and lower stream power than Wesney Creek. Wesney Creek was actively transporting $<$40 cm boulders during the flood in 2015 yet Smithys Creek had barely any change. The high sediment load and stream power is allowing the Wesney Creek fan to maintain its cuspate form while also constricting the Eglinton River on the true right of the valley.

Where Smithys Creek exits the fault-controlled, bedrock gorge, it is no more than 20 m above the Eglinton River floodplain. Because of this, there is very little space for any sediment to accumulate and a fan to form (Bull, 1977; Lewin et al., 2005). Wesney Creek on the other hand, exits the valley approximately 100 m above Eglinton Valley floor, allowing sufficient space for a fan to form and be preserved.

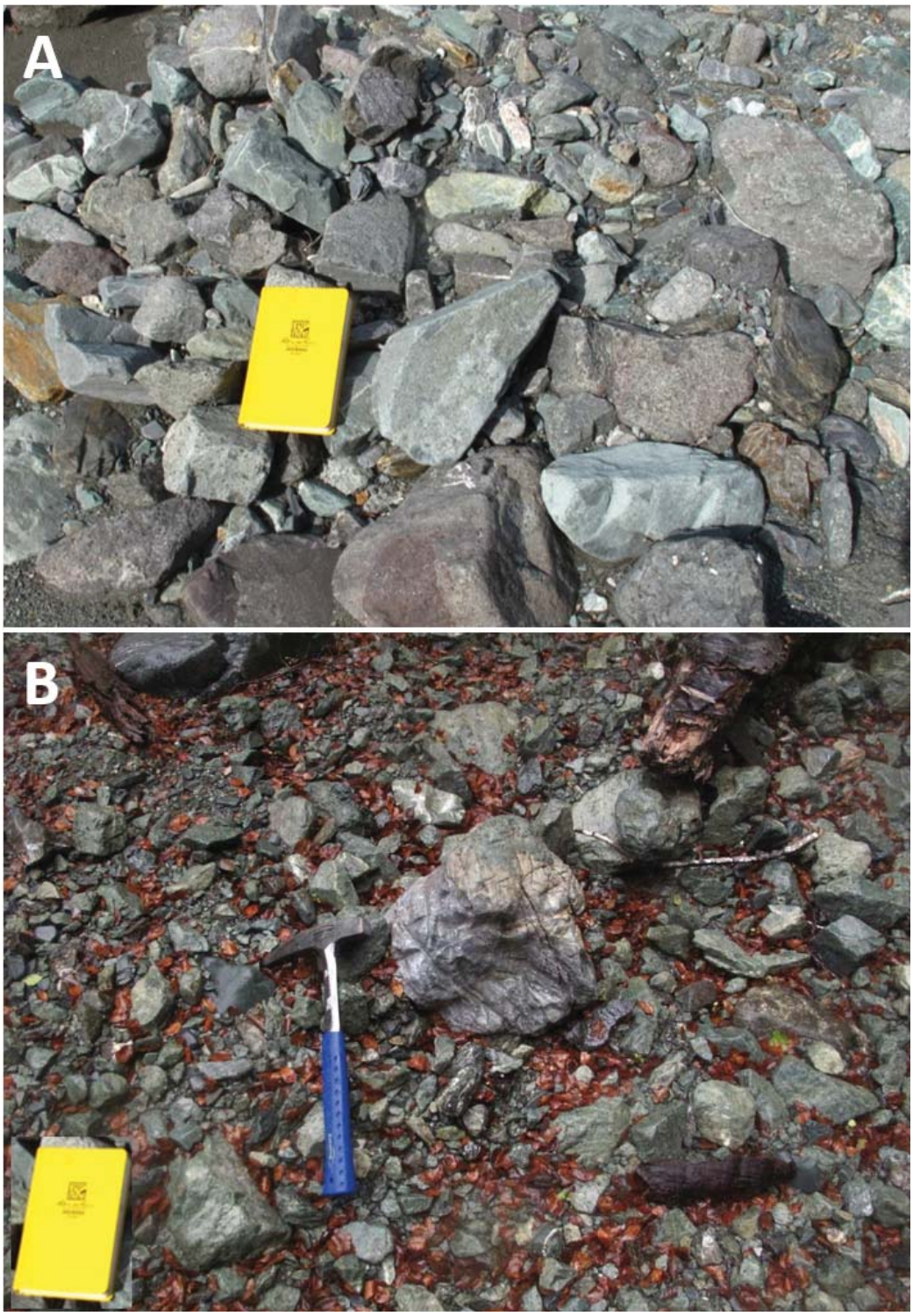

Figure 6.9: Clast sizes beside the active channels of Wesney Creek (A) and Smithys Creek (B). The difference in clast size here is primarily conditioned by available stream power.

6.3.5 A lack of river terraces

There is a distinct lack of river terraces within the Eglinton Valley and most likely due to low uplift rates. The lack of terraces contrasts what can be found in many of the larger catchments in New Zealand such as the Waimakariri Valley (Canterbury; Gage, 1958) and the Wairau Valley (Marlborough; McCalpin, 1992). Typical factors promoting the formation of river terraces in deglaciated landscapes include a decline in sediment input and high uplift rates (Ballantyne, 2002; Bridgland and Westaway, 2008). A lowering of the base-level can also prompt fluvial incision which may be driven by uplift and also by down-valley lake- or sea-level lowering.

Uplift rates in the Eglinton Valley region are relatively low (~0.5-1 mm a^{-1}) when compared to Waimakariri and Wairau valleys in the central and northern Southern Alps that experience uplift rates of ~5 mm a^{-1}. This alone can help explain why there are no river terraces found in Eglinton Valley, or in any of the tributaries draining into Lake Te Anau. Another factor influencing the lack of terraces could be if the level of Lake Te Anau had gradually risen throughout the Holocene, though there does not appear to be any studies done on this at the time of writing. The neighbouring Dart Valley does have river terraces which is possibly due to base-level changes as the level of Lake Wakatipu (that the Dart River drains into) has been recorded to fluctuate in the past (Thomson, 1996; McColl and Davies, 2011).

6.3.5.1 Sediment delivery into Eglinton Valley

There are currently no valley glaciers contributing to the sediment load of the Eglinton River, therefore, the sediment moving through the Eglinton Valley system is proposed to be a mix of reworked glacial and mass movement deposits, as well as a little sediment supplied from the tributary catchments during high rainfall events. The Eglinton River has incised a narrow, winding, 4.68 km long gorge into the Lake Gunn Landslide deposit (Figure 6.10). The total sediment that has since been reworked by the Eglinton River is ~4.6 million m^3 (approximated from Google Earth and a LINZ topographic map using the gorge length, depth, and average width of 4,680 m, 20 m, and 50 m respectively). These reworked landslide sediments would have contributed approximately 0.3 m of aggradation to the ~15 million m^2 (the approximate floodplain area of the entire valley) Eglinton floodplain down stream from the landslide. In addition, the the valley floor has probably been built up from paleo-lake deposits, alluvial fan sediments, and reworking of within channel and bank sediments.

The Eglinton River appears to now be at equilibrium (i.e. no active aggradation or degradation) within a 1-2 m deep channel in the modern floodplain. Well developed tussock and grassy vegetation throughout the floodplain indicates the floodplain is currently stable, with no recent (at least >100 years) signs of channel

avulsion or overbank deposits. In the exposed sections in the river banks in two locations, thick deposits of very fine-grained sediments were identified. This finding builds on the story of what makes up the modern floodplain and is further discussed in Subsection 6.3.6.

Figure 6.10: Annotated image of the northern section of the Lake Gunn Landslide deposit with the incised Eglinton River shown in blue.

6.3.6 Multiple dammed lakes

This study has found evidence that the Eglinton Valley held three lakes, two of which have since drained, and the third being Lake Gunn. The possibility of Eglinton Valley being blocked by a RA or alluvial fan and prompting the formation of a temporary lake is very high due to the high relief, seismically active region, sediment input from tributaries, and glacial history as all these factors commonly influence lake formation (Costa and Schuster, 1988; Schuster et al., 1998; Korup, 2002).

6.3.6.1 Wesney Creek Fan as a valley dam

Wesney Creek Fan appears to have been much larger in the past, possibly crossing the entire width of the valley and impounding a small lake. The river has truncated part of the up-valley extent of the fan (can be seen in Figure 6.1), leaving a raised 'terrace' ~10 m above the modern river channel (where clast sample EG R 2, with an AI of 7, was collected). This dips gently, over a distance of 200 m, to ~1 m above the modern channel near the fan toe. At this point, a steep-sided (dipping 80°to the north, 50°to the east, 60°to the west, and 30°to the south) 'lump' abruptly rises ~8 m above the fan. The lithology of the lump (sample EG R 1, collected from underneath an uprooted tree) is the same as the Wesney Creek Fan lithologies (sample EG Q 1) and different to the adjacent Earl Mountains. This similarity indicates it probably

originated from the Wesney Creek catchment in the Livingston Mountains and may be part of a much older, larger fan prior to the Eglinton River eroding it (further discussed in Subsubsection 6.3.6.3). The internal sedimentary structure of the fan (e.g. bedding) and hummock was concealed with very thick soil development and vegetation growth.

Where a paleo-lake may have existed, one would expect to find an exposed stratigraphic section of slack-water sediments (see Section 5.5). Sandy silts are found in several locations upstream of Wesney Creek Fan, with the best preserved sample being exposed in a ~2 m section (Figure 6.11). Similar sorts of fine sands are not found south of Wesney Creek suggesting the northern sediments are a product of valley blockage at Wesney Creek, and not farther down-valley. This discovery provides evidence that Wesney Creek Fan stretched a few more metres across to the other side of the valley, blocking the river, and forming a lake. This would have allowed the fine sediment to build up up-valley of the fan (as shown in Figure 6.11). A similar scenario has recently occurred in the neighbouring Dart Valley where the Te Koroka/Slip Stream debris-flow fan dammed the Dart River at Dredge Flat, impounding a lake (Cox et al., 2014).

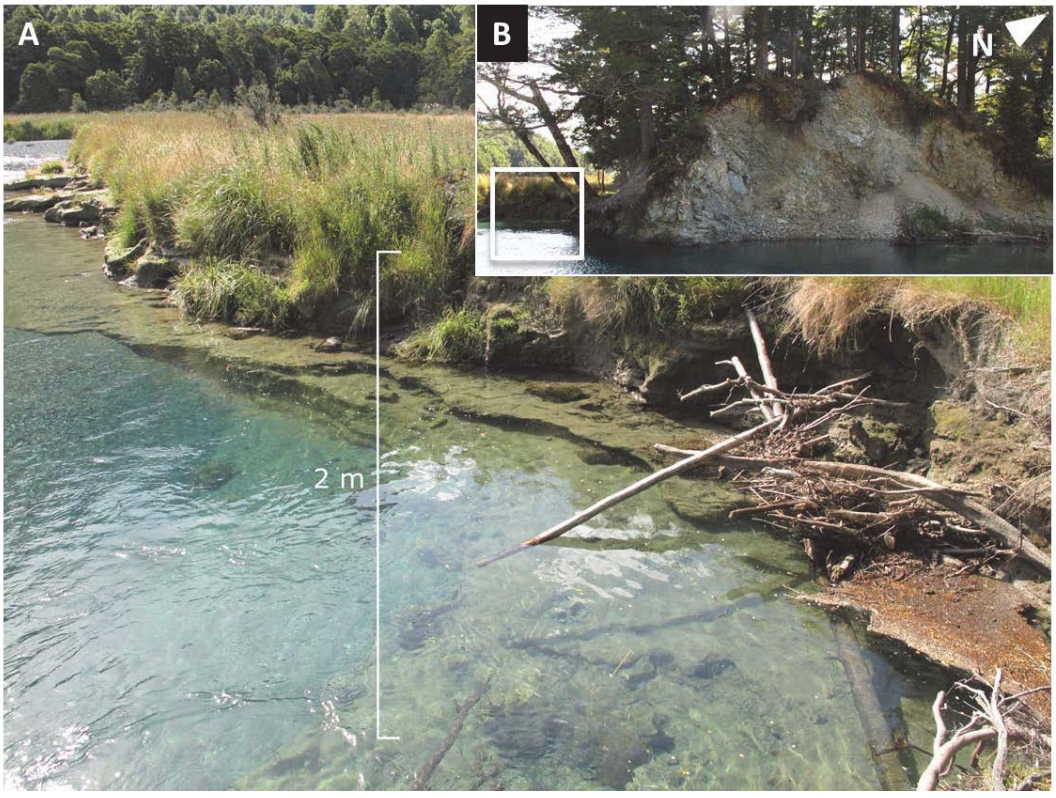

Figure 6.11: 2 m section of sandy silt exposed within the active channel of the Eglinton River beside the Lower Deer Flat hummocks. A) An indication of the depth of the sandy silt above and below water, B) exposed Deer Flat hummock with location of A outlined in white.

6.3.6.2 Deer Flat rock avalanche as a dam

1.5 km north of the Deer Flat RA deposits, and approximately adjacent to Malvora Lake, ~1.4 m of fine sandy silts are exposed in the river bank, above a sharp contact with rounded clasts beneath it (Figure 6.12). These silts are considered to be separate to the Wesney Creek lake sediments due to a ~10 m elevation difference (visible in Figure 6.13). The elevation of the floodplain at Malvora Lake is ~350 m, and at the Deer Flat Hummock exposure of the Wesney Creek lake sediments it is ~340 m. This finding suggests the Deer Flat RA deposits also blocked the valley, allowing another lake to form. If this is the case, it was held in place long enough for the ~1.4 m of sediment to build up before breaching.

Figure 6.12: An exposed section within the modern channel of the Eglinton River adjacent to Malvora Lake. A) Shows location of B (white outline) with photo taken facing SW down Eglinton Valley, B) 1.4 m section of sandy silt with a sharp contact over rounded cobbles.

By conducting an elevation profile (using Google Earth Pro 7.1.4) from Wesney Creek Fan to Smithys Creek, it is clear that the entire valley floor is raised above the Wesney Creek Fan with two depressions where lakes may have been held in the past (Figure 6.13). This elevation is attributed to excess fine sediment built-up during the existence of the lakes, first against the Wesney Creek Fan, then later, against the Deer Flat RA deposits (further discussed in Subsubsection 6.3.6.3).
Up-river from Malvora Lake, the Kiosk Creek Fan abuts the river on the true left thus hiding any outcrops of floodplain, while on the true right, the modern floodplain is only 0.5 - 1 m above the current river level with no more visible sections of sandy silt deposits. In this case, it is difficult to say how much farther up the valley (than the outcrop in Figure 6.12) this particular lake may have reached.

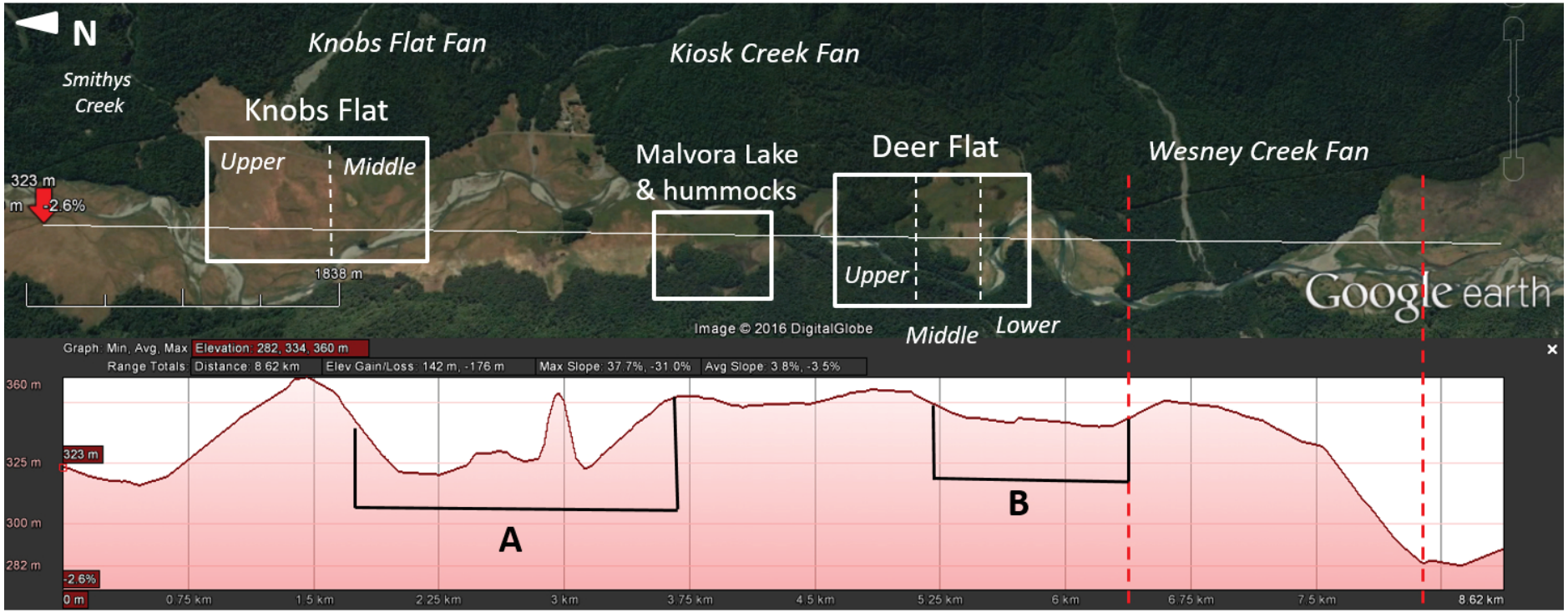

Figure 6.13: Annotated Google Earth Pro 7.1.4 image showing the long-valley elevation profile from Smithys Creek to Wesney Creek Fan (annotated with red dashed line to show the fan elevation on the profile). A) Low surface within the valley that potentially held a lake that was impounded by the Deer Flat RA with a hummock where Sample EG E 1 was taken indicated by the large spike in the profile. B) Low surface between the Wesney Creek Fan and Deer Flat RA deposits where ~2 m of fine sandy silt was found. Note that the photo in Figure 6.12 was located in the river channel by Malvora Lake and hummocks (outlined).

6.3.6.3 Sequence of paleo-lake events

Considering the two areas of visible, fine, silty sediments, it is suggested that there were two major paleo-lakes within Eglinton Valley; the Deer Flat RA lake may have formed, followed by the formation of the Wesney Creek Fan lake, potentially as a direct result due to the restriction in Eglinton River stream power. Apart from the exposures of the fine-grained sediments there is no other evidence of the former lake/s within the valley such as delta foreset beds or paleo-shorelines. However, the steep walls on both sides of the valley have, in the past, been very efficient at conveying sediment into the valley floor, potentially burying any evidence of the shorelines as has been suggested to have occurred in other locations e.g. Wassmer et al., (2004).

No visible mixing of lacustrine-type sediments in the Deer Flat hummocks was observed (as was found by Hancox et al., (2013) in the Lake Gunn Landslide), indicating they were probably not deposited into a lake. The GPR line that was conducted between the two hummocks at Lower Deer Flat (Figures 5.4 and 6.11) clearly indicate fine, stratified sediments building up around the previously deposited hummocks. This suggests the Lower Deer Flat hummocks (and probably the other Deer Flat hummocks) were emplaced prior to the fine-grained sedimentation that then built up around and between the hummocks as a result of the Wesney Creek Fan lake being formed. If this was the case, the Deer Flat RA occurred first, blocked the valley, restricting the Eglinton River for possibly weeks to years, and formed a lake.

In the weeks to decades after the Deer Flat RA caused a lake to form up-stream, the Wesney Creek Fan built out across the valley, forming another lake. Two major factors could have influenced the aggradation of the Wesney Creek fan:

1. A reduction in Eglinton River stream power leading to less sediment being removed from the fan toe due to an upstream blockage e.g. the Deer Flat RA, and/or

2. An influx of sediment as a result of an external trigger, such as an earthquake or heavy rain event, allowed the fan to build out rapidly.

A reduction in water flowing down the Eglinton River can reduce tributary fan toe erosion, unless the tributary sediment supply exceeds the erosional capacity of the river, the fan can continue to extend (e.g. this is actively occurring at the Te Koroka/Slip Stream debris-flow fan in the Dart River at Dredge Flat; Cox et al., 2014). Wesney Creek catchment appears to be supplying a large amount of sediment to the system with many active, and formerly active, scree slopes (Figure 6.14).

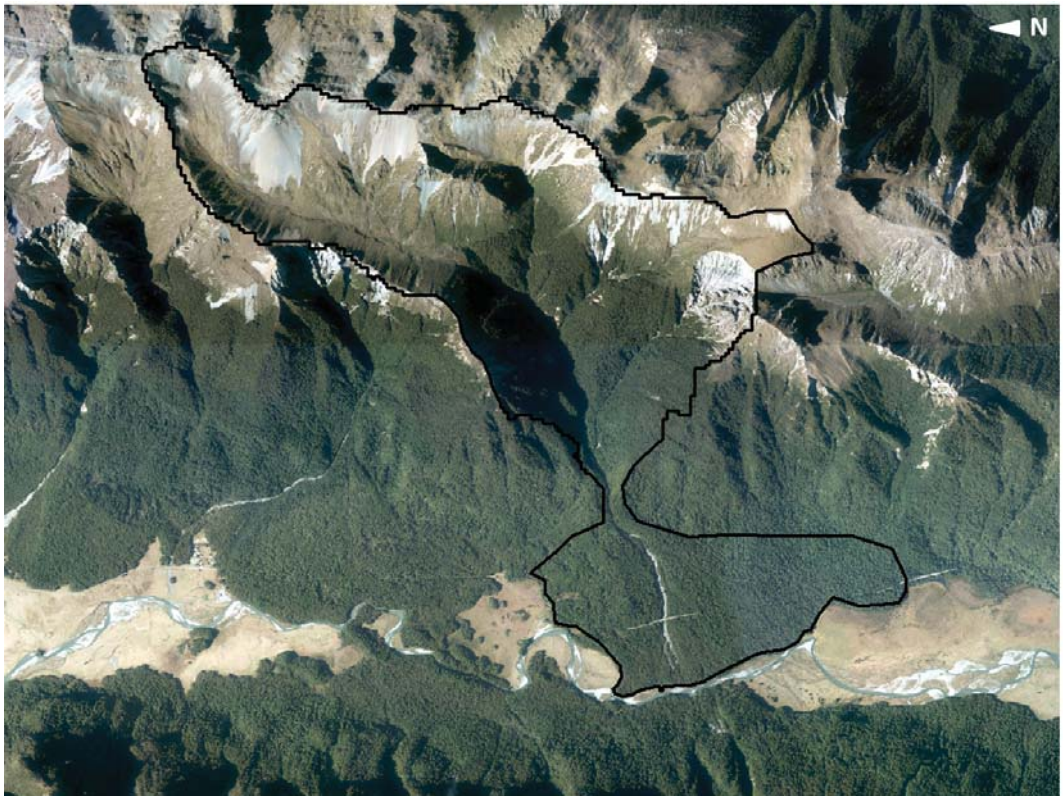

Figure 6.14: Outline of Wesney Creek catchment and fan (black line) showing the large amount of active (and previously active) scree slopes providing sediment available for transport through the fluvial system.

Given a slight reduction in stream power from the Eglinton River, due to the Deer Flat RA blockage, as well as excess sediment supply from the Wesney Creek catchment, the Wesney Creek Fan was potentially able build up and extend across the entire valley. At some point in time, the Eglinton River found the lowest point in the fan and incised a channel. Field work investigations suggest this channel may have formed between the modern fan and the lump (introduced in Subsubsection 6.3.6.1; Figure 6.15). As the river incised the fan, a heavy rain event, or an outburst from the Deer Flat RA dam, may have prompted the Eglinton River to avulse to the current channel between the hummock and the Earl Mountains.

Figure 6.15: Schematic diagram showing the active channels of Wesney Creek and Eglinton River (dark blue lines). White box surrounds the location of the 'lump' on the western side of the suggested paleo-channel (dotted, light blue line)of the Eglinton River prior to avulsion into its current channel. Base image: Google Earth.

6.4 Conditions for agglomerate formation

This study has found quantitative evidence, for the first time, that agglomerates can be formed in mass movements other than RA; they can also form in very large translational slides (the process responsible for the Lake Gunn Landslide; Hancox et al., 2013). This is important as it shows that the presence of agglomerates can not be used to distinguish a relict RA deposit from a relict complex translational rockslide deposit. It also shows that, where there is $<100\%$ agglomerates in the sample, the conclusion that the rest of the sample must therefore be non-mass movement in origin can not be made without other information including morphology, glacial history, and provenance analysis.

Reznichenko (2012) discovered that submicron agglomerations of grains form during a high stress RA event and not during low stress glacial transport, however, no minimum stress threshold for agglomerates formation has been established. While this study does not present a minimum threshold, it does highlight that the presence of agglomerates within any mass movement deposit indicates that the mass movement had sufficient comminution (high intensity fracturing) to allow sufficient quantities of sub-micron particles to form agglomerates.

The Lake Gunn Landslide collection location, near the distal deposits, was formed of massive, highly crushed, very angular-rounded course sands to cobbles-sized fragments with visible shear bands of finer crushed material throughout (Figure 4.11). Sample I was collected from one of these shear bands yet there was a negligible difference in the amount of agglomerated particles counted between this sample and samples J and K from the massive crushed sections nearby.

Unlike in the environments in which Reznichenko (2012) developed the agglomerate technique, with quartz-rich sediments, within Eglinton Valley, quartz is extremely rare, so all minerals (including epidotes, olivines, pyroxenes, and amphiboles) were used in the identification. With these minerals being less chemically stable than quarts, it introduces the possibility that some of the microtextures exhibited by some of the grains (e.g. the rough faces on sample N in Figure 5.22 or possible silica precipitation in Figure 5.23) may not be textures that have developed during mass movement transport. As all steps were taken to ensure there were no loose, clay-sized particles on the samples, this study has shown that using agglomerates in determining a high- or low-energy transport regimes is possible, however, using them to distinguish RA deposits from other forms of mass movement may not be so simple.

Chapter 7

Conclusion

7.1 Introduction

The aim of this chapter is to reinforce the primary findings of this study and suggest a number of ideas to build on the ideas considered here. Although further investigation is required to detail absolute ages and determine below-ground extent of the hummocky topography, this study contributes explicit evidence the post-glacial slope movements have previously been unrecognised in the Eglinton Valley.

7.2 A geomorphic model for Eglinton Valley floor

Based on the geomorphological mapping informed by geophysics, sedimentology, and provenance analysis, the following landforms and processes have been identifed:

- Glacial depositional processes are likely to be responsible for the majority of the Middle and Upper Knobs Flat hummocks.
- Moraine has been identified around Eglinton Flat, supporting Valkengoed's 2011 suggestion.
- RA deposits have been recognised throughout Deer Flat, Malvora Lake, and Knobs Flat.
- Paleo-lake deposits have been identified and the processes responsible for these include the Deer Flat RA causing the upper lake, followed by an expansion of the Wesney Creek alluvial fan forming the lower lake.
- The active and partially active tributaries, high stream power of the Eglinton River, and cross-valley sediment variability are considered responsible for the formation and preservation of the extensive alluvial fans throughout the valley.
- A distinct absence of river terraces is noted and explained by low rates of uplift in the region, valley aggradation as a result of sediment input from the Lake Gunn Landslide and tributary valleys, and no discernible change in base-level

that could be recognised though the recessional moraine at the entrance into Te Anau Valley may have influenced this in the past.

7.2.1 Glacial deposits

This study demonstrates that there are a number of glacial deposits within the Eglinton Valley and, in particular, in the northern half of the valley. These include the hummocky deposits surrounding Eglinton Flat and a number of the deposits within Knobs Flat. The New Zealand Geopreservation Inventory probably correctly identifies the glacial kame field at Knobs Flat, with one exception, the hummock that, based on its overall lithological characteristics, morphology, and proximity to a source area on the valley wall adjacent, is suggested to be RA in oorigin.

7.2.2 Rock avalanche deposits

In deglaciated valleys there is a tendency to attribute morphological features to glacial processes (Davies et al., 2013). A large number of previously unrecognised RA deposits have been identified within the deglaciated Eglinton Valley. This finding promotes the geomorphic significance of such processes and provides an insight into the potential hazard of future RA events in the touristic Eglinton Valley. It also provides yet another example where post-glacial slope-failure has, until now, gone unrecognised (*sensu* Hewitt, 1999).

7.2.3 Recognition of paleo-lakes

Paleo-lake deposits have, for the first time, been identified in Eglinton Valley. Lakes are common in many deglaciated valleys, and are generally held in place by moraine sequences (e.g. Lakes Pukaki, Wanaka, and Te Anau, all situated within the Southern Alps, NZ). This study recognises the often shorter-lived lakes that can form following RA events and alluvial fan aggradation. Both of these scenarios are recognised in the wider NZ (e.g. Mount Adams 1999 RA, and Te Koroka/Slip Stream debris-flow fan in the Dart Valley) and are now found in Eglinton Valley.

7.3 Future work

A number of wider implications emerge from this study. While succinct morphological mapping and macro- and micro-sediment analysis has identified a number of important features including RA deposits, this study, and the overall geomorphic history of the Eglinton Valley, can be built on with the following recommendations.

This study found that agglomerates do not need to make up 100% of a microsediment sample for a deposit that is purely RA derived. Instead, the amount of agglomerates found within any particular sample may reflect a distance from source

relationship with agglomerates hypothesised to become more prevalent in the more distal (and therefore more comminuted) parts of the deposit. It is suggested that this be tested on a modern, long run-out, rock avalanche. Establishing the relationship between agglomerate abundance and travel distance could provide a useful means of reconstructing RA transport and deposit dynamics. Another finding is that agglomerates are not restricted to formation in RA's, but are also capable of being formed in other styles of mass movement, such as large translational rockslides e.g. Lake Gunn Landslide.

Measuring absolute ages on the hummocky topography within Eglinton Valley would better constrain the timing of deposition and help build a more robust timeline of events through the Holocene. From the TCND process that was nearly completed during this study, it seems highly likely that conducting ^{10}Be dating on pyroxene minerals will work, given the samples have a fraction of quartz that can also be dated to constrain the errors (which is possible in Eglinton Valley).

The novel method of using TCND on micro-quartz grains from New Zealand appeared promising. This should be attempted in the future.

Further mapping and dating work is required to better constrain the extent of the paleo-lakes within Eglinton Valley. Coring and/or radiocarbon dating of more of the minor lakes within the valley (e.g. Malvora Lake) would help constrain when they began forming in relation to deglaciation or other, unidentified, valley blockages.

Further GPR work is recommended on the glacial hummocks at Knobs Flat in order to determine their spatial extent below the surface. This would provide a clearer insight as to whether they are small individual deposits or one large deposit as this difference can be used to determine how long a glacier may have had to pause at this location to deposit the sediments involved. This data would help broaden the knowledge of the climatic patterns within the Eglinton Valley over time.

Geomorphic mapping, TCND, and sedimentological analysis on the proposed recessional moraine where Eglinton Valley enters Te Anau Valley would be beneficial as this would provide an insight into whether this feature has had an influence on base-level changes in Eglinton Valley and/or provide a better constraint on Te Anau Glacier recession.

Further mapping, clast analysis, and TCND is suggested on the newly recognised RA deposits at Deer Flat, Malvora Lake, and Lower Knobs Flat which may help to ascertain whether these landforms were produced from one very large RA, or multiple events.

References

Abdrakhmatok, K., Strom, A., 2006. Dissected rockslide and rock avalanche deposits; Tien Shan, Kyrgyzstan. In: Evans, S.G., Mugnozza, G.S., Strom, A., Hermanns, R.L. (Eds). Landslides from Massive Rock Slope Failure. Springer Netherlands, Dordrecht, pp. 551–570. DOI: 10.1007/978-1-4020-4037-5_29. URL: http://dx.doi.org/10.1007/978-1-4020-4037-5_29.

Alexander, D., Davies, T., Shulmeister, J., 2014. Formation of the Waiho Loop terminal moraine, New Zealand. Journal of Quaternary Science 29.4, 361–369. DOI: 10.1002/jqs.2707. URL: http://dx.doi.org/10.1002/jqs.2707.

Alley, R., Cuffey, K., Evenson, E., Strasser, J., Lawson, D., Larson, G., 1997. How glaciers entrain and transport basal sediment: Physical constraints. Quaternary Science Reviews 16.9, 1017–1038.

Alloway, B.V., Lowe, D.J., Barrell, D.J., Newnham, R.M., Almond, P.C., Augustinus, P.C., Bertler, N.A., Carter, L., Litchfield, N.J., McGlone, M.S., 2007. Towards a climate event stratigraphy for New Zealand over the past 30 000 years (NZ-INTIMATE project). Journal of Quaternary Science 22.1, 9–35.

Almond, P., Moar, N., Lian, O., 2001. Reinterpretation of the glacial chronology of South Westland, New Zealand. New Zealand Journal of Geology and Geophysics 44.1, 1–15.

Ambrosi, C., Crosta, G.B., 2006. Large sackung along major tectonic features in the Central Italian Alps. Engineering Geology 83.1, 183–200.

Anderson, B., Mackintosh, A., 2006. Temperature change is the major driver of late-glacial and Holocene glacier fluctuations in New Zealand. Geology 34.2, 121–124.

Angeli, M., Gasparetto, P., Menotti, R., Pasuto, A., Silvano, S., Soldati, M., 1996. Rock avalanche. In: Dikau, R., Brunsden, D., Schrott, L., Ibsen, M. (Eds). Landslide recognition. Wiley, Chichester, pp. 190–201.

Ballantyne, C.K., 1995. Paraglacial debris-cone formation on recently deglaciated terrain, western Norway. The Holocene 5.1, 25–33.

Ballantyne, C.K., 2002. Paraglacial geomorphology. Quaternary Science Reviews 21.18–19, 1935–2017. DOI: http://dx.doi.org/10.1016/S0277-3791(02)

00005-7. URL: http://www.sciencedirect.com/science/article/pii/S0277379102000057.

Ballantyne, C.K., Stone, J., 2004. The Beinn Alligin rock avalanche, NW Scotland: cosmogenic 10Be dating, interpretation and significance. The Holocene 14.3, 448–453.

Barrell, D., 2011. Quaternary glaciers of New Zealand. In: Quaternary Glaciations-Extent and Chronology: a closer look: Ehlers, J, pp. 1047–1064.

Barrett, P., 1980. The shape of rock particles, a critical review. Sedimentology 27.3, 291–303.

Barth, N., 2014. The Cascade rock avalanche: implications of a very large Alpine Fault-triggered failure, New Zealand. Landslides 11.3, 327–341.

Beavan, J., Denys, P., Denham, M., Hager, B., Herring, T., Molnar, P., 2010. Distribution of present-day vertical deformation across the Southern Alps, New Zealand, from 10 years of GPS data. Geophysical Research Letters 37.16.

Benn, D., 2004. Clast morphology. In: Evans, D., Benn, D. (Eds). A practical guide to the study of glacial sediments. Arnold, London. Chap. 4, pp. 78–92.

Benn, D., Evans, D., 2010. Glaciers and Glaciation. Arnold, London, p. 802.

Benn, D.I., Ballantyne, C.K., 1993. The description and representation of particle shape. Earth Surface Processes and Landforms 18.7, 665–672. DOI: 10.1002/esp.3290180709.

Benn, D.I., Ballantyne, C.K., 1994. Reconstructing the transport history of glacigenic sediments: a new approach based on the co-variance of clast form indices. Sedimentary Geology 91.1-4, 215–227.

Benn, D.I., Evans, D.J., 1996. The interpretation and classification of subglacially-deformed materials. Quaternary Science Reviews 15.1, 23–52.

Berryman, K.R., Cochran, U.A., Clark, K.J., Biasi, G.P., Langridge, R.M., Villamor, P., 2012. Major earthquakes occur regularly on an isolated plate boundary fault. Science 336.6089, 1690–1693.

Blair, T.C., 1999. Form, facies, and depositional history of the North Long John rock avalanche, Owens Valley, California. Canadian Journal of Earth Sciences 36.6, 855–870.

Blair, T.C., McPherson, J.G., 1994. Alluvial fan processes and forms. In: Geomorphology of desert environments. Springer, pp. 354–402.

Blard, P.-H., Bourles, D., Pik, R., Lavé, J., 2008. In situ cosmogenic 10 Be in olivines and pyroxenes. Quaternary Geochronology 3.3, 196–205.

Boulton, G., 1978. Boulder shapes and grain-size distributions of debris as indicators of transport paths through a glacier and till genesis. Sedimentology 25.6, 773–799.

Boulton, G., Deynoux, M., 1981. Sedimentation in glacial environments and the identification of tills and tillites in ancient sedimentary sequences. Precambrian Research 15.3-4, 397–422.

Bourles, D., Raisbeck, G., Yiou, F., 1989. 10Be and 9Be in marine sediments and their potential for dating. Geochimica et Cosmochimica Acta 53.2, 443–452.

Brevik, E.C., Konen, M.E., 2003. Problems and Suggestions Concerning the Use of Glacially Deposited Sediment Terminology by Soil Scientists. Soil survey horizons 44.2, 64–70.

Bridgland, D.R., 1986. Clast lithological analysis. Quaternary Research Association.

Bridgland, D., Westaway, R., 2008. Climatically controlled river terrace staircases: a worldwide Quaternary phenomenon. Geomorphology 98.3, 285–315.

Bull, W.B., 1977. The alluvial-fan environment. Progress in physical geography 1.2, 222–270.

Campbell, H., 2005. Partitioning of plate boundary deformation in South Westland, New Zealand: controls from reactivated structures. Department Of Geology, University of Otago, University of Otago, Dunedin.

Chinn, T., 1975. Late Quaternary snowlines and cirque moraines within the Waimakariri watershed. University of Canterbury, Christchurch, p. 213.

Chinn, T., 1979. Moraine forms and their recognition on steep mountain slopes. Moraines and varves. Rotterdam, AA Balkema, 51–57.

Clark, P.U., Dyke, A.S., Shakun, J.D., Carlson, A.E., Clark, J., Wohlfarth, B., Mitrovica, J.X., Hostetler, S.W., McCabe, A.M., 2009. The last glacial maximum. science 325.5941, 710–714.

Collins, J.A., 2015. In situ cosmogenic 10Be in pyroxene with an application to surface exposure dating. Victoria University of Wellington. URL: `http://hdl.handle.net/10063/4851`.

Costa, J.E., 1984. Physical geomorphology of debris flows. In: Developments and applications of geomorphology. Springer, pp. 268–317.

Costa, J.E., Schuster, R.L., 1988. The formation and failure of natural dams. Geological Society of America Bulletin 100.7, 1054–1068.

Cox, S., McSaveney, M.J., Rattenbury, M., Hamling, I.J., 2014. *Activity of the landslide Te Horo and Te Koroka fan, Dart River, New Zealand, during January 2014*. Report.

Crosta, G.B., Frattini, P., Fusi, N., 2007. Fragmentation in the Val Pola rock avalanche, Italian alps. Journal of Geophysical Research: Earth Surface (2003 - 2012) 112.F1.

Crozier, M.J., 2005. Multiple-occurrence regional landslide events in New Zealand: hazard management issues. Landslides 2.4, 247–256.

Crozier, M.J., 2010. Deciphering the effect of climate change on landslide activity: A review. Geomorphology 124.3, 260–267.

Cruden, D., Hungr, O., 1986. The debris of the Frank Slide and theories of rockslide-avalanche mobility. Canadian Journal of Earth Sciences 23.3, 425–432.

Cruden, D., Krahn, J., 1978. Frank rockslide, Alberta, Canada. In: Voight, B. (Ed). Rockslides and avalanches: 1. Elsevier, New York, pp. 97–112.

Davies, T.R., 1982. Spreading of rock avalanche debris by mechanical fluidization. Rock Mechanics 15.1, 9–24.

Davies, T.R., McSaveney, M., 2002. Dynamic simulation of the motion of fragmenting rock avalanches. Canadian Geotechnical Journal 39.4, 789–798.

Davies, T.R., McSaveney, M., Hodgson, K., 1999. A fragmentation-spreading model for long-runout rock avalanches. Canadian Geotechnical Journal 36.6, 1096–1110.

Davies, T.R., Warburton, J., Dunning, S.A., Bubeck, A.A., 2013. A large landslide event in a post-glacial landscape: rethinking glacial legacy. Earth Surface Processes and Landforms 38.11, 1261–1268.

Davis, J., Annan, A., 1989. Ground-penetrating radar for high-resolution mapping of soil and rock stratigraphy. Geophysical prospecting 37.5, 531–551.

Deline, P., 2005. Change in surface debris cover on Mont Blanc massif glaciers after the 'Little Ice Age′ termination. The Holocene 15.2, 302–309.

Deline, P., 2009. Interactions between rock avalanches and glaciers in the Mont Blanc massif during the late Holocene. Quaternary Science Reviews 28.11–12, 1070–1083.

Deline, P., Hewitt, K., Reznichenko, N., Shugar, D., 2015. Rock avalanches onto glaciers. Landslide Hazards, Risks and Disasters. Elsevier, Amsterdam, 263.

Dikau, R., Brunsden, D., Schrott, L., Ibsen, M., 1996. Landslide recognition: identification, movement, and causes. Wiley, Chichester.

Dufresne, A., Davies, T., 2009. Longitudinal ridges in mass movement deposits. Geomorphology 105.3, 171–181.

Dufresne, A., Bosmeier, A., Prager, C., 2016. Sedimentology of rock avalanche deposits case study and review. Earth-Science Reviews.

Dunning, S., 2006. The grain size distribution of rock-avalanche deposits in valley-confined settings. Italian Journal of Engineering Geology and Environment 1, 117–121.

Dunning, S., Mitchell, W., Rosser, N., Petley, D., 2007. The Hattian Bala rock avalanche and associated landslides triggered by the Kashmir Earthquake of 8 October 2005. Engineering Geology 93.3, 130–144.

Dunning, S., Petley, D., Strom, A., 2005. The morphologies and sedimentology of valley confined rock-avalanche deposits and their effect on potential dam hazard. Landslide Risk Management. AT Balkema, Amsterdam, 691–704.

Dunning, S.A., 2004. Rock avalanches in high mountains - a sedimentological approach. University of Luton, UK.

Dunning, S.A., Armitage, P., 2011. The grain-size distribution of rock-avalanche deposits: implications for natural dam stability. In: Natural and artificial rockslide dams. Springer, pp. 479–498.

Dunning, S.A., Rosser, N.J., McColl, S.T., Reznichenko, N.V., 2015. Rapid sequestration of rock avalanche deposits within glaciers. Nature communications 6.

Dykstra, J.L., 2012. The Post-LGM Evolution of Milford Sound, Fiordland, New Zealand: Timing of Ice Retreat, the Role of Mass Wasting and Implications for Hazards. Thesis,

Evans, D.J., Phillips, E., Hiemstra, J., Auton, C., 2006. Subglacial till: formation, sedimentary characteristics and classification. Earth-Science Reviews 78.1, 115–176.

Evans, D.J., Twigg, D.R., 2002. The active temperate glacial landsystem: a model based on Breioamerkurjokull and Fjallsjokull, Iceland. Quaternary science reviews 21.20, 2143–2177.

Fischer, L., Kääb, A., Huggel, C., Noetzli, J., 2006. Geology, glacier retreat and permafrost degradation as controlling factors of slope instabilities in a high-mountain rock wall: the Monte Rosa east face. Natural Hazards and Earth System Science 6.5, 761–772.

Gage, M., 1958. Late Pleistocene glaciations of the Waimakariri Valley, Canterbury, New Zealand. New Zealand journal of geology and geophysics 1.1, 123–155.

Glade, T., Crozier, M.J., 2005a. A review of scale dependency. In: Glade, T., Anderson, M., Crozier, M.J. (Eds). Landslide hazard and risk. Wiley, Chichester. Chap. 3, pp. 75–138.

Glade, T., Crozier, M.J., 2005b. The nature of landslide hazard impact. In: Glade, T., Anderson, M., Crozier, M.J. (Eds). Landslide hazard and risk. Wiley, Chichester. Chap. 2, pp. 43–74.

Golledge, N.R., Mackintosh, A.N., Anderson, B.M., Buckley, K.M., Doughty, A.M., Barrell, D.J., Denton, G.H., Vandergoes, M.J., Andersen, B.G., Schaefer, J.M., 2012. Last Glacial Maximum climate in New Zealand inferred from a modelled Southern Alps icefield. Quaternary Science Reviews 46, 30–45.

Gosse, J.C., Phillips, F.M., 2001. Terrestrial in situ cosmogenic nuclides: Theory and application. Quaternary Science Reviews 20.14. Cited By :823 Export Date: 8 September 2015, 1475–1560.

Graham, I., Mortimer, N., 1992. Terrane characterisation and timing of metamorphism in the Otago Schist, New Zealand, using Rb-Sr and K-Ar geochronology. New Zealand journal of geology and geophysics 35.4, 391–401.

Grindley, G., 1958. The Geology of the Eglinton Valley, Southland. New Zealand Geological Survey.

Guelke-Stelling, M., Blanckenburg, F. von, 2012. Fe isotope fractionation caused by translocation of iron during growth of bean and oat as models of strategy l and ll plants. Plant and soil 352.1-2, 217–231.

Haeberli, W., Kääb, A., Paul, F., Chiarle, M., Mortara, G., Mazza, A., Deline, P., Richardson, S., 2002. A surge-type movement at Ghiacciaio del Belvedere and a developing slope instability in the east face of Monte Rosa, Macugnaga, Italian Alps. Norsk Geografisk Tidsskrift-Norwegian Journal of Geography 56.2, 104–111.

Hallet, B., Hunter, L., Bogen, J., 1996. Rates of erosion and sediment evacuation by glaciers: a review of field data and their implications. Global and Planetary Change 12.1, 213–235.

Hambrey, M.J., 1994. Glacial environments. UCL Press, London.

Hambrey, M.J., Ehrmann, W., 2004. Modification of sediment characteristics during glacial transport in high-alpine catchments: Mount Cook area, New Zealand. Boreas 33.4, 300–318.

Hancox, G.T., 1999. Mt Adams rock avalanche of 6 October 1999 and the subsequent formation and breaching of a large landslide dam in Poerua River, Westland, New Zealand. GNS Science.

Hancox, G.T., Dellow, G.D., Perrin, N.D., 1997. Earthquake-induced landsliding in New Zealand and implications for MM intensity and seismic hazard assessment. GNS Science.

Hancox, G.T., Langridge, R.M., Perrin, N.D., Vandergoes, M., Archibald, G., 2013. Recent mapping and radiocarbon dating of three giant landslides in northern Fiordland, New Zealand. Vol. 1012/45. GNS Science, p. 52.

Hancox, G.T., McSaveney, M.J., Manville, V.R., Davies, T.R., 2005. The October 1999 Mt Adams rock avalanche and subsequent landslide dam-break flood and effects in Poerua river, Westland, New Zealand. New Zealand Journal of Geology and Geophysics 48.4, 683–705.

Hancox, G.T., Perrin, N.D., 1994. Green Lake Landslide: A very large ancient rock slide in glaciated terrain, Fiordland, New Zealand. GNS Science.

Hancox, G.T., Perrin, N.D., 2009. Green Lake Landslide and other giant and very large postglacial landslides in Fiordland, New Zealand. Quaternary Science Reviews 28.11, 1020–1036.

Hancox, G., Cox, S., Turnbull, I., Crozier, M., 2004. Landslides and other ground damage caused by the MW7. 2 Fiordland earthquake of 22 August 2003. In: Proceedings of the 9th Australia New Zealand Conference on Geomechanics, Auckland. Vol. 7.

Hancox, G., Perrin, N., Dellow, G., 2002. Recent studies of historical earthquake-induced landsliding, ground damage, and MM intensity in New Zealand. Bulletin of the New Zealand Society for Earthquake Engineering 35.2, 59–95.

Harvey, A., 2002. The role of base-level change in the dissection of alluvial fans: case studies from southeast Spain and Nevada. Geomorphology 45.1, 67–87.

Hayward, B.W., Kenny, J.A., 1998. Inventory and maps of important geological sites and landforms in the Southland Region, including the Subantarctic Islands. Vol. MP100. Geological Society of New Zealand, p. 41. URL: `http://www.geomarine.org.nz/NZGI`.

Heim, A., 1932. Landslides and human lives (translated by NA Skermer). Vancouver: Bi-Tech Publishers.

Heim, A., 1882. Der Bergsturz von Elm. Zeitschrift der Deutschen Geologischen Gesellschaft, 74–115.

Henderson, R., Thompson, S., 1999. Extreme rainfalls in the Southern Alps of New Zealand. Journal of Hydrology (NZ) 38.2, 309–330.

Hewitt, K., 1999. Quaternary Moraines vs Catastrophic Rock Avalanches in the Karakoram Himalaya, Northern Pakistan. Quaternary Research 51.3, 220–237.

Hewitt, K., 2002. Styles of rock-avalanche depositional complexes conditioned by very rugged terrain, Karakoram Himalaya, Pakistan. Reviews in Engineering Geology 15, 345–377.

Hewitt, K., 2009. Glacially conditioned rock-slope failures and disturbance-regime landscapes, Upper Indus Basin, northern Pakistan. Geological Society, London, Special Publications 320.1, 235–255.

Hewitt, K., Clague, J.J., Orwin, J.F., 2008. Legacies of catastrophic rock slope failures in mountain landscapes. Earth-Science Reviews 87.1, 1–38.

Holmes, C.D., 1947. Kames. American Journal of Science 245.4, 240–249.

Hoppe, G., 1952. Hummocky moraine regions with special reference to the interior of Norrbotten. Geografiska Annaler 34, 1–72.

Howarth, J.D., Fitzsimons, S.J., Norris, R.J., Langridge, R., Vandergoes, M.J., 2015. A 2000 yr rupture history for the Alpine fault derived from Lake Ellery, South Island, New Zealand. Geological Society of America Bulletin, B31300. 1.

Imre, B., Laue, J., Springman, S.M., 2010. Fractal fragmentation of rocks within sturzstroms: insight derived from physical experiments within the ETH geotechnical drum centrifuge. Granular matter 12.3, 267–285.

Ivy-Ochs, S., Poschinger, A., Synal, H.-A., Maisch, M., 2009. Surface exposure dating of the Flims landslide, Graubünden, Switzerland. Geomorphology 103.1, 104–112.

Ivy-Ochs, S., Kerschner, H., Kubik, P.W., Schluchter, C., 2006. Glacier response in the European Alps to Heinrich Event 1 cooling: the Gschnitz stadial. Journal of Quaternary Science 21.2, 115–130.

Jackson, L.E., 2002. Landslides and landscape evolution in the Rocky Mountains and adjacent Foothills area, southwestern Alberta, Canada. Reviews in Engineering Geology 15, 325–344.

Jones, R.S., 2015. Late cenozoic behaviour of two Transantarctic Mountain outlet glaciers. Victoria University of Wellington.

Keefer, D.K., 1999. Earthquake-induced landslides and their effects on alluvial fans. Journal of Sedimentary Research 69.1.

Kennedy, I.T., Petley, D.N., Williams, R., Murray, V., 2015. A systematic review of the health impacts of mass Earth movements (landslides). PLoS currents 7.

Kim, K., Sutherland, R., 2004. Uplift rate and landscape development in southwest Fiordland, New Zealand, determined using 10 Be and 26 Al exposure dating of marine terraces. Geochimica et Cosmochimica Acta 68.10, 2313–2319.

Korup, O., 2002. Recent research on landslide dams-a literature review with special attention to New Zealand. Progress in Physical Geography 26.2, 206–235.

Korup, O., 2005. Distribution of landslides in southwest New Zealand. Landslides 2.1, 43–51.

Korup, O., Clague, J.J., 2009. Natural hazards, extreme events, and mountain topography. Quaternary Science Reviews 28.11, 977–990.

Korup, O., Clague, J.J., Hermanns, R.L., Hewitt, K., Strom, A.L., Weidinger, J.T., 2007. Giant landslides, topography, and erosion. Earth and Planetary Science Letters 261.3, 578–589.

Korup, O., McSaveney, M.J., Davies, T.R., 2004. Sediment generation and delivery from large historic landslides in the Southern Alps, New Zealand. Geomorphology 61.1, 189–207.

Landis, C., 1980. Little Ben Sandstone, Maitai Group (Permian): nature and extent in the Hollyford-Eglinton region, South Island, New Zealand. New Zealand journal of geology and geophysics 23.5-6, 551–567.

Larsen, S.H., Davies, T.R.H., McSaveney, M.J., 2005. A possible coseismic landslide origin of late Holocene moraines of the Southern Alps, New Zealand. New Zealand Journal of Geology and Geophysics 48.2, 311–314.

Larson, G.J., Menzies, J., Lawson, D.E., Evenson, E.B., Hopkins, N.R., 2015. Macro- and micro-sedimentology of a modern melt out till-Matanuska Glacier, Alaska, USA. Boreas.

Lawson, D.E., 1981. *Sedimentological characteristics and classification of depositional processes and deposits in the glacial environment*. Report. DTIC Document.

Lewin, J., Macklin, M.G., Johnstone, E., 2005. Interpreting alluvial archives: sedimentological factors in the British Holocene fluvial record. Quaternary Science Reviews 24.16–17, 1873–1889. DOI: http://dx.doi.org/10.1016/j.quascirev.2005.01.009. URL: http://www.sciencedirect.com/science/article/pii/S027737910500034X.

LINZ, 2014. *Southland 0.75m Rural Aerial Photos (2005 - 2011)*. Web Page. URL: https://data.linz.govt.nz/layer/1934-southland-075m-rural-aerial-photos-2005-2011/.

Livingstone, S.J., Evans, D.J., Cofaigh, C.Ó., Hopkins, J., 2010. The Brampton kame belt and Pennine escarpment meltwater channel system (Cumbria, UK): morphology, sedimentology and formation. Proceedings of the Geologists' Association 121.4, 423–443.

McCalpin, J., 1992. Glacial geology of the upper Wairau valley, Marlborough, New Zealand. New Zealand Journal of Geology and Geophysics 35.2, 211–222.

McColl, S., Draebing, D., in press. Rock slope (in-)stability in the proglacial zone: State of the Art. In: Heckmann, T., Morch, D. (Eds). Geomorphology of proglacial systems - Landform and sediment dynamics in recently deglaciated alpine landscape. Springer Science. Chap. 4.

McColl, S.T., 2012. Paraglacial rock-slope stability. Geomorphology 153, 1–16.

McColl, S.T., Davies, T.R., 2013. Large ice-contact slope movements: glacial buttressing, deformation and erosion. Earth Surface Processes and Landforms 38.10, 1102–1115.

McColl, S., Davies, T., 2011. Evidence for a rock-avalanche origin for 'The Hillocks' "moraine", Otago, New Zealand. Geomorphology 127.3, 216–224.

McSaveney, M., 2002. Recent rockfalls and rock avalanches in Mount Cook national park, New Zealand. Reviews in Engineering Geology 15, 35–70.

McSaveney, M., Davies, T., 2006. Rapid rock-mass flow with dynamic fragmentation: inferences from the morphology and internal structure of rockslides and rock avalanches. Landslides from Massive rock Slope Failure.(Evans, SG; Scarascia Mugnozza, G, 285–304.

McSaveney, M., Davies, T., 2007. Rockslides and their motion. Progress in landslide science, 113–133.

McSaveney, M., Davies, T., Hodgson, K., 2000. "A contrast in deposit style and process between large and small rock avalanches". In: *Proceedings of the 8th International Symposium on Landslides, Cardiff, UK*, pp. 26–30.

Mortimer, N., Gans, P., Calvert, A., Walker, N., 1999. Geology and thermochronometry of the east edge of the Median Batholith (Median Tectonic Zone): a new perspective on Permian to Cretaceous crustal growth of New Zealand. Island Arc 8.3, 404–425.

Nicoletti, P.G., Sorriso-Valvo, M., 1991. Geomorphic controls of the shape and mobility of rock avalanches. Geological Society of America Bulletin 103.10, 1365–1373.

Niewiarowski, W., 1965. Conditions of occurrence and distribution of kame landscapes in the Peribalticum within the area of the last glaciation. Geographia Polonica 6, 6.

Norris, R.J., Toy, V.G., 2014. Continental transforms: A view from the Alpine Fault. Journal of Structural Geology 64, 3–31.

O'Donnell, C.F., Christie, J., Corben, C., Sedgeley, J.A., Simpson, W., 1999. Rediscovery of short-tailed bats (Mystacina sp.) in Fiordland, New Zealand: preliminary observations of taxonomy, echolocation calls, population size, home range, and habitat use. New Zealand Journal of Ecology 23.1, 21–30.

Paul, M., Eyles, N., 1990. Constraints on the preservation of diamict facies (melt-out tills) at the margins of stagnant glaciers. Quaternary Science Reviews 9.1, 51–69.

Petley, D., 2012. Global patterns of loss of life from landslides. Geology 40.10, 927–930.

Powers, M.C., 1953. A new roundness scale for sedimentary particles. Journal of Sedimentary Research 23.2.

Price, R., 1969. Moraines, sandar, kames and eskers near BreiDamerkurjokull, Iceland. Transactions of the Institute of British Geographers, 17–43.

Purdie, J., Fitzharris, B., 1999. Processes and rates of ice loss at the terminus of Tasman Glacier, New Zealand. Global and Planetary Change 22.1, 79–91.

Putnam, A.E., Denton, G.H., Schaefer, J.M., Barrell, D.J.A., Andersen, B.G., Finkel, R.C., Schwartz, R., Doughty, A.M., Kaplan, M.R., Schluchter, C., 2010. Glacier advance in southern middle-latitudes during the Antarctic Cold Reversal. Nature Geosci 3.10. 10.1038/ngeo962, 700–704. DOI: `http://www.nature.com/ngeo/journal/v3/n10/abs/ngeo962.html#supplementary-information`. URL: `http://dx.doi.org/10.1038/ngeo962`.

Reading, H.G., 2009. Sedimentary environments: processes, facies and stratigraphy. John Wiley and Sons.

Reznichenko, N.V., 2012. Rock Avalanches on Glaciers: Processes and Implications. University of Canterbury, Christchurch. URL: `http://hdl.handle.net/10092/6524`.

Reznichenko, N.V., Davies, T.R., Winkler, S., 2015. Revised palaeoclimatic significance of Mueller Glacier moraines, Southern Alps, New Zealand. Earth Surface Processes and Landforms.

Reznichenko, N.V., Davies, T.R., Shulmeister, J., Larsen, S.H., 2012a. A new technique for identifying rock avalanche-sourced sediment in moraines and some paleoclimatic implications. Geology 40.4, 319–322.

Reznichenko, N.V., Davies, T.R., Shulmeister, J., Winkler, S., 2012b. Influence of rock avalanches upon the formation of moraines and their subsequent palaeoclimatic interpretation: a critical appraisal. Zeitschrift für Geomorphologie, Supplementary Issues 56.4, 37–54.

Reznichenko, N., Davies, T., Robinson, T., De Pascale, G., 2013. Rock avalanche deposits in Alai Valley, Central Asia: misinterpretation of glacial record. Vol. 15. EGU General Assembly Conference Abstracts, p. 182.

Rhoades, D., Van Dissen, R., 2003. Estimates of the time-varying hazard of rupture of the Alpine Fault, New Zealand, allowing for uncertainties. New Zealand Journal of Geology and Geophysics 46.4, 479–488.

Robinson, T.R., Davies, T.R., Reznichenko, N.V., De Pascale, G.P., 2014. The extremely long-runout Komansu rock avalanche in the Trans Alai range, Pamir Mountains, southern Kyrgyzstan. Landslides, 1–13.

Robinson, T., Davies, T., 2013. Review article: Potential geomorphic consequences of a future great (M w= 8.0+) Alpine Fault earthquake, South Island, New Zealand. Natural Hazards and Earth System Science 13.9, 2279–2299.

Rosenblum, S., Brownfield, I.K., 2000. Magnetic susceptibilities of minerals. US Geological Survey, US Departmetn of the Interior.

Rother, H., Shulmeister, J., Fink, D., Alexander, D., Bell, D., 2015. Surface exposure chronology of the Waimakariri glacial sequence in the Southern Alps of New Zealand: Implications for MIS-2 ice extent and LGM glacial mass balance. Earth and Planetary Science Letters 429, 69–81.

Ryder, J.M., 1971. The Stratigraphy and Morphology of Para-glacial Alluvial Fans in South-central British Columbia. Canadian Journal of Earth Sciences 8.2, 279–298. DOI: 10.1139/e71-027. URL: http://dx.doi.org/10.1139/e71-027.

Schaefer, J.M., Denton, G.H., Barrell, D.J., Ivy-Ochs, S., Kubik, P.W., Andersen, B.G., Phillips, F.M., Lowell, T.V., Schluchter, C., 2006. Near-synchronous interhemispheric termination of the last glacial maximum in mid-latitudes. Science 312.5779, 1510–1513.

Schumm, S.A., 1979. Geomorphic thresholds: the concept and its applications. Transactions of the Institute of British Geographers, 485–515.

Schuster, R., Wieczorek, G., Hope, D., 1998. Landslide dams in Santa Cruz County, California, resulting from the earthquake. US Geological Survey professional paper 1551C.

Shakesby, R.A., 1989. Variability in neoglacial moraine morphology and composition, Storbreen, Jotunheimen, Norway: within-moraine patterns and their implications. In: Geografiska Annaler. Series A. Physical Geography. 1/2. Vol. 71. Wiley, pp. 17–29.

Sharp, M., 1983. Glacial geomorphology. Progress in Physical Geography 7.2, 229–239.

Sharp, M., Gomez, B., 1986. Processes of debris comminution in the glacial environment and implications for quarts sand-grain micromorphology. Sedimentary Geology 46.1, 33–47.

Shepherd, A., 2015. *Glaciers and Glacial Landforms*. Web Page. URL: http://slideplayer.com/slide/5963823/.

Shreve, R.L., 1968. The Blackhawk landslide. Geological Society of America Special Papers 108, 1–48.

Shugar, D.H., Rabus, B.T., Clague, J.J., Capps, D.M., 2012. The response of Black Rapids Glacier, Alaska, to the Denali earthquake rock avalanches. Journal of Geophysical Research: Earth Surface 117.F1.

Shulmeister, J., Davies, T.R., Evans, D.J., Hyatt, O.M., Tovar, D.S., 2009. Catastrophic landslides, glacier behaviour and moraine formation–A view from an active plate margin. Quaternary Science Reviews 28.11, 1085–1096.

Siebert, L., 1984. Large volcanic debris avalanches: characteristics of source areas, deposits, and associated eruptions. Journal of volcanology and geothermal research 22.3, 163–197.

Smith, G., Davies, T., McSaveney, M., Bell, D., 2006. The Acheron rock avalanche, Canterbury, New Zealand—morphology and dynamics. Landslides 3.1, 62–72.

Smith, L.N., 2001. Columbia Mountain landslide: late-glacial emplacement and indications of future failure, Northwestern Montana, USA. Geomorphology 41.4, 309–322.

Strom, A., 2006. Morphology and internal structure of rockslides and rock avalanches: grounds and constraints for their modelling. In: Landslides from Massive Rock Slope Failure. Springer, pp. 305–326.

Strom, A.L., Korup, O., 2006. Extremely large rockslides and rock avalanches in the Tien Shan Mountains, Kyrgyzstan. Landslides 3.2, 125–136.

Suggate, R.P., Almond, P.C., 2005. The last glacial maximum (LGM) in western South Island, New Zealand: implications for the global LGM and MIS 2. Quaternary Science Reviews 24.16, 1923–1940.

Suggate, R., 1990. Late pliocene and quaternary glaciations of New Zealand. Quaternary science reviews 9.2, 175–197.

Sutherland, R., Kim, K., Zondervan, A., McSaveney, M., 2007. Orbital forcing of mid-latitude Southern Hemisphere glaciation since 100 ka inferred from cosmogenic nuclide ages of moraine boulders from the Cascade Plateau, southwest New Zealand. Geological Society of America Bulletin 119.3-4, 443–451.

Swift, D.A., Nienow, P.W., Spedding, N., Hoey, T.B., 2002. Geomorphic implications of subglacial drainage configuration: rates of basal sediment evacuation controlled by seasonal drainage system evolution. Sedimentary Geology 149.1, 5–19.

Tessier, A., Campbell, P.G., Bisson, M., 1979. Sequential extraction procedure for the speciation of particulate trace metals. Analytical chemistry 51.7, 844–851.

Thomson, R., 1996. Prehistoric changes in the level of Lake Wakatipu. An Outline Study Prepared for the Otago Regional Council.

Tiwari, G., Tiwari, R., Singh, K., 2004. SEM surface microtextures of quartz grains from Ganga and Yamuna river sediments, Allahabad, UP. Geological Society of India 63.5, 515–521.

Tovar, D.S., Shulmeister, J., Davies, T., 2008. Evidence for a landslide origin of New Zealand′s Waiho Loop moraine. Nature Geoscience 1.8, 524–526.

Tschudi, S., Ivy-Ochs, S., Schluchter, C., Kubik, P., Rainio, H., 2000. 10Be dating of Younger Dryas Salpausselka l formation in Finland. Boreas 29.4, 287–293.

Turnbull, I., 2000. Geology of the Wakatipu Area Institute of Geological and Nuclear Sciences 1:250 000 geological map 18..1 sheet + 72 p. Institute of Geological and Nuclear Sciences Limited, Lower Hutt, New Zealand.

Turnbull, J.M., Davies, T.R., 2006. A mass movement origin for cirques. Earth Surface Processes and Landforms 31.9, 1129–1148.

Valkengoed, B. van, 2011. Pollen evidence for Holocene climate change in the Eglinton Valley, western Southland. University of Otago. URL: `http://hdl.handle.net/10523/1757`.

Vandergoes, M.J., Newnham, R.M., Denton, G.H., Blaauw, M., Barrell, D.J., 2013. The anatomy of Last Glacial Maximum climate variations in south Westland, New Zealand, derived from pollen records. Quaternary Science Reviews 74, 215–229.

Vandergoes, M.J., Newnham, R.M., Preusser, F., Hendy, C.H., Lowell, T.V., Fitzsimons, S.J., Hogg, A.G., Kasper, H.U., Schluchter, C., 2005. Regional insolation forcing of late Quaternary climate change in the Southern Hemisphere. Nature 436.7048, 242–245.

Wadell, H., 1932. Volume, shape, and roundness of rock particles. The Journal of Geology, 443–451.

Wandres, A.M., Bradshaw, J.D., Weaver, S., Maas, R., Ireland, T., Eby, N., 2004. Provenance analysis using conglomerate clast lithologies: a case study from the Pahau terrane of New Zealand. Sedimentary Geology 167.1, 57–89.

Wassmer, P., Schneider, J., Pollet, N., Schmitter-Voirin, C., 2004. Effects of the internal structure of a rock–avalanche dam on the drainage mechanism of its impoundment, Flims sturzstrom and Ilanz paleo-lake, Swiss Alps. Geomorphology 61.1, 3–17.

Weidinger, J.T., Korup, O., 2009. Frictionite as evidence for a large Late Quaternary rockslide near Kanchenjunga, Sikkim Himalayas, India—Implications for extreme events in mountain relief destruction. Geomorphology 103.1, 57–65.

Weidinger, J.T., Korup, O., Munack, H., Altenberger, U., Dunning, S.A., Tippelt, G., Lottermoser, W., 2014. Giant rockslides from the inside. Earth and Planetary Science Letters 389, 62–73.

Whitehouse, I.E., Griffiths, G.A., 1983. Frequency and hazard of large rock avalanches in the central Southern Alps, New Zealand. Geology 11.6, 331–334.

Whitehouse, I., 1983. Distribution of large rock avalanche deposits in the central Southern Alps, New Zealand. New Zealand journal of geology and geophysics 26.3, 271–279.

Williams, J., 1975. Geology of the Upper Eglinton area. status of the median tectonic line. Thesis, URL: `http://hdl.handle.net/10523/5936`.

Williams, J., 1978. Eglinton Volcanics-stratigraphy, petrography, and metamorphism. New Zealand Journal of Geology and Geophysics 21.6, 713–732.

Williams, M., Cook, E., Kaars, S. van der, Barrows, T., Shulmeister, J., Kershaw, P., 2009. Glacial and deglacial climatic patterns in Australia and surrounding regions from 35 000 to 10 000 years ago reconstructed from terrestrial and near-shore proxy data. Quaternary Science Reviews 28.23, 2398–2419.

Williams, P.W., 1996. A 230 ka record of glacial and interglacial events from Aurora Cave, Fiordland, New Zealand. New Zealand Journal of Geology and Geophysics 39.2, 225–241.

Williams, P.W., McGlone, M., Neil, H., Zhao, J.-X., 2015. A review of New Zealand palaeoclimate from the Last Interglacial to the global Last Glacial Maximum. Quaternary Science Reviews 110, 92–106.

Winkler, S., Nesje, A., 1999. Moraine formation at an advancing temperate glacier: Brigsdalsbreen, western Norway. Geografiska Annaler: Series A, Physical Geography 81.1, 17–30.

Xu, Q., Shang, Y., Asch, T. van, Wang, S., Zhang, Z., Dong, X., 2012. Observations from the large, rapid Yigong rock slide–debris avalanche, southeast Tibet. Canadian Geotechnical Journal 49.5, 589–606.

Yetton, M.D., 2000. The probability and consequences of the next Alpine Fault earthquake, South Island, New Zealand. University of Canterbury, Christchurch.

Appendix A

Beryllium separation chemistry

A.1 Beryllium separation chemistry

Original method by Blard et al., (2008)
Modified by Collins (2015)
Further modified by Goldie Walker, April 2016

A.1.1 Leach 1 - hydroxylammonium-chloride

- Weigh approx. 5 g of each sample into individual labeled 180 ml Savillex beakers of a known weight.

  Note: The purer the pyroxene sample, the less mass is needed. E.g. 90% pyroxene can be weighed in at ~4 g.

- Slowly pour in 25 ml 0.04M $NH_2OH.HCl$ in 25% acetic acid and leach for 12 hours on a 95°C hotplate.

- Remove from hotplate and allow to cool for 15 minutes.

- Decant excess solution into acid waste.

- Wash sediment into 50 ml centrifuge tubes using MilliQ water.

- Centrifuge for 5 minutes at 3000 rpm.

- Rinse the solution into acid waste.

- Add ~15 ml MilliQ water to the centrifuge tube and shake to mix.

  Repeat the rinsing two more times. Water should run clear.

- After final rinse, wash the sediment back into the original Savillex beaker using MilliQ water.

- Dry the sediment on a 100°C hotplate (approx. 2 hours).

- Precisely weigh the sample to determine the mass of material eliminated by this leaching step.

A.1.2 Leach 2 - hydrochloric acid

- Add a small amount of 1M HCl to the sediment and swirl to combine.
- Wash the mixture into 50 ml centrifuge tubes using more 1M HCl if needed.
- Top the centrifuge tubes up to 25 ml with 1M HCl.
- Agitate on 20°C hotdog rollers for 24 hours.
- Centrifuge for 5 minutes at 3000 rpm.
- Rinse the solution into acid waste.
- Add ~15 ml MilliQ water to the centrifuge tube and shake to mix.

  Repeat the rinsing two more times. Water should run clear.
- After final rinse, wash the sediment back into the original Savillex beaker with MilliQ water.
- Dry the sediment overnight in a 70°C oven.

  Note: The hotplate and the oven can be used interchangeably to dry the sediment prior to weighing.
- Precisely weigh the sample to determine the mass of material eliminated by this leaching step.

Appendix B

Geomorphic map of Eglinton Valley

The A2-sized geomorphic map (Figure 6.1) has been supplied separately for ease of visualisation.